FP7 2013 Cooperation Work Programme
Theme 6: Environment (Including Climate Change)

Novel indicators for identifying critical *INFRA*structure at *RISK* from Natural Hazards

Deliverable D8.2

Case Study Results

Primary Author	Julie Clarke, Robert Corbally, Eugene OBrien/Roughan & O'Donovan Ltd. (ROD)
WP	8
Submission Date	29/11/2016
Primary Reviewer	Teresa Salceda, Miguel Segarra/Dragados (DSA)
Dissemination Level	PU

This project has received funding from the European Union's Seventh Programme for research, technological development and demonstration under grant agreement No 603960.

Project Information

Project Duration: 1/10/2013 - 30/09/2016

Project Coordinator: Professor Eugene OBrien

Roughan & O' Donovan Limited

eugene.obrien@rod.ie

Work Programme: 2013 Cooperation Theme 6:

Environment (Including Climate Change).

Call Topic: Env.2013.6.4-4 Towards Stress Testing of Critical Infrastructure Against Natural Hazards-FP7-ENV-2013-two stage.

Project Website: www.infrarisk-fp7.eu

Partners:

Roughan & O' Donovan Limited, Ireland

Eidgenössische Technische Hochschule Zürich, Switzerland.

Dragados SA, Spain.

Gavin and Doherty Geosolutions Ltd., Ireland.

Probabilistic Solutions Consult and Training BV, Netherlands.

Agencia Estatal Consejo Superior de Investigaciones Científicas, Spain.

University College London, United Kingdom.

PSJ, Netherlands.

Stiftelsen SINTEF, Norway.

Ritchey Consulting AB, Sweden.

University of Southampton (IT Innovation Centre), United Kingdom.

Document Information

Version	Date	Description	Primary Author
Version01	15/07/2016	Table of contents for consortium comment	Julie Clarke
	17/06/2015	Section 5.3.4.1 and 5.3.4.2	Pierre Gehl, Dina D'Ayala
	16/09/2016	Section 6.6.3.1	Teresa Salceda Page, Silvia Goni Ibanez, Miguel Segarra
	17/09/2016	Section 6.6.1	Pieter van Gelder
	19/09/2016	Section 5.3.2	Mariano Garcia-Fernandez, Maria Jose Jimenez
	25/09/2016	Section 6.5	Peter Prak
Version02	11/11/2016	ROD rev01	Julie Clarke, Cathal Leahy, Lorcan Connolly, Robert Corbally, Sheila Nolan
	29/11/2016	Final version for submission	Julie Clarke, Robert Corbally, Eugene OBrien

Executive Summary

This deliverable presents the results of two European case studies that were analysed to demonstrate the systematic application of the tools and methodologies that have been developed in the INFRARISK project. The case studies are located along the trans-European (TEN-T) network, which provides critical infrastructure corridors throughout Europe and facilitates the effective transportation of people and goods, supporting economies and contributing to the European single market. Each case study focuses on a particular transport infrastructure network (i.e. road or rail) and a particular source hazard (i.e. earthquake or rainfall). Stress tests are performed for the case studies according to the overarching risk assessment methodology that has been developed in the INFRARISK project. The first case study consists of a regional road network in the province of Bologna in northern Italy. Stress tests are performed for low probability, high consequence seismic hazard scenarios and the cascading landslide hazard effects. The direct consequences are quantified in terms of the cost of repairs for structural elements along the road network (i.e. bridges, tunnels and road sections). In addition, the indirect consequences are quantified in terms of the travel time increases encountered by road users as a result of the network disruption, as well as the associated economic losses at national level. The second case study consists of a rail network in Croatia for which stress tests are performed for low probability, high consequence flooding scenarios. Similarly, the direct consequences are quantified in terms of the costs of physical repairs to the network and the indirect consequences are determined in terms of the travel delay times for passengers and freight transport.

Table of Contents

1.0 INTRODUCTION

1.1 Motivation

Modern societies rely on transport infrastructure for the effective transportation of people and goods. The European Union (EU) has over 4.5 million km of paved roads and 212,500 km of rail lines, and the European single market is highly dependent on reliable road and rail infrastructure for the mobility of people and for the distribution of goods. For example, approximately 49.4% of distributed goods in the EU are transported via road and 72.3% of EU passengers travel on roads. Overall, road transport generates approximately 2% of Europe's GDP and has generated approximately 5 million jobs (European Commission, 2012). Rail transport in the EU is equally important, which supports approximately 11.7% of all distributed goods and 6.6% of passengers in the EU (European Commission, 2015).

To improve the connectivity between European countries, the EU has allocated €26 billion for the period 2014-2022 to the development of a trans-European transport network (TEN-T), consisting of nine core network corridors, that forms the backbone for transportation in Europe's single market (European Commission, 2016). It is anticipated that by 2050, freight transport activity will have increased by approximately 80% compared to 2005, and passenger transport is expected to increase by 51% by then (European Commission, 2011).

However, extreme natural hazard events have the potential to cause devastating impacts to transport infrastructure, resulting in significant disruption for road and rail passengers, and associated economic losses. For example, the Northridge earthquake that occurred in Los Angeles, California, in 1994 caused severe damage to the regional highway system, which included the collapse of a section of the main freeway connecting Los Angeles to Northern California. The earthquake event generated a year's worth of highway repair activities and caused significant transport disruption to the region that resulted in the closure of businesses and schools following the event (DeBlasio et al., 2002). Similarly, an extreme flood event that occurred along the Austrian-Slovakian border in 2006 caused damage to approximately 10 km of an important rail line linking Vienna to the Czech Republic, generating repair costs of more than €41.4 million and causing a complete shutdown of passenger and freight operations for several months (Moran et al., 2010; Kellermann et al., 2015). Overall, transport infrastructure plays a vital role in terms of the resilience of societies to natural hazards, facilitating the transportation of emergency goods and services as part of disaster management activities immediately following natural hazard events, and enabling societies to 'bounce back' following such events by avoiding the disruption of daily activities and preventing economic losses.

1.2 The Challenge

In Europe, an increasing number of extreme natural hazard events have occurred in recent decades due to a combination of climate change effects, and changes in physical and social systems. For the period between 1998 and 2009, almost 100,000 fatalities occurred due to natural hazards and more than 11 million people were affected, resulting in losses of approximately €200 billion (European Environment Agency, 2010). These natural hazards have included earthquakes, floods, and landslides. For example, the 2009 earthquake that occurred in the L'Aquila region of Italy resulted in

approximately €2 billion in losses. Additionally, flooding that occurred in the Elbe Basin in 2002 in Italy resulted in approximately €20 billion in losses and landslides that occurred in the town of Sarno, Italy, in 1998 claimed 160 lives.

To ensure the protection of critical transport infrastructure, the INFRARISK project has developed a stress test framework for critical road and rail networks due to low probability, high consequence natural hazard scenarios (van Gelder and van Erp, 2016; Hackl et al., 2016). Stress tests for critical transport infrastructure involve the application of a set of adverse conditions to determine the potential losses due to an extreme natural hazard scenario. The outcome of such tests can be employed by decision makers to assist in the protection of critical transport infrastructure to ensure that undesirable losses are avoided.

1.3 Aims and Objectives

This deliverable describes the application of the stress test framework that has been developed in work package (WP) 6 of the INFRARISK project (van Gelder and van Erp, 2016) to two example case studies. The case studies consist of a road network in Italy and a rail network in Croatia (Ni Choine and Martinovic, 2014), and the stress tests were performed according to the overarching risk assessment methodology developed in WP4 of the project (Hackl et al., 2016).

The objective of this deliverable is to present the results of the case studies that were conducted in WP8 of the INFRARISK project. The aim of the case studies was to test the applicability and validate the effectiveness of the tools and methodologies developed, and the ultimate goal is to demonstrate reliable stress tests for critical European transport infrastructure. The proposed stress test framework provides important insights in relation the risk associated with transport networks due to natural hazards that can be used by infrastructure owners or managers, for example, to facilitate decision making regarding the protection of critical transport infrastructure.

1.4 Limitations and Assumptions

Although the case studies consisted of existing European transport networks, it was not possible to verify the data, nor was it possible to validate the results. Therefore, the case studies were conducted to solely demonstrate the systematic application of the tools and methodologies developed in the INFRARISK project. Notably, the results presented in this deliverable should not be employed by decision makers in relation to the transport networks that are described herein.

Insofar as possible, it was ensured that the terminology employed throughout this deliverable was consistent with the terminology adopted in the INFRARISK project, as outlined by Adey and Hackl (2014).

1.5 Deliverable Structure

Section 2 of this deliverable provides a review of the current literature and methodologies in relation to risk assessment for road and rail transport infrastructure due to natural hazards. This is followed by an overview of the stress test framework (van Gelder and van Erp, 2016) and the overarching risk assessment methodology (Hackl et al., 2016) developed as part of the INFRARISK project in Section 3. Section 4 provides a description of the selected case studies and is focused on the ‘Initiate’ task of

the general process for ensuring acceptable levels of risk, as described by Hackl et al. (2016). This is followed by a description of stress tests that were conducted for each of the selected case studies in Sections 5 and 6, respectively. These sections focus upon the 'Conduct Risk Assessment' task of the general process described by Hackl et al. (2016) and present the results of the stress tests conducted. Finally, a summary of this research is described in Section 7 and conclusions are presented.

2.0 BACKGROUND

Risk assessment for transport networks due to natural hazards plays an important role in terms of mitigation planning as part of risk management activities to improve the resilience of existing infrastructure to extreme events. Risk assessment methodologies form an integral part of disaster management activities and can be used to increase disaster preparedness and to prevent unwanted losses in the face of extreme natural hazard events, as outlined in the Hyogo Framework for Action (ISDR, 2005) and the Sendai Framework for Disaster Reduction (United Nations, 2015). Such strategies are becoming ever more pertinent due to the increasing trends in terms of the occurrence and severity of meteorological natural hazards due to climate change impacts (IPCC, 2014). Furthermore, the impacts of geophyisical natural hazards are becoming increasingly severe due to changing demographic and socioeconomic population characteristics (Huppert and Sparks, 2006).

For distributed transport infrastructure, such as road and rail networks, there is significant complexity associated with the determination of the associated risk due to natural hazards as a result of the spatial and temporal variability of such networks. Furthermore, the impacts of natural hazards events on a distributed transport network occur in the form of both direct consequences, such as structural damage, and indirect consequences, such as travel delays, as well as economic and social losses (Tacnet et al., 2012).

2.1 Risk Assessment for Road and Rail Networks

With increasing trends towards the use of probabilistic risk assessment methodologies to account for the aleatoric uncertainty, or randomness, associated with the occurrence of natural hazards, as well as the epistemic uncertainty associated with the response behaviour of existing structures, such approaches have been adopted for transport networks in recent years. For spatially distributed road or rail networks, risk assessment methodologies are significantly more complex than the analysis of individual structures due to the fact that the spatial correlation across the network should be considered in the analysis to enable the quantification of network losses. The application of such methodologies at network level has been prompted by various natural hazard events over the past number of decades that have caused network disruption at regional and national levels.

2.1.1 Earthquake Hazards

To evaluate the risk due to earthquake hazards, Chang et al. (2000) performed a risk assessment for a road network, which considered several probabilistic hazard scenarios. Fragility functions were employed to characterise the seismic vulnerability of the highway bridges and damage multipliers were subsequently applied to individual links, which represented highway segments, to characterise the functionality loss in terms of a network performance degradation index. Recently, seismic risk assessment methodologies for transport networks have been extended to consider the damage interactions with the surrounding built environment (Argyroudis et al., 2015) and the impact of transport disruption on local communities (Miller and Baker, 2016).

Such risk assessment methodologies consider the spatial correlation of seismic ground motions for earthquake scenarios that are commonly generated using a Monte Carlo simulation method (Crowley and Bommer, 2006; Shiraki et al., 2007). However, this can lead to a computationally

demanding risk assessment analysis and, therefore, several studies have proposed methods to reduce the number of seismic hazard scenarios by providing a representative subset of scenarios to estimate the associated risk. For example, Jayaram and Baker (2010) employed importance sampling to sample only large magnitude seismic events and also adopted K-Means clustering to further reduce the number of ground motion intensity maps. Furthermore, Han and Davidson (2012) introduced an optimization method to minimise the sampling variability across the earthquake scenarios considered.

Within the INFRARISK project, Jiménez and García-Fernández (2016) have developed a seismic hazard methodology to consider low probability ground motions that can be specifically used to perform stress tests for spatially distributed infrastructure networks. The approach is based on Monte Carlo simulation techniques and provides the same results that are generated using conventional probabilistic hazard assessment where the same input models are specified. However, the methodology proposed by Jiménez and García-Fernández (2016) has several advantages; namely, the creation of a long-duration synthetic earthquake catalogue to derive low-probability amplitudes, providing a more powerful and flexible handling of the associated uncertainties and generating a direct link with the probabilistic risk analysis. The approach does not affect the mean hazard values, enabling a distribution of maximum amplitudes that allows a general extreme-value distribution to be obtained. This facilitates the analysis of the occurrence of extreme ground motion scenarios (i.e. those with a very low probability of exceedance) from unlikely combinations.

2.1.2 Flood Hazards

For flood risk assessment, the majority of methodologies have been developed for building structures. For example, Apel et al. (2004) and Apel et al. (2006) employed simple stochastic models that were calibrated based on the results of complex deterministic models and developed a risk assessment framework based on the following modules: 1) hydrological load, 2) flood routing, 3) levee failure, and 4) damage estimation. The risk assessment was used to quantify the associated losses in terms of property damage and damage functions were employed to relate the inflow of water volume during and after a levee failure for a particular region to the total property damage encountered. Similarly, Jonkman et al. (2008) proposed an integrated framework for the assessment of the associated economic losses due to catastrophic flooding, in which the physical damage was initially modelled according to a hydrodynamic model to simulate the flood flow and damage functions for individual assets. The economic losses associated with infrastructure damage (i.e. indirect consequences) were subsequently estimated based on the disruption of existing links within and between the various sectors of the regional and national economy.

More recently, Vorogushyn et al. (2010) employed a probabilistic methodology for flood hazard risk assessment that considered dike failures and proposed an inundation hazard assessment model. The model comprised three main modules: 1) an unsteady 1D hydrodynamic model using derived synthesis input hydrographs, 2) a probabilistic dike breach model, 3) a 2D raster-based inundation model. The analysis was performed according to a Monte Carlo simulation method to account for the aleatoric uncertainty associated with the flood hazard, as well as the epistemic uncertainty associated with the dike failure process.

For flood hazard assessment, detailed modelling of the steps involved in the entire flood process chain (i.e. from precipitation to inundation), involving the associated meteorological, hydrological, hydraulic and geotechnical processes, is computationally expensive (Menzel, et al. 2006). Modelling approaches are generally categorised as macro, meso or micro (Messner, et al. 2007). In general, macro-level approaches are adopted for the flood assessment of large areas at either national or international scale, for which a relatively low level of precision is generally employed (DEFRA 2001). For meso-level approaches, more detail is considered in the analysis and these approaches are generally adopted at regional scale (Kok, et al. 2005). Micro-level methodologies involve the greatest level of detail and are normally conducted at local scale (Penning-Rowsell, et al. 2005).

2.1.3 Landslide Hazards

For road and rail transport networks, parts of these networks are commonly located adjacent to earthwork slopes, such as cuttings and embankments, which pose a risk to the network due to hydrological and geological processes, e.g. rainfall-triggered landslides. For example, Nguyen et al. (2015) demonstrated the application of an agent-based model to simulate the impacts of landslides on a mountainous road network to evaluate the transport disruption and to determine optimal restoration planning. Similarly, risk assessment methodologies have been developed for landslide-prone regions to quantify the losses, in terms of physical damage associated with landslide occurrences (Remondo et al., 2005; Cardinali et al., 2002).

For road and rail transport infrastructure specifically, Jaiswal et al. (2010) demonstrated a quantitative risk assessment methodology to consider various landslide hazard scenarios. The consequences were considered in terms of the financial losses due to infrastructure and vehicle damage (i.e. direct consequences). Additionally, the indirect consequences were considered in terms of the traffic disruption and the associated business losses and loss of revenue to the railway department.

For rainfall-triggered landslides specifically, a procedure for developing fragility functions to quantify the vulnerability of transport infrastructure to shallow landslides for specific slopes has been developed in the INFRARISK project (D'Ayala and Gehl, 2015). Such an approach has the potential to be incorporated as part of a quantitative risk assessment methodology in conjunction with hazard modelling for extreme weather events to determine the potential losses for existing transport infrastructure for a range of hazard scenarios.

3.0 GENERAL METHODOLOGY

The purpose of this deliverable is to demonstrate reliable stress tests for critical transport infrastructure due to natural hazards. To do so, stress tests were performed for two case studies at regional and pan-European scale according to the stress test framework that was developed for critical transport infrastructure as part of the INFRARISK project (van Gelder and van Erp, 2016). Stress tests refer to the analysis of a particular system under a specific set of adverse conditions to determine the potential losses, and are commonly employed in other industries such as finance, mechanics and nuclear industries, as described by Avdeeva and van Gelder (2014). For transport infrastructure, the stress test framework developed by van Gelder and van Erp (2016) facilitates the development of a probabilistic output disruption for transport networks in terms of the potential losses due to an adverse scenario through the application of 'virtual shocks' simulated according to a numerical representation of the infrastructure network. This outcome distribution can be used to assist decision makers, such as infrastructure owners and managers, regarding the protection of existing and future-planned infrastructure, and contributing to the resilience of critical transport networks.

Within the context of the INFRARISK project, transport infrastructure located along the European TEN-T road and rail networks was considered as 'critical infrastructure' (Figure 1). These network routes constitute important trans-European corridors that facilitate the effective transportation of goods and people and, therefore, are very important for the European single market. The stress tests performed for the case studies considered low probability, high consequence hazard events. Low probability refers to return periods that exceed those that are included in current design codes and an 'event' refers to a measure of the hazard intensity (D'Ayala and Gehl, 2014). To consider 'high consequence' events, the hazard scenarios were linked to critical network elements along the network, which will be described in Sections 5 and 6 for the selected case studies, respectively.

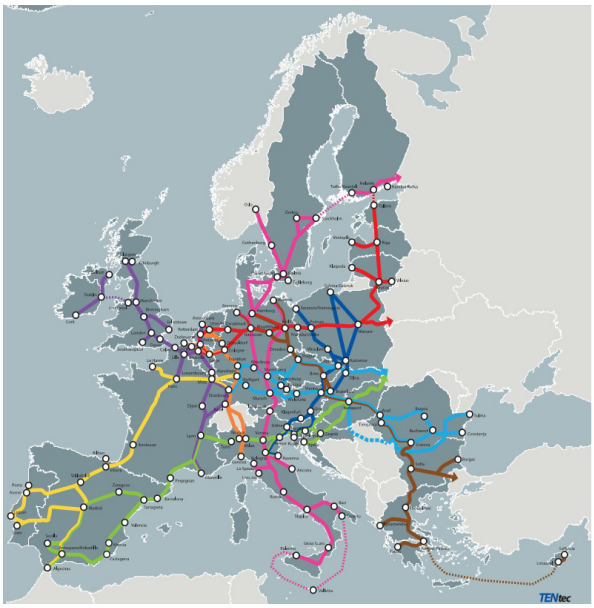

Figure 1: European TEN-T network corridors

The stress tests were performed for the case studies according to the overarching risk assessment methodology developed in the INFRARISK project (Hackl et al., 2016), which describes a general process that supports the evaluation of the risks associated with road and rail infrastructure networks due to natural hazards. The general risk assessment process consists of three main tasks: 1) initiate, 2) conduct risk assessment, 3) conduct intervention program, as illustrated in Figure 2.

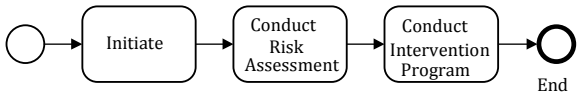

Figure 2: General process to ensure acceptable levels of risk (Hackl et al., 2016)

Section 4 of this deliverable will focus on the 'Initiate' task, which is used to generate ideas in relation to how the risk assessment will be conducted. Meanwhile, the 'Conduct Risk Assessment' task is used to determine whether the level of infrastructure-related risk is acceptable or not. Within the 'Conduct Risk Assessment' task, five sub-tasks have been defined by Hackl et al. (2016), as illustrated in Figure 3: i) setup the risk assessment, ii) determine approach, iii) define system, iv) estimate risk and v) evaluate risk. Using this risk assessment methodology, stress tests were performed for the selected case studies, as described in Sections 5.0 and 6.0, respectively. Notably, the third task in the general process described by Hackl et al. (2016), 'Conduct Intervention Program', was not considered as part of the stress tests described herein although the results of the stress tests have the potential to be used to determine the optimal intervention program according to the decision theory proposed by van Gelder and van Erp (2016).

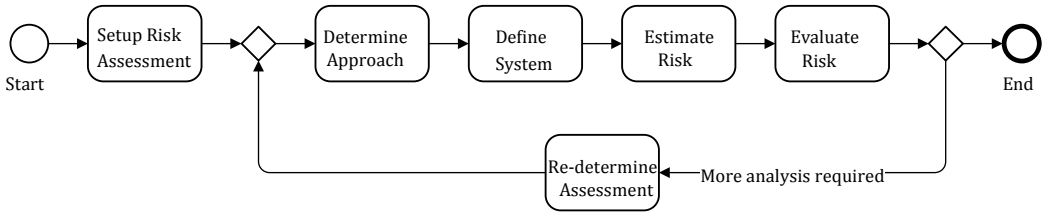

Figure 3: Risk assessment task (Hackl et al., 2016)

4.0 SELECTED CASE STUDIES

Two case studies were examined in WP8 of the INFRARISK project. The selected case studies were previously introduced by Ni Choine and Martinovic (2014). However, the scope of these case studies, as presented in this deliverable, has been modified for reasons of computational demand and data availability. The first case study presented in this deliverable consists of an existing road network in the province of Bologna in northern Italy. The second case study presented consists of an existing rail network in northern Croatia. Each case study focused on a specific source hazard (i.e. earthquake or rainfall) and considers cascading hazard effects.

In this section the 'Initiate' task of the general process for ensuring acceptable levels of risk described by Hackl et al. (2016) is described. This task involved generating ideas in relation to the process of determining whether or not risk levels are deemed to be acceptable for the selected case studies. To do so, structured brainstorming was conducted according to a series of General Morphological (GMA) and Bayesian Networks (BN) workshops for the case studies. The workshops were attended by representative members of the INFRARISK consortium who, for each of the selected case studies, considered various aspects relating to natural hazards and the existing transport infrastructure, such as the following: the type of hazards that could occur; the TEN-T infrastructure that could potentially be affected by the hazards; the type and location of the transport infrastructure networks; the physical condition of the transport infrastructure; and the required level of network service. Further information in relation to both GMA and BN methodologies can be found in Appendices B.3 and C.3 of INFRARISK Deliverable 4.2 (Hackl et al., 2016).

As part of the 'Initiate' task, an internal 'Case Study Guidelines' document was also developed for each of the selected case studies. This was used to structure each of the case studies and to define the steps associated with conducting stress tests according to the 'Risk Assessment' process described by Hackl et al. (2016). In each case, the most prevalent source hazard was identified and it was decided whether or not to consider associated cascading hazards. The spatial extent of each of the selected case study transport networks was clearly defined and the vulnerability of the network elements to the selected hazards was identified. Baseline data was subsequently gathered for each of the case studies and detailed steps to conduct the stress tests were subsequently specified. For example, Figure 4 illustrates a process that was developed for the Italian road network case study using Business Process Model and Notation (BPMN) (www.bpmn.org).

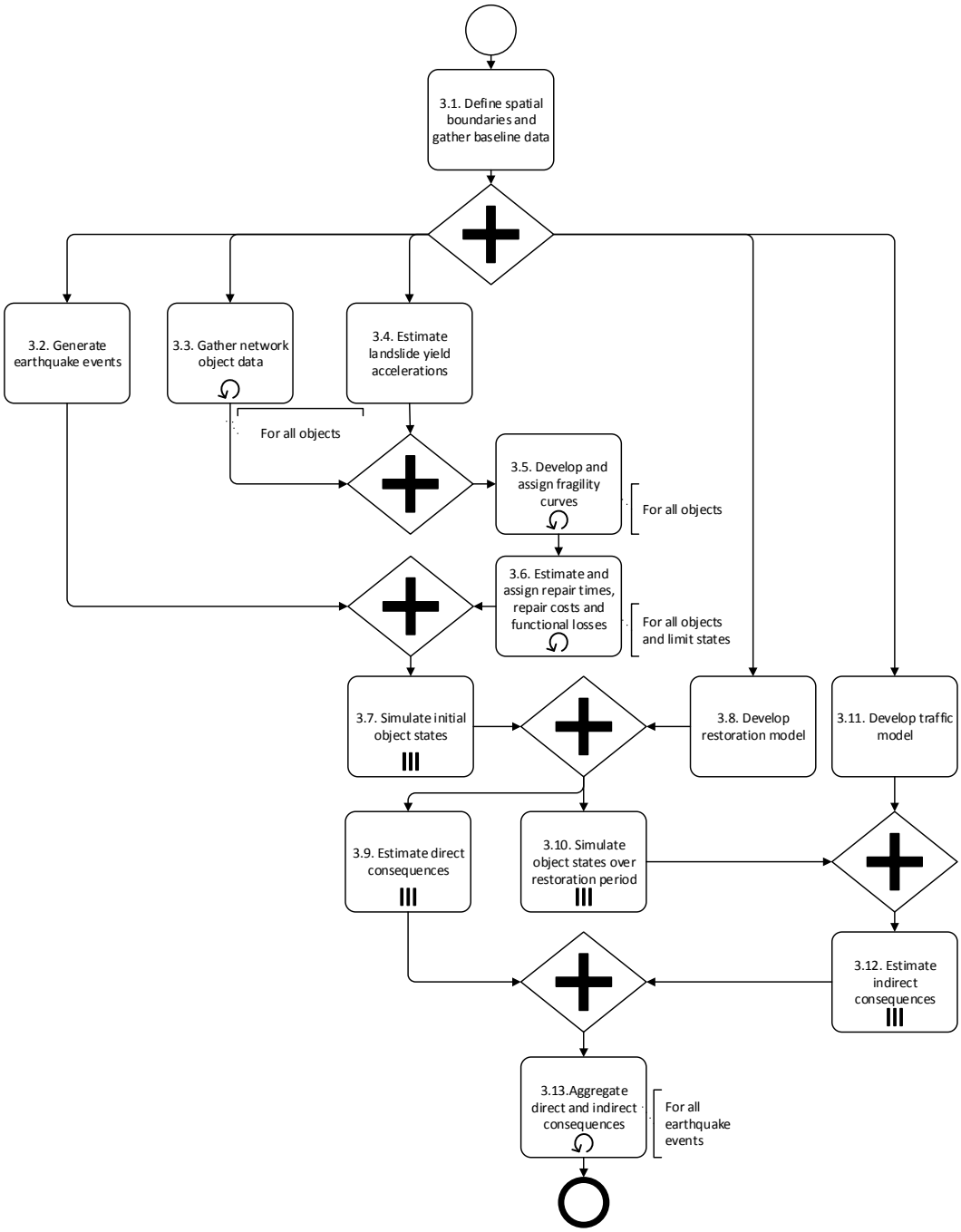

Figure 4: BPMN visualization of 'Conduct Risk Assessment' task for Italian case study

For each of the case studies, the guidelines documents specified that both spatial and temporal aspects were considered in terms of the network risk assessment. Furthermore, the potential network losses were specified in terms of the direct and indirect consequences. The direct consequences were defined in terms of the cost associated with restoring the network to the level of service that existed prior to the natural hazard event, and were considered to be directly attributable to the infrastructure manager. The indirect consequences were defined in terms of the additional losses due to the functionality loss of the transport network, such as additional travel

times encountered by network users and the associated economic losses. Details of this 'Initiate' task are described in the following sections for each of the selected case studies.

4.1 Italian Road Network

For this first case study, a road network in the province of Bologna, northern Italy, was examined. The selected road network is located in the metropolitan area of Bologna, which has a population of approximately one million people and is one of the most important business centres in Italy. The road network is located along the Scandinavian-Mediterranean TEN-T corridor, which provides an important north-south axis for the European economy, as shown in Figure 5. The selected region is exposed to earthquakes, floods and landslides, as described by Ni Choine and Martinovic (2014). Based on the structured brainstorming conducted as part of the 'Initiate' task, it was decided to consider earthquake and landslide hazards in the stress testing of the selected road network. The susceptibility of the province of Bologna to earthquakes and landslides is illustrated in Figure 6.

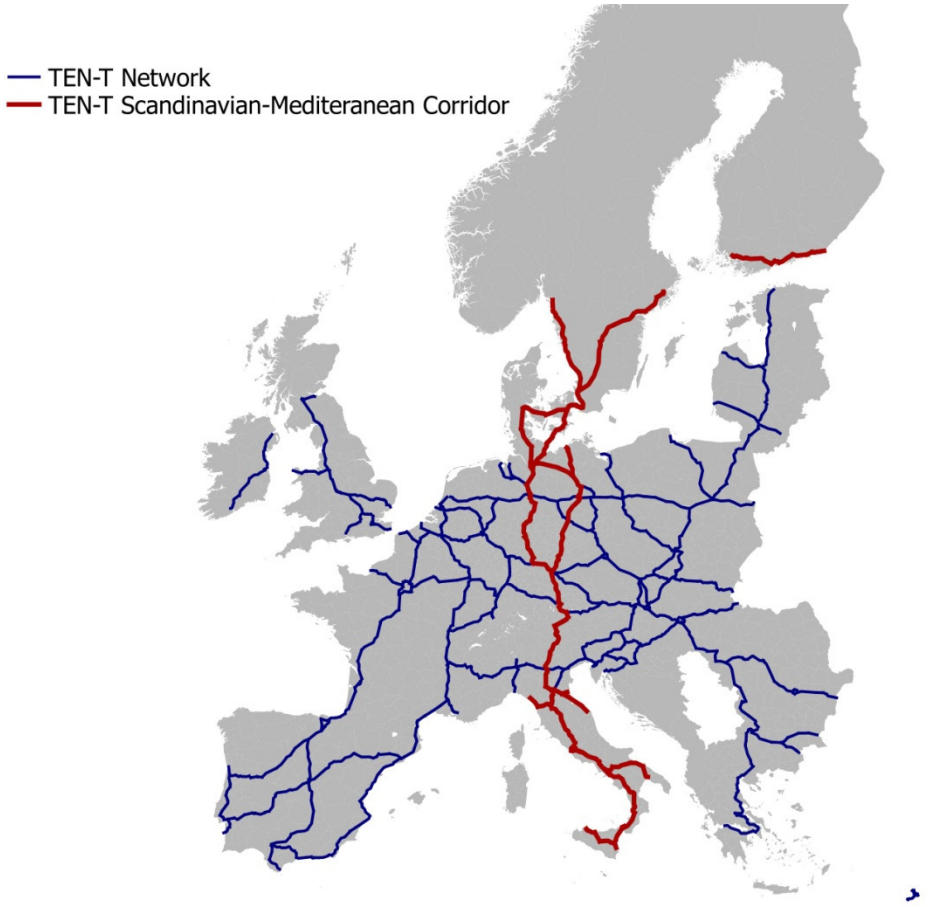

Figure 5: Scandinavian-Mediterranean corridor of European TEN-T network

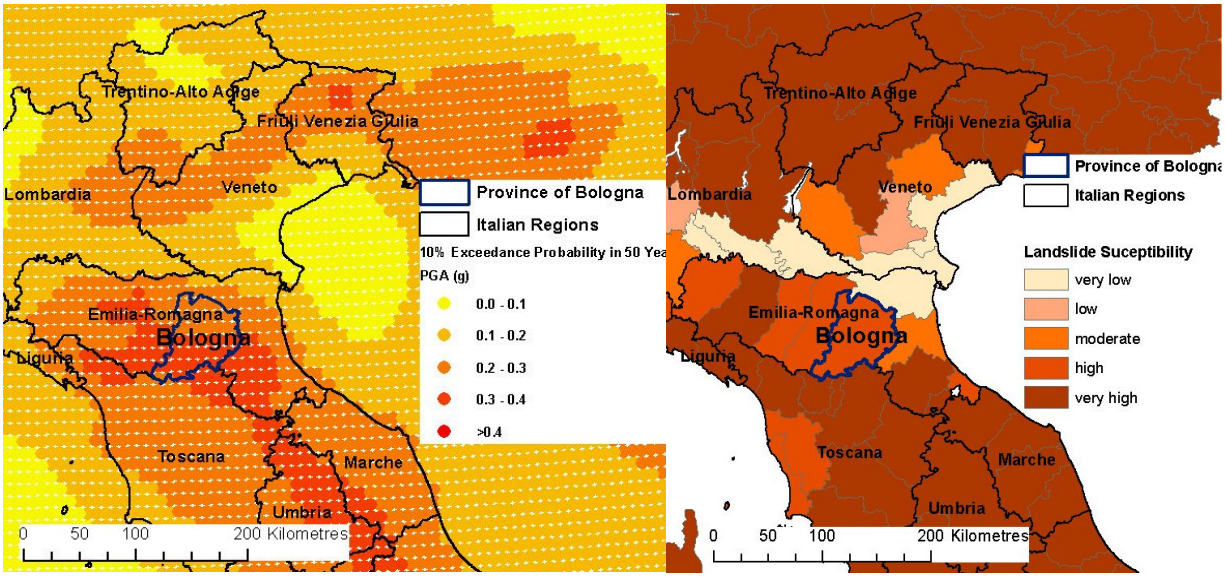

a) Earthquake hazard (Giardini et al., 2013)

b) Landslide hazard (Gunther et al., 2013)

Figure 6: Susceptibility of Bologna to earthquake and landslide hazards

An initial data collection phase was conducted for the Italian case study. Details of the information obtained are outlined in Table 1.

4.2 Croatian Rail Network

For the second case study, a rail network in Croatia was examined. This network is located along the Mediterranean corridor of the European TEN-T network, which forms a vital link from the port of Rijeka to the city of Zagreb, which provides international connections to Slovenia and Hungary, as shown in Figure 7. The selected region is exposed to earthquakes, floods and landslides, as described by Ni Choine and Martinovic (2014). Based on the structured brainstorming conducted as part of the 'Initiate' task, it was decided to consider floods and landslide hazards in the stress testing of the selected rail network. The susceptibility of Croatia to floods and landslides is illustrated in Figure 8.

Variable	Information	URL
Road Network	Open Street Map data available: • Geo position of infrastructure (polylines) • Length • Number of intersections • Bridge locations • Tunnel locations Data extracted from Google maps or elsewhere: • Bridge structural characteristics • Tunnel structural characteristics • Number of lanes • Max speed • Toll rates	http://download.geofabrik.de/europe/italy.html
Building	Geo position and outline of buildings	http://download.geofabrik.de/europe/italy.html
Land use	Open Street Map land use	http://download.geofabrik.de/europe/italy.html
Land cover	Corine Land Cover 2006 raster data. Resolution: 100 × 100 m	http://www.eea.europa.eu/data-and-maps/data/corine-land-cover-2006-raster-3
Population Density	European Population density disaggregated with Corine Land Cover 2000.	http://www.eea.europa.eu/data-and-maps/data/population-density-disaggregated-with-corine-land-cover-2000-2#tab-gis-data
Hydrological Network	DBPrior 10K data includes: Elements of Water (Elementi Idirici); Lakes (Specchi acqua);	http://www.centrointerregionale-gis.it/DBPrior/DBPrior1.asp
Digital Elevation Model	Resolution: 10 × 10 m. DEM is broken into separate tiles. Tile labels can be found at: http://tinitaly.pi.ingv.it/download.html	http://tinitaly.pi.ingv.it
Seismic Hazard	EU FP7 project share developed this seismic hazard map.	http://www.share-eu.org/node/90
Landslide Susceptibility	European landslide expert group developed this landslide susceptibility map.	http://eusoils.jrc.ec.europa.eu/library/themes/landslides/#ELSUS
Flood Hazard	100 year European flood hazard map	http://onlinelibrary.wiley.com/doi/10.1002/hyp.9947/abstract
Soil Maps	1:250000 soil map covers Emilia Romagna region	http://ambiente.regione.emilia-romagna.it/geologia-en/cartografia/webgis-banchedati/soil-maps-of-emilia-romagna-region

Table 1: Baseline data for Italian case study

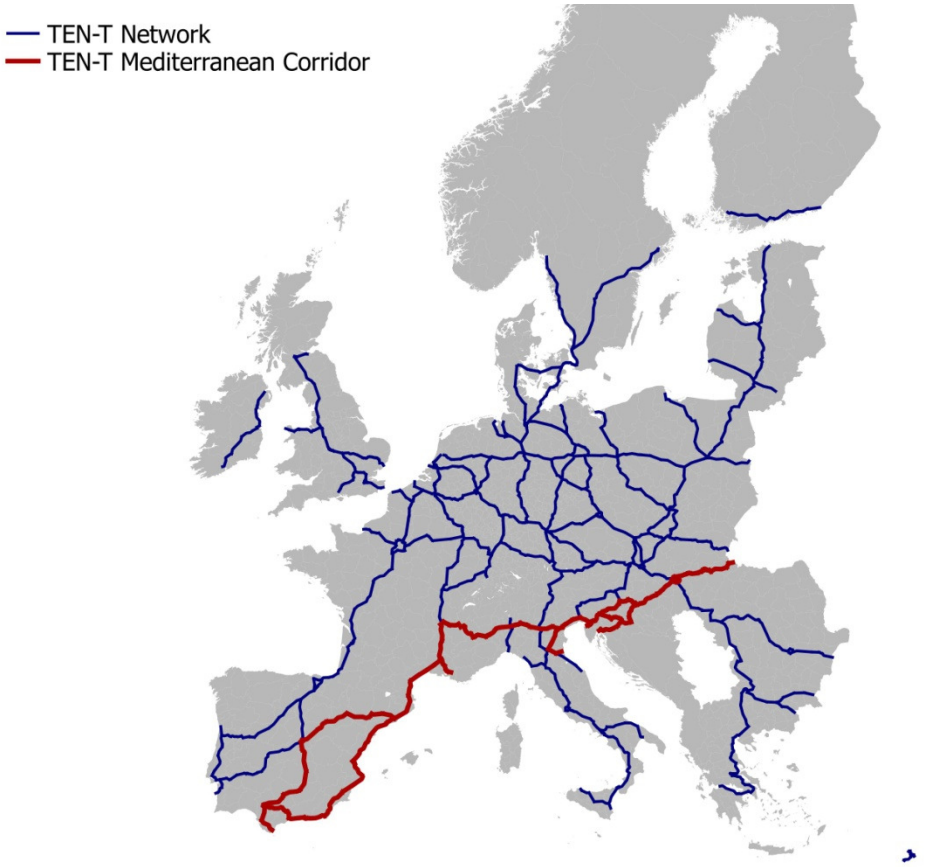

Figure 7: Mediterranean corridor of European TEN-T network

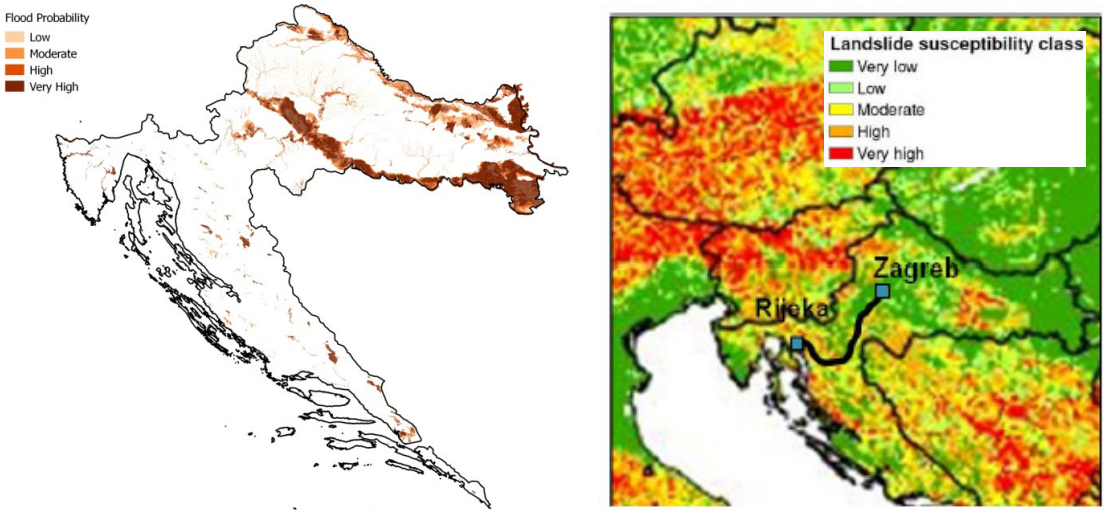

a) Flood hazard (http://korp.voda.hr/) b) Landslide hazard (Gunther et al., 2013)

Figure 8: Susceptibility of Croatia to flood and landslide hazards

An initial data collection phase was conducted for the Croatian case study. Details of the information obtained are outlined in Table 2.

Variable	Information	URL
Road Network	Open Street Map data consists of geo position of road network in Network, broken down into priority levels (motorway, primary, secondary, etc.). Geo position of TEN-T road network is also available.	http://download.geofabrik.de/europe/croatia.html
Rail Network	Open Street Map data consists of geo position of rail lines. Infrastructure element data to be extracted from reports, publications, info from Croatian Railways: • Bridge locations and structural characteristics • Tunnel locations and structural characteristics • Max speed Freight and passenger transport	http://download.geofabrik.de/europe/croatia.html
Buildings	Geo position and outline of buildings	http://download.geofabrik.de/europe/croatia.html
Land use	Open Street Map land use	http://download.geofabrik.de/europe/croatia.html
Land cover	Corine Land Cover 2006 raster data. Resolution: 100 × 100 m	http://www.eea.europa.eu/data-and-maps/data/corine-land-cover-2006-raster-3
Population Density	European Population density disaggregated with Corine Land Cover 2000.	http://www.eea.europa.eu/data-and-maps/data/population-density-disaggregated-with-corine-land-cover-2000-2#tab-gis-data
Hydrological Network	Geo position of rivers	http://download.geofabrik.de/europe/croatia.html
Digital Elevation Model	DEM Resolution: 30 × 30 m. Data sources: SRTSM, ASTER GDEM.	http://www.eea.europa.eu/data-and-maps/data/eu-dem#tab-european-data
Seismic Hazard	EU FP7 project share developed this seismic hazard map.	http://www.share-eu.org/node/90
Landslide Susceptibility	European landslide expert group developed this landslide susceptibility map.	http://eusoils.jrc.ec.europa.eu/library/themes/landslides/#ELSUS
Flood Hazard	100 year European flood hazard map	http://onlinelibrary.wiley.com/doi/10.1002/hyp.9947/abstract

Table 2: Baseline data for Croatian case study

5.0 ITALIAN ROAD NETWORK

This section will describe the application of the 'Conduct Risk Assessment' phase of the overarching risk assessment methodology described by Hackl et al. (2016) that was used to perform stress tests for the Italian road network case study. The 'Conduct Risk Assessment' phase comprises five main tasks: 1) set up risk assessment, 2) determine approach, 3) define system, iv) estimate risk and v) evaluate risk, which will be described for the Italian case study in the following sections.

5.1 Risk Assessment

The objective of the stress tests for the Italian case study was to determine the potential losses due to the impact of low probability, high consequence seismic hazard scenarios on the road network. As part of the 'set up risk assessment' task in the risk assessment process, it was decided that the impacts would be analysed in terms of both the direct and indirect consequences. Direct consequences refer to the costs associated with the earthquake occurrence that are considered directly attributable to the road infrastructure owner or manager. Indirect consequences refer to the additional losses encountered as a result of the road network disruption; for example, the additional travel time encountered by network users and the associated economic losses.

Spatial boundaries were defined in terms of the area to consider in terms of the low probability, high consequence seismic scenarios and the associated landslide cascading effects, and the potential for physical infrastructure damage. However, since transport disruption due to natural hazards has the potential to impact regions beyond the directly affected area, the indirect consequences due to the hazard scenario were analysed for regions beyond these spatial boundaries. Specifically, the consequences to the surrounding Italian regions were analysed in terms of travel delays for road passengers and the associated economic losses.

As there is generally a large degree of uncertainty associated with seismic ground motions, landslide occurrences and the physical vulnerability of road infrastructure elements, a risk assessment approach that considered and accounted for these uncertainties was adopted for the stress tests. Uncertainty quantification is important for providing accurate risk assessments, as discussed in D'Ayala and Gehl (2015). Furthermore, the consideration of uncertainty enables the potential losses to be quantified in terms of a distribution of values, enabling decision makers to assess the level of risk more accurately.

5.2 Approach

For the road network examined as part of the Italian case study, a quantitative approach was employed to conduct the stress tests. This was deemed to be an appropriate approach for determining the risk to the road network due to the low probability, high consequence scenarios examined. The adopted quantitative approach to risk assessment was based on the methodologies described by D'Ayala and Gehl (2014) and D'Ayala and Gehl (2015) and was supported by the use of models.

The quantitative analysis was conducted according to a series of modules, as defined by Hackl et al. (2016). This facilitated an iterative risk assessment process and enabled increased complexity to be adopted for individual modules, where deemed necessary.

5.3 System Definition

This section describes the overall 'system', which refers to the following:

- Definition of the road network spatial boundaries.
- Definition of the earthquake and cascading landslide hazards.
- Definition of the road network infrastructure and the vulnerability of this infrastructure to the hazards considered.
- Definition of the potential losses in terms of physical repair works.
- Definition of the potential functionality loss of the road network.
- Definition of the potential disruption for users of the road network.
- Definition of the potential economic loss due to travel disruption.

For each of the above, the selected boundaries (spatial and temporal), events, scenarios, relationships and models are described herein.

5.3.1 Spatial Boundaries

The spatial boundaries of the selected road network in the province of Bologna, Italy are illustrated in Figure 9. The road network consists of 3410 km of roads and covers an area of approximately 990 km^2.

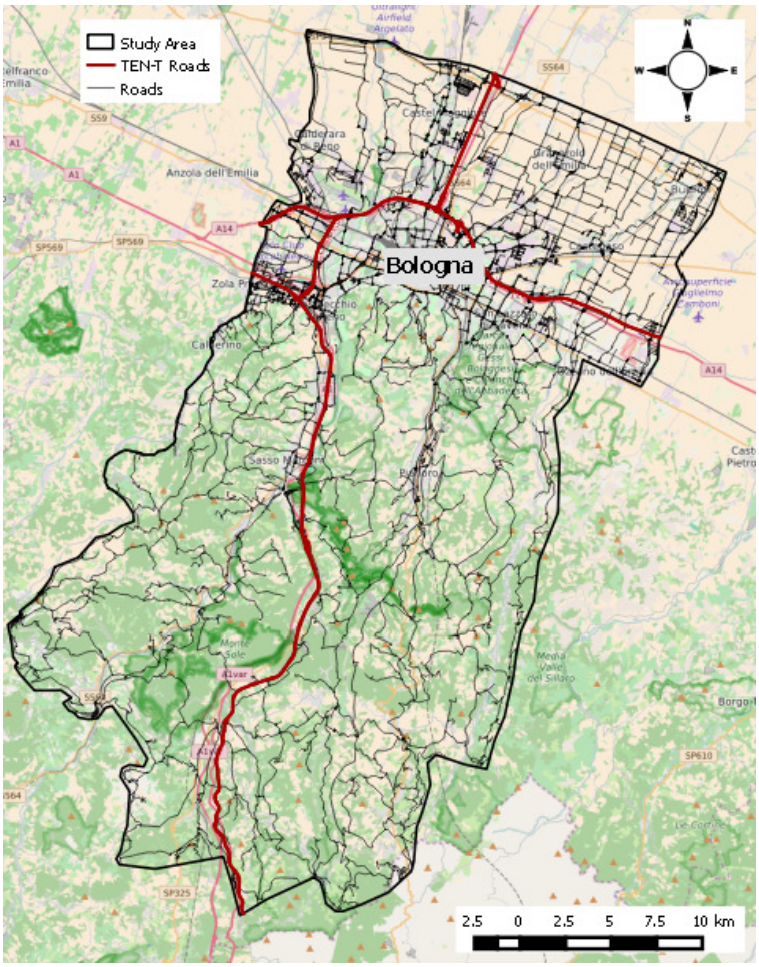

Figure 9: Spatial extent of Italian case study road network

5.3.2 Seismic Hazard Model

Low probability, extreme seismic hazard scenarios were considered for the Italian road network. To do so, the seismic hazard model developed by Jiménez and García-Fernández (2016) was employed, which provided a database of extreme ground-motion (GM) field scenarios that corresponded to various scenarios based on a selection of the following parameters: 1) seismic activity model, 2) ground motion model, 3) hazard level, and 4) percentile of extreme ground motion values.

The seismic activity models employed by Jiménez and García-Fernández (2016) were derived from the area source model used in the European SHARE project (Woessner et al., 2015). The GM-fields were generated based on a single rectangular source area for the seismic activity model measuring 400 km by 500 km (see Figure 10). For each source, seismicity parameters that corresponded to a minimum magnitude of 5.0 were used to generate a synthetic earthquake catalogue that corresponded to 3 million years. Four average source activity models were derived and implemented in the seismic hazard model: 1) high, 2) moderate, 3) moderate-to-low, and 4) low. Ground motion modelling was implemented through two generic models: 1) low attenuation and 2) high attenuation. Both models were based on the ground motion models for soils characterized by V_{S30} = 760 m/s developed by Atkinson and Adams (2015). Hazard levels (annual probability of exceeding ground motion values at the reference site) of 4×10^{-4}, 2×10^{-4}, and 10^{-4} per year were considered that correspond to mean return periods of 2,500, 5,000, and 10,000 years, respectively. Finally, three options of fractiles of extreme ground-motion values at the reference site were available: 1) 0.50, 2) 0.75 and 3) 0.90 (50^{th}, 75^{th}, and 90^{th} percentiles, respectively). Based on the combination of these parameters, 72 extreme motion hazard deterministic 'scenarios' were specified by Jiménez and García-Fernández (2016) in terms of Peak Ground Acceleration (PGA) values for a hazard area measuring 100 km by 200 km at the centre of the source area (see Figure 10).

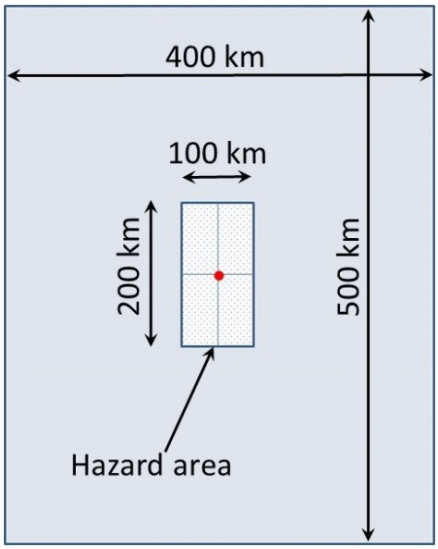

Figure 10: Hazard area (100 km x 200 km)
Note: the red dot corresponds to the centre point of the hazard area and the grey background represents the seismic source area

Spatial random variability for the GM-fields was introduced in the model developed by Jiménez and García-Fernández (2016) to remove the symmetry that would result from implementation of generic ground-motion models, but to maintain the degree of spatial correlation expected, as outlined by Jayaram and Baker (2009). To do so, two-dimensional random fields were generated based on an approach that involved moving an average disk over a uniform grid of points, each having a random realization of the standard normal distribution. After 10,000 random fields were generated, the 18 random fields that resulted in a distortion of less than 0.1% of the ground-motion value at that point were selected and were subsequently applied to the extreme motion hazard deterministic scenarios in order to introduce spatial random variability.

For the Italian case study, a high activity model (SHARE Active) was selected and a low attenuation ground motion model was specified (ENA, 2012). The three hazard levels (i.e. the annual exceedance probability) were considered for the case study, each for a fractile of extreme ground-motion values at the reference site equal to 0.90. Three extreme motion hazard deterministic 'scenarios', or GM-fields, were therefore considered for the Italian case study. These GM-fields were linked to a reference site located at the centre of the hazard area, as shown in Figure 11. The reference site corresponded to the location of a 'critical network element' that was identified using the 'betweenness centrality' method, as described by Medda and Taalab (2016).

Figure 11: Sample GM field linked to reference site in selected study area

5.3.3 Cascading Landslide Hazard

Cascading hazard effects were also considered in terms of earthquake-triggered landslides. To characterise the susceptibility of the selected region to earthquake-triggered landslides, a rigid sliding block displacement approach was employed to estimate values of landslide yield acceleration (k_y) for the region. This approach was proposed by Newmark (1965) and Saygili and Rathje (2009), as outlined in INFRARISK Deliverable D3.1 (D'Ayala and Gehl, 2014). The yield acceleration (k_y) of the sliding block represents the horizontal acceleration that results in a factor of safety equal to 1.0 for the slope, at which sliding of the block initiates.

To calculate k_y values for the study area, slope values were derived from the digital elevation model (DEM) for the region (see Figure 12a). The resolution of the DEM was 10m x 10m and, therefore, k_y values were calculated according to a raster grid of the same resolution. The geotechnical parameters ϕ' (the internal friction angle of the soil), c' (the effective friction angle of the soil) and γ (unit weight of the soil) were derived based on geological information for the selected region (see Figure 12b), whereby four main geological classifications were identified, as outlined in Table 3. A failure surface thickness, t, equal to 2.4 m was assumed, as commonly adopted for shallow slope

failures (Jibson et al., 2000; Saygili and Rathje, 2009). For the saturation ratio, *m*, a value of 0.2 was assumed (i.e. 20% saturation of the failure surface depth), which was considered to be appropriate for the geographical location of the selected case study.

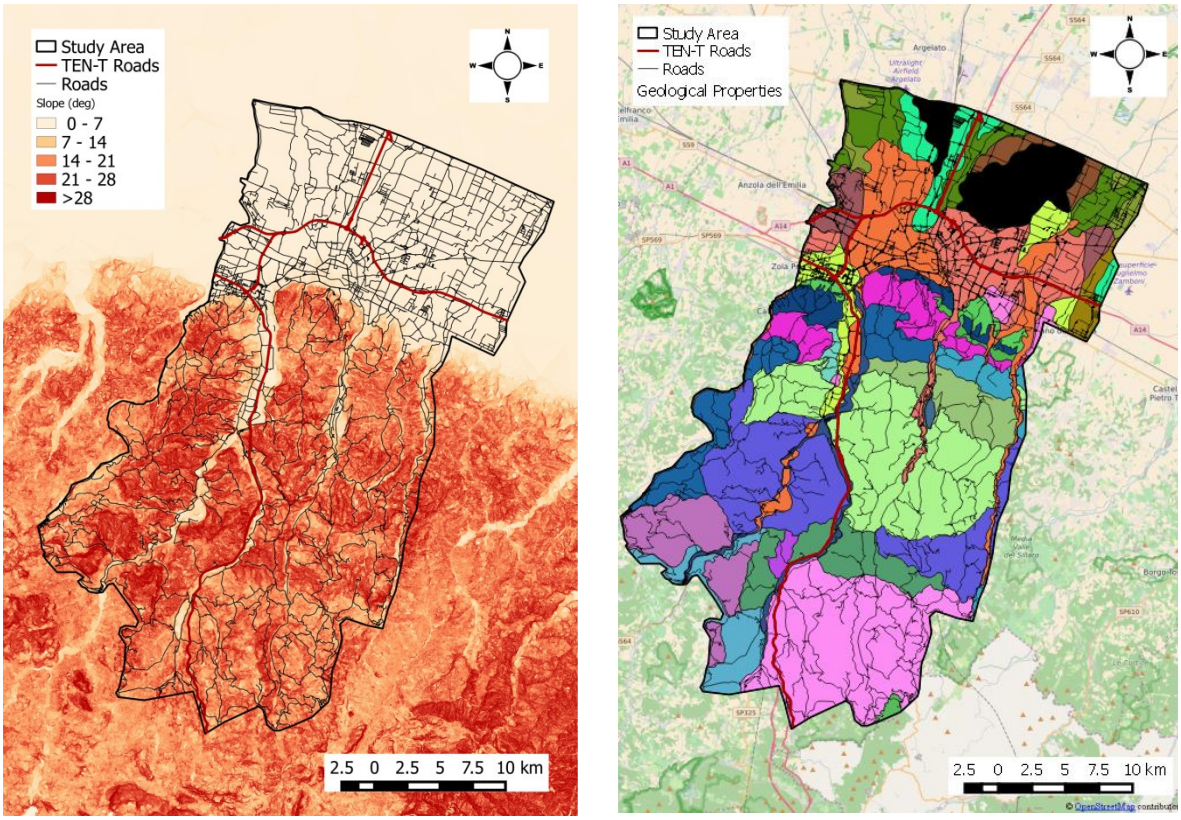

a) Slope b) Geology

Figure 12: Input data for landslide yield acceleration (k_y) calculation

Geological Classification	ϕ' (deg)	c' (kPa)	γ (kN/m^3)
Silts/Clays	28	5	18
Sands/Gravels	40	1	20
Rocks ('Soft')	45	10	23
Rocks ('Hard')	45	30	24

Table 3: Geotechnical properties for four main geological classifications in Italian case study region

The calculated values of k_y for the selected region are illustrated in Figure 13, whereby values in the northern part of the selected region (where the road network is most dense) are relatively uniform due to the fact that this area is relatively flat. The most onerous values of k_y occur in an area of specific geology (see Figure 12b), where values vary between 0 and 0.4*g*.

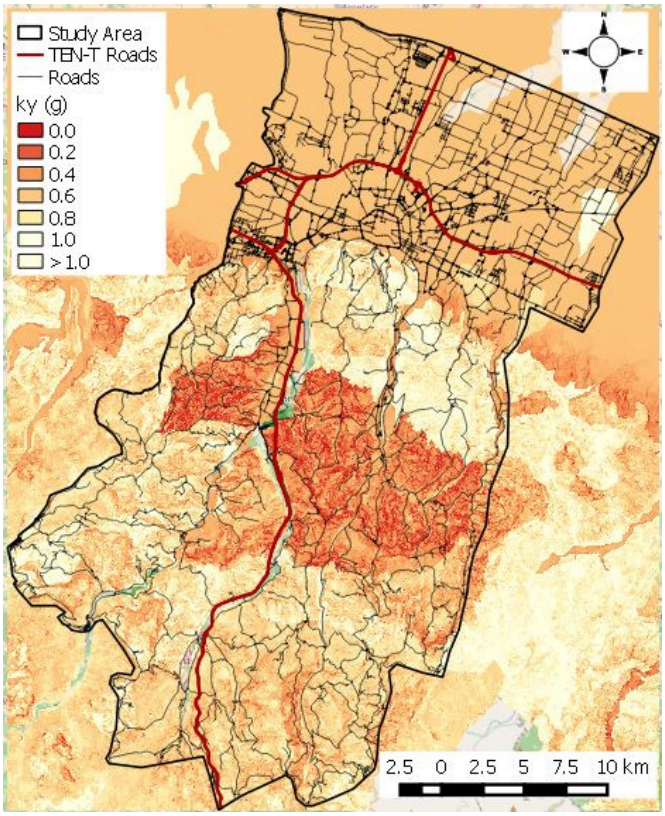

Figure 13: Landslide yield acceleration (k_y) values for selected region

5.3.4 Network Vulnerability

The susceptibility of the selected Italian road network to earthquake and earthquake-triggered landslides was assessed according to the vulnerability of the network bridges, tunnels and individual sections of road pavement, as outlined in Table 4. These were considered as 'infrastructure events', i.e. an event that is a change in infrastructure that may lead to a change in infrastructure use or a change in human behaviour, as described by Hackl et al. (2016).

Network Element	Hazard
Bridges	Earthquakes
Tunnels	Earthquakes
Road sections	Earthquake-triggered landslides

Table 4: Network elements and associated hazards for Italian case study

The bridges and tunnels located along the selected road network were identified using Open Street Maps and their location was subsequently verified using Google Street View. In total, 315 road bridges and 24 tunnels were identified along the selected road network. The location of the network bridges and tunnels is illustrated in Figure 14 and a list of these network elements is provided in Appendix A.

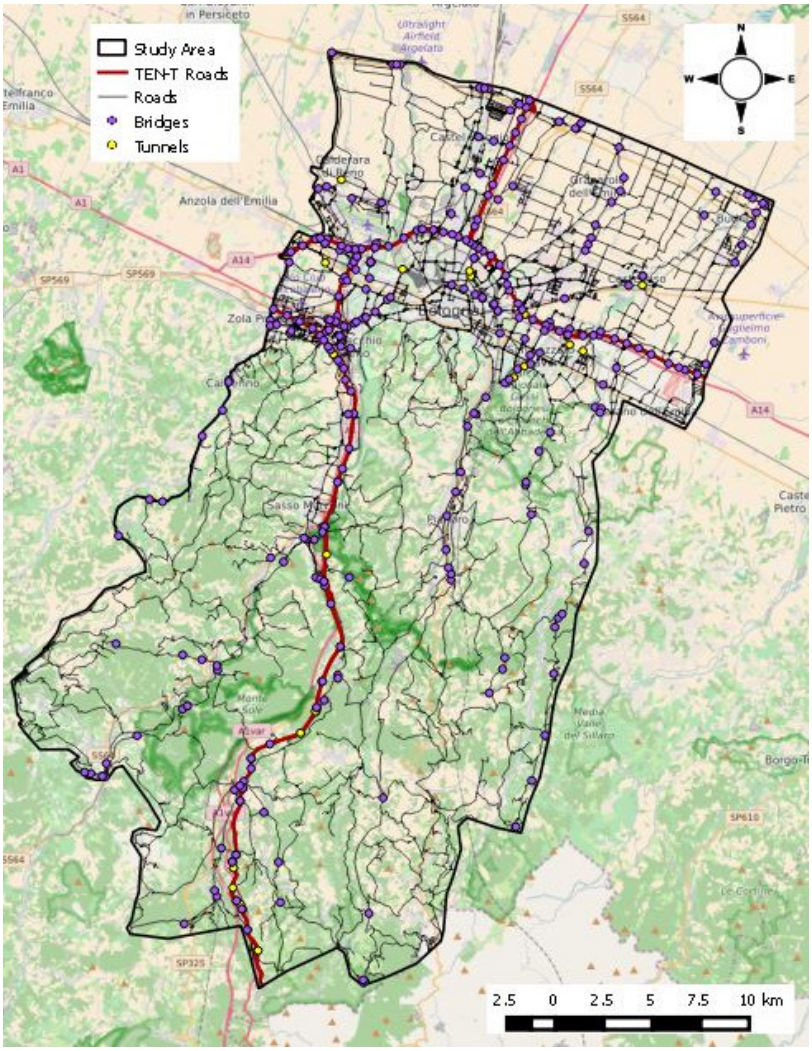

Figure 14: Location of bridges and tunnels along selected Italian road network

The geographic location of the road network for the selection region was also obtained using Open Street Maps and individual polylines to represent road segments were classified according to the road type (i.e. motorway, trunk, primary, tertiary, secondary, regional or unclassified) and the number of lanes in each direction.

To characterise the vulnerability of the network elements to the selected hazards specified in Table 4, fragility functions were assigned to individual network elements, as described in the following sections. Fragility functions provide the probability of exceedance for specified damage states as a function of the hazard intensity measure and are commonly employed as a probabilistic tool for the vulnerability assessment of a given structural system, as described by D'Ayala and Gehl (2015). They are commonly defined for a variety of damage states and their form is generally that of a cumulative lognormal distribution, according to lognormal distribution, according to Equation 1, where *ds* is a damage state threshold of interest for a particular structure, α and β are the median and dispersion values of the fragility function respectively, and ϕ is a standard normal cumulative distribution function.

$$P\left(DS \geq \frac{ds}{IM}\right) = \varphi\left(\frac{log\, IM - log\, \alpha}{\beta}\right) \quad \textbf{(1)}$$

5.3.4.1 Seismic vulnerability of bridges

Due to the large number of bridges (315) along the road network, the development of fragility functions for individual bridges was not feasible. As such, fragility functions were assigned to the bridges based on an existing database that was developed in the European SYNER-G project (Silva et al., 2014). This recently compiled database provides a taxonomy of parameters, as outlined in Table 5, that can be used to assign fragility functions from the database to existing bridges. Based on this taxonomy, structural data was gathered for the bridges along the selected road network according to a visual inspection of each individual structure using Google Street View. A list of these structural characteristics is presented in Appendix C of INFRARISK Deliverable 3.2 (D'Ayala and Gehl, 2015). In many cases, the structural taxonomy parameters were unknown due to the limitations of the visual inspection using Google Street View.

Parameter	Properties
Material (MM1)	Concrete (C) Masonry (M) Steel (S) Iron (I) Wood (W) Mixed (MX)
Material (MM2)	Reinforced concrete (RC) Pre-stressed reinforced concrete (PC) Unreinforced masonry (URM) Reinforced masonry (RM) High strength concrete (HSC) Average strength concrete (ASC) Low strength concrete (LSC) Fired brick (FB) Hollow clay tile (HC) Stone (S) Lime mortar (LM) Cement mortar (CM) Mud mortar (MM) Concrete masonry unit (CMU) Autoclaved aerated concrete (AAC) High % voids (H%) Low % voids (L%) Regular Cut (Rc) Rubble (Ru)
Type of Deck (TD1)	Girder bridge (Gb) Arch bridge (Ab) Suspension bridge (Sb) Cable-stayed bridge (Csb) Moveable bridge (Mb)
Type of Deck (TD2)	Solid slab (Ss) Slab with voids (Sv) Box girder (B) Modern arch bridge (MA) Ancient arch bridge (AA) Precasr brams with concrete topping (Pbc)
Deck Characteristics (DC)	*Width*
Deck Structural System (DSS)	Simply supported (Ssu) Continuous (Co)
Pier to Deck Connection (PDC)	Not isolated (monolithic) (Nis) Isolated (through bearings (Is) Combination (Com) Fixed bearings (Fb) Elastomeric bearings (Eb)
Pier to Deck Connection (PDC) (cont.)	Sliding bearings (Sb) Seismic isolation/dissipation devices (SeisD)
Type of pier to superstructure connection (TC1)	Single-column pier (ScP) Multi-column pier (McP)
Number of piers for column (NP)	*Number*
Type of section of the pier (TS1)	Cylindrical (Cy) Rectangular (R) Oblong (Ob) Wall-type (W)
Type of section of the pier (TS2)	Solid (So) Hollow (Ho)
Height of the pier (HP)	*Height*
Spans (Sp)	Single span (Ssp) Multi spans (Ms)
Span characteristics (SC)	Number of spans (Ns) Span length (SL)
Type of connection to the abutments (TCa)	Free (F) Monolithic (M) Isolated (through bearings, isolators) (Isl) Free transverse translation (Ftt) Constrained transverse translation (Ctt) Fixed bearings (Fb) Elastomeric bearings (Eb) Sliding bearings (Sb) Seismic isolation/dissipation devices (SeisD)
Skew (Sk)	*Angle*
Bridge Configuration (BC)	Regular or semi-regular (R) Irregular (IR)
Foundation Type (FT)	Shallow foundation (SF) Deep foundation (DF) Single pile (Sp) Multiple piles with pile cap (Mps)
Seismic Design Level (SDL)	No seismic design (design for gravity loads only) (NSD) Low-code (LC) Medium-code (MC) High-code (HC)

Table 5: Bridge taxonomy parameters (Hancilar and Taucer, 2013)

Based on the identified taxonomy parameters for each network bridge, fragility functions were subsequently assigned based on bridge typologies that were derived based on bridges that had common taxonomy parameters and using the SYNER-G database (Silva et al., 2014). In total, 45 bridge typologies were identified in the selected case study area, as outlined in Appendix A. The fragility functions were defined in terms of four damage states (DS) that are commonly defined in the literature: 1) slight damage, 2) moderate damage, 3) extensive damage, and 4) complete damage. Further information in relation to this procedure is described in INFRARISK Deliverable 3.2 (D'Ayala and Gehl, 2015).

Where multiple fragility functions were associated with a given bridge typology, two methods were employed to assign fragility functions: 1) a combined fragility model (Shinozuka et al., 2000), 2) the use of median fragility functions with their 16%-84% confidence bounds, as described by D'Ayala and Gehl (2015). Example fragility functions for bridge typology 1 are presented in Figure 15, where the selected Intensity Measure (IM) in this instance is Peak Ground Acceleration (PGA), which is expressed in terms of *g* (9.81m/s^2). The fragility functions for all 45 typologies are illustrated in Figure 16 and Figure 17 for the combined fragility function model and the median fragiltiy model with confidence bounds, respectively. The median and dispersion parameters for the fragility functions assigned to each bridge typology along the selected road network are presented in Appendix A.

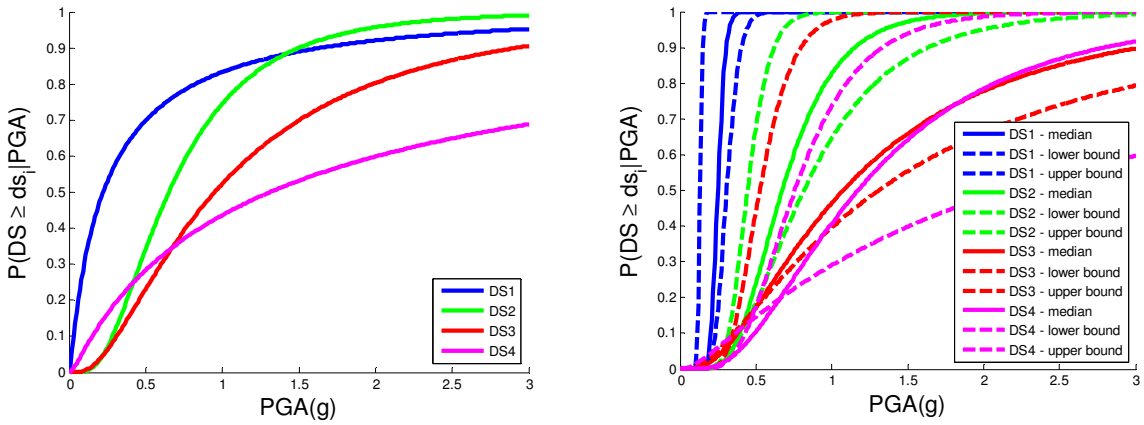

a) Combined fragility model

b) Median fragility model with 16%-84% confidence bounds

Figure 15: Fragility functions for bridge typology 1

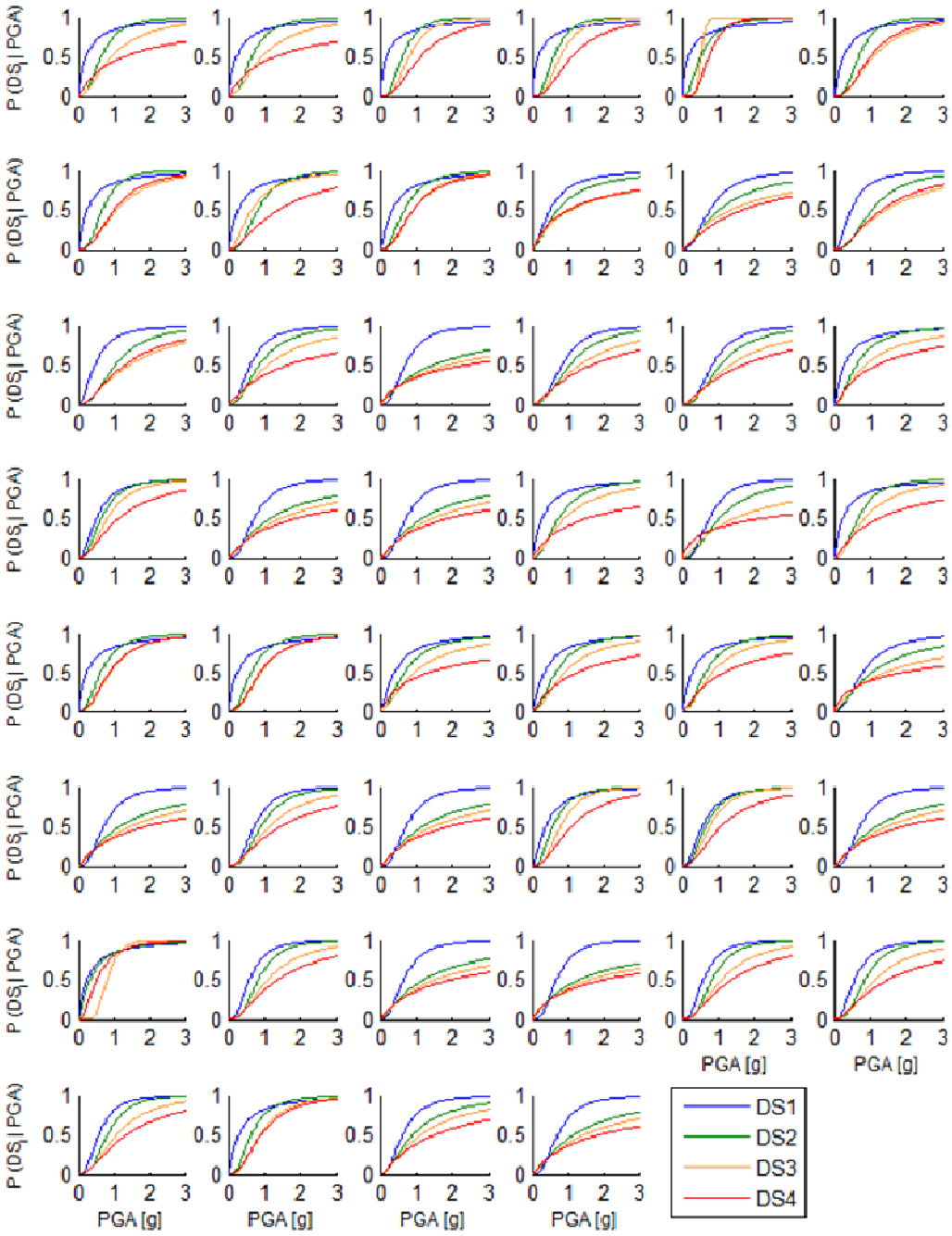

Figure 16: Combined fragility function model for the 45 bridge typologies

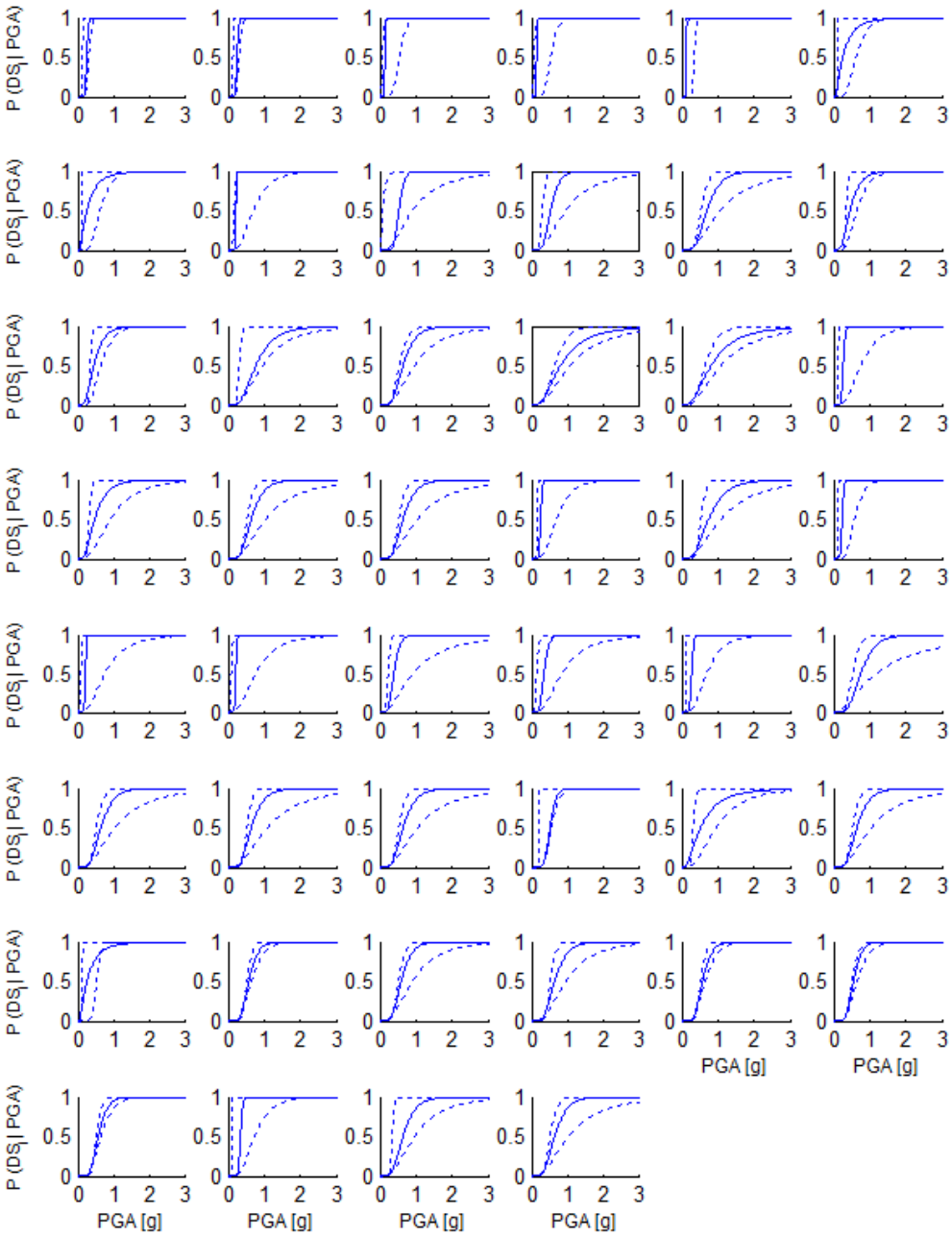

Figure 17: Median fragility function model with confidence bounds for the 45 bridge typologies
Note: Damage State 1 (Slight) shown only

5.3.4.2 Seismic vulnerability of tunnels

A similar approach was adopted for the network tunnels, whereby fragility functions were assigned to individual structures based on a taxonomy of parameters defined by Argyroudis and Kaynia (2014), as outlined in Table 6. Based on this taxonomy, structural data was gathered for the tunnels along the case study road network according to a visual inspection of each individual structure using Google Street View. Fragility functions were subsequently assigned to the tunnels based on typologies using the database of fragility functions for tunnels that was developed in the SYNER-G project (Silva et al., 2014). For the case study tunnels, 5 typologies were identied, as outlined in Appendix A. The fragility functions were defined in terms of four damage states (DS) that are

commonly defined in the literature: 1) slight damage, 2) moderate damage, 3) extensive damage, and 4) complete damage. Further information in relation to this procedure is described in INFRARISK Deliverable 3.2 (D'Ayala and Gehl, 2015).

Similar to bridges, two methods were employed to assign fragility functions based on the tunnel typology: 1) a combined fragility model (Shinozuka et al., 2000) and 2) the use of median fragility functions with their 16%-84% confidence bounds, as shown in Figure 18 for tunnel typology 1, where the selected Intensity Measure (IM) in this instance is Peak Ground Acceleration (PGA). The fragility functions for all 5 tunnel typologies are illustrated in Figure 19 and Figure 20 for the combined fragility function model and the median fragiltiy model with confidence bounds, respectively. The median and dispersion parameters for the fragility functions assigned to each tunnel typology along the case study road network are presented in Appendix A.

Parameter	Properties
Construction Method	Bored (B) Cut & Cover (CC) Immersed (I)
Shape	Circular (C) Rectangular (R) Horseshoe (H)
Depth	Surface (Su) Shallow (Sh) Deep (D)
Geological Conditions	Rock (EC8 soils class A) Alluvial (EC8 soil classes B and higher)
Supporting System	Concrete (C) Masonry (M) Steel (S)

Table 6: Tunnel taxonomy parameters (Argyroudis and Kaynia, 2014)

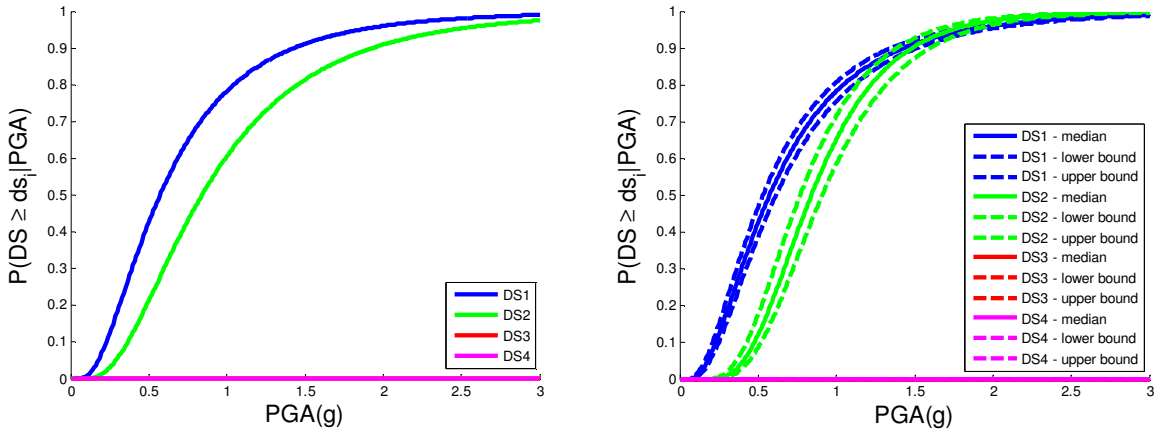

a) Combined fragility model

b) Median fragility model with 16%-84% confidence bounds

Figure 18: Fragility functions for tunnel typology 1

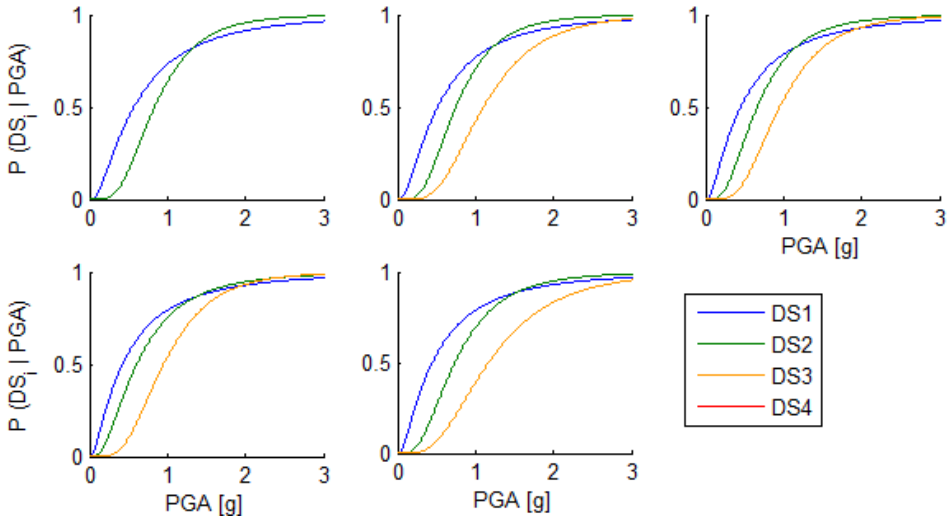

Figure 19: Combined fragility function model for the 5 tunnel typologies

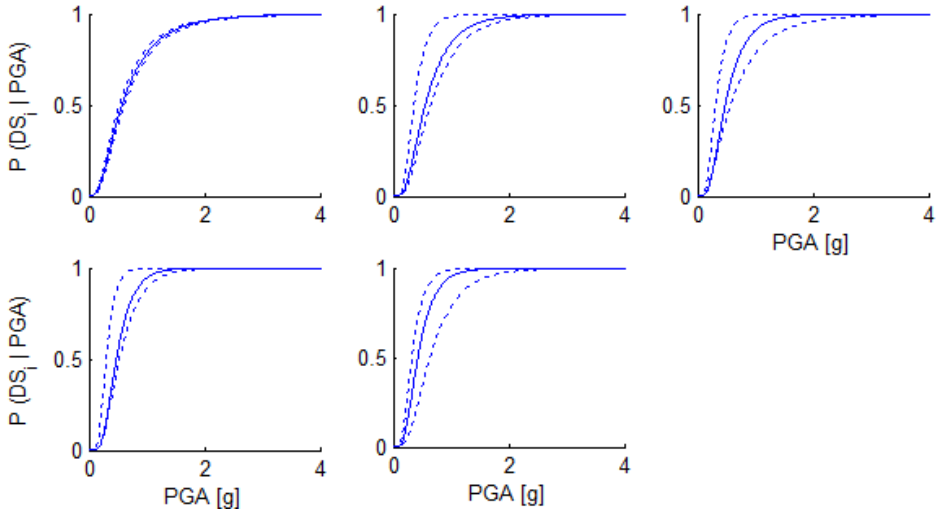

Figure 20: Median fragility function model with confidence bounds for the 5 tunnel typologies
Note: Damage State 1 (Slight) shown only

5.3.4.3 Vulnerability of road sections to earthquake-triggered landslides

Fragility functions were also assigned to individual road sections along the network to characterise the vulnerability due to earthquake-triggered landslides. To do so, a method developed in the European SAFELAND project was adopted (Pitilakis et al., 2011). This method employs the fragility functions that were previously developed by the National Institute of Building Sciences (2004) based on empirical data and expert judgement, but modifies them to account for local slope characteristics, in terms of landslide yield acceleration values (k_y), and to represent the functions in terms of Peak Ground Acceleration (PGA) values rather than Peak Ground Displacement (PGD). The fragility functions were defined for two road types; major and urban, and in terms of three damage states: 1) slight damage, 2) moderate damage, 3) extensive/complete damage. Desciptions of these damage states, as well as further information in relation to the method described by Pitilakis et al. (2011), can be found in INFRARISK Deliverable 3.2 (D'Ayala and Gehl, 2015).

To assign fragility functions to individual road sections, the case study road network was divided into 10 m segments since the Digital Elevation Model (DEM) for the case study region had a resolution of 10 m×10 m. Fragility functions were not assigned to road sections located adjacent to slopes of less than 10 degrees as the risk of landslide-induced damage for these sections was deemed to be negligible. For the remaining road segments, fragility functions were individually assigned based on the associated landslide yield acceleration (k_y) values and the road type. For road segments that consisted of three or more lanes in each direction, these were classified as 'major' roads. All other road sections were classifid as 'urban' roads. Example fragility functions for road sections adjacent to slopes are presented in Figure 21.

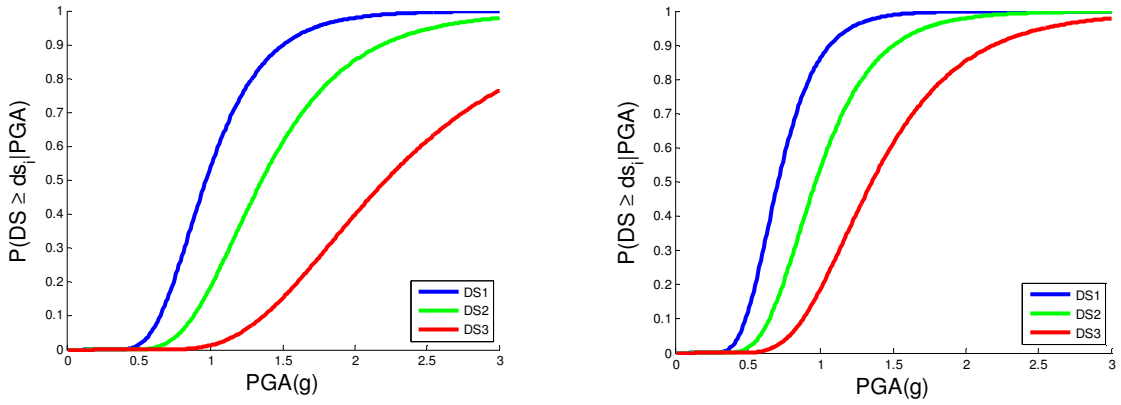

a) Major roads b) Urban roads

Figure 21: Example fragility functions for road sections located adjacent to slopes >10°

5.3.5 Functionality Loss

The vulnerability of the selected Italian road network to earthquake and earthquake-triggered landslides was also assessed according to potential functionality loss associated with physical network damage. This may be defined as a 'network use event' according to the methodology proposed by Hackl et al. (2016) since it considers events that may result in a change in how the infrastructure is used that may lead to a change in human behaviour.

The potential functionality loss of the network was defined according to the functionality loss associated with the individual damage states defined for the various network elements considered in the analysis (i.e. bridges, tunnels and road sections). Two functionality loss measures were adopted in the analysis that relate to the traffic modelling described in Section 5.3.6; speed reduction and lane capacity reduction. Additionally, loss measures in terms of repair cost and repair time were defined for each network element damage state, as outlined in Table 7. For bridges and tunnels, the values are given per individual structure. For roads, the values are defined per 10 m segment of roadway. Furthermore, the repair times assume that a single work crew is assigned to conduct the repairs. Further information in relation to functionality loss measures is described by D'Ayala and Gehl (2015).

	Speed Reduction (%)	Lane Capacity Reduction (%)	Repair Cost (Euro)	Repair Time (Days)
Bridges				
No Damage	0	0	0	0
Slight	20	20	100000	120
Moderate	25	50	750000	120
Extensive	100	100	1000000	150
Complete	100	100	1000000	150
Tunnels				
No Damage	0	0	0	0
Slight	75	75	150000	120
Moderate	100	100	1000000	120
Extensive	100	100	3000000	120
Complete	100	100	10000000	365
Road Sections				
No Damage	0	0	0	0
Slight	40	40	500	1
Moderate	60	60	1000	1
Extensive/Complete	100	100	3500	1

Table 7: Functional capacity loss measures

5.3.6 Travel Delays

The vulnerability of the selected road network was subsequently assessed according to the potential for passenger travel delays. This is defined as a 'societal event' according to the methodology proposed by Hackl et al. (2016) since it is an event that is associated with a change in human behaviour. To quantify the increase in travel times for road users, traffic modelling was conducted according to a traffic equilibrium model for various 'scenarios', which were characterised according to the physical damage of the network elements and the associated functionality loss for the corresponding section of roadway. The results of these traffic 'scenarios' were then compared to the results of a traffic analysis under normal operating conditions for the road network (i.e. no physical damage) to calculate the increase in travel times for road users.

The traffic modelling was performed according to Network Explorer for Traffic Analysis (NEXTA); an open-source software that acts as a graphical user interface for DTALite (Light-weight Dynamic Traffic Assignment Engine), which is a traffic assignment model (Zhou and Taylor, 2014). The model required input data in the form of Origin-Destination (O-D) passenger information and the analysis is based on the premise that all passengers seek to minimise their travel time. Further information is described in INFRARISK Deliverable 5.3 (Medda and Taalab, 2016).

5.3.6.1 Regional Traffic Analysis

The potential for traffic delays was initially assessed at regional level for the selected case study area outlined in Figure 9. To do so, the selected road network was imported into the NEXTA software as a series of nodes and links, as illustrated in Figure 22. Each node represented a road junction and each link represented an individual road segment, whereby information regarding the type of link, number of lanes, speed limit and lane capacity was included. In total, there were 18,097 links and

18,969 nodes. Further information regarding the importation of a road network into the NEXTA software can be found in Appendix A of INFRARISK Deliverable 5.3 (Medda and Taalab, 2016).

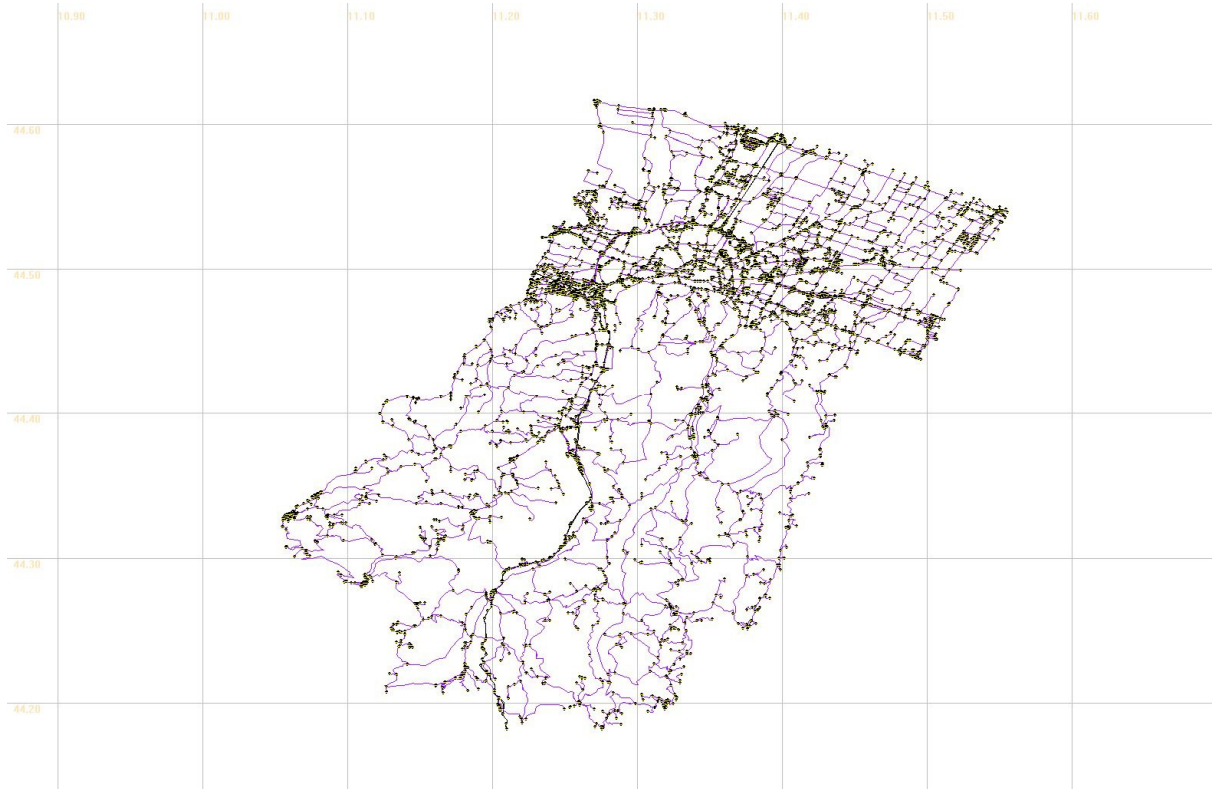

Figure 22: Links and nodes to represent selected case study regional road network

The traffic demand for the road network was characterised according to Origin-Destination (O-D) road passenger data for the province of Bologna. This data was gathered during the 2011 Italian general population census and provided information regarding the daily travel arrangements for residents within this region in terms of their usual place of work or study (http://www.istat.it/). The data was categorised according to the communes located in the province of Bologna. Within the selected case study region, 21 of these r communes are located within the selected case study region and were defined as O-D zones in the traffic model, as illustrated in Figure 23. The corresponding commune names are provided in Table 8.

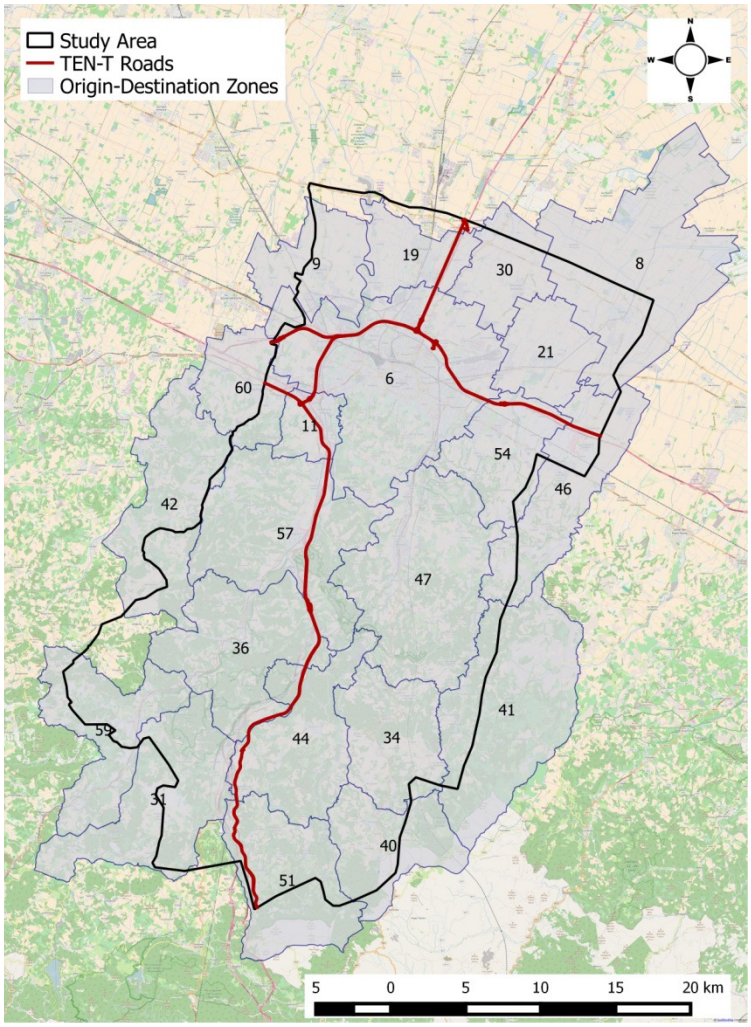

Figure 23: O-D zones for regional traffic analysis

For each O-D trip record, information regarding daily passenger movements in terms of origin zone, destination zone, mode of transport, departure time and journey duration was available. For the traffic analysis using NEXTA, daily trips that were conducted using private cars were considered. Since approximately 50% of the O-D data consisted of intra-zonal trips (i.e. trips for which the origin and destination zones were the same), which could not be considered in the analysis due to a limitation of the NEXTA software, the number of O-D trips according to private cars was doubled for the selected case study region in an effort to provide a realistic network traffic representation. This data was subsequently imported into NEXTA in the form of an O-D matrix, which is outlined in Appendix A.

In total, 80,700 passenger trips were simulated for the regional traffic analysis. For each trip, the node where the journey commenced within the origin zone and the node where the same journey was completed within the corresponding destination zone were randomly selected. Since the O-D records considered daily passenger trips with the timeframe of 07:15 to 09:15, the traffic analysis using NEXTA was performed for this time period.

O-D Zone ID	Italian Commune
6	Bologna
8	Budrio
9	Calderara di Reno
11	Casalecchio di Reno
19	Castel Maggiore
21	Castenaso
30	Granarolo dell'Emilia
31	Grizzana Morandi
34	Loiano
36	Marzabotto
40	Monghidoro
41	Monterenzio
42	Monte San Pietro
44	Monzuno
46	Ozzano dell'Emilia
47	Pianoro
51	San Benedetto Val di Sambro
54	San Lazzaro di Savena
57	Sasso Marconi
59	Vergato
60	Zola Predosa

Table 8: O-D zones for regional traffic analysis

Each link was classified according to the type of road that the segment represented, which was obtained from Open Street Maps. Notably, residential roads were not considered in the analysis since it was assumed that these roads would not impact the traffic movement between O-D zones and that their inclusion in the model would unnecessarily increase the overall model complexity. The road types corresponded to link types that were defined in the NEXTA software and an associated number of lanes, speed and lane capacity (i.e. the maximum service flow rate per lane), as outlined in Table 9.

Road Type	Link Type	No. of Lanes (per direction)	Speed (mph)	Lane Capacity (vehicles per hour)
Motorway	Freeway	3	80	1700
Trunk	Principal Arterial	3	30	1000
Primary	Highway	1	30	1000
Secondary	Major Arterial	1	20	1000
Tertiary	Minor Arterial	1	20	1000
Unclassified	Collector	1	20	1000

Table 9: Road characteristics defined in regional traffic analysis

The number of lanes specified for each road type was established based on the road network data that was obtained from Open Street Maps. Although data was also available from Open Street Maps for each road segment in terms of speed and lane capacity, an initial traffic analysis performed according to these values demonstrated that the NEXTA traffic analysis appeared to underestimate journey times for passengers (based on a comparison to journey times estimated using Google

Maps). It was assumed that the reason for this underestimation of journey times was due to the fact that signalised junctions were not considered in the traffic analysis and, therefore, the delays encountered by road users at signalised junctions were not factored into the analysis. Consequently, the values of speed and lane capacity were adjusted accordingly so that the journey durations corresponded to those estimated using Google maps, and the values outlined in Table 9 were ultimately adopted in the model.

To evaluate the potential travel disruption for passengers due to the seismic hazard scenarios considered in the analysis, a traffic analysis was performed for the various network scenarios in terms of the functionality loss (i.e. speed and lane capacity reduction) that corresponded to the various damage states of the network elements according to Table 7. For the network tunnels and bridges, the associated functionality loss was assigned to the link to which the network element corresponded based on the geographical location of the relevant bridge or tunnel. Similarly, the functionality loss for individual road sections was assigned to the link in the NEXTA traffic which was associated with the individual road section.

5.3.6.2 National Traffic Analysis

The potential for passenger travel delays was also assessed at national scale by performing a traffic analysis for the existing road network on the Italian mainland. In this way, the consequences of damage to the selected case study road network were analysed for an area consisting of approximately 300,000 km^2. For the traffic analysis at national scale, motorways, trunk roads and primary roads were considered as it was assumed that the omission of smaller roads such as secondary, tertiary and unclassified roads would not impact traffic movement at this scale.

The nodes and links to represent the national road network were imported into the NEXTA software, as shown in Figure 24. In total, the national road network consisted of 7,143 links and 2,468 nodes. Each node represented a road junction and each link represented an individual road segment, which was classified based on the road type according to the type of link, the number of lanes, the speed limit and the lane capacity, as outlined in Table 10. Similar to the regional traffic analysis, appropriate values of speed and lane capacity were established based on a calibration of the model using Google Maps.

Figure 24: Links and nodes to represent national road network

Road Type	Link Type	No. of Lanes (per direction)	Speed (mph)	Lane Capacity (vehicles per hour)
Motorway	Freeway	3	50	1000
Trunk	Principal Arterial	3	50	1000
Primary	Highway	1	50	1000

Table 10: Road characteristics defined in national traffic analysis

The traffic demand for the national road network was characterised according to Origin-Destination (O-D) road passenger data that was obtained from the European ETISPLUS project (ETISPLUS, 2012). This provided data in terms of origin and destination zones for passenger trips that are conducted for either business, private, vacation or commuting purposes. The O-D zones considered for this data correspond to the official NUTS3 zones for mainland Italy (Eurostat, 2015). In total, 90 O-D zones were considered for the national traffic analysis, as shown in Figure 25. The corresponding names for the O-D zones are provided in Table 11. In total, 870,601 passenger trips were simulated for the national traffic analysis, which was representative of traffic along the network for a single hour. This data was subsequently imported into NEXTA in the form of an O-D matrix.

To evaluate the potential travel disruption for passengers due to the seismic hazard scenarios considered in the analysis, a national traffic analysis was initially performed for an 'undamaged' network. The results of this analysis were subsequently compared to the results of traffic analyses performed for various network scenarios in terms of the functionality loss (i.e. speed and lane capacity reduction) for the links located in the selected study area, to compute the additional travel times for passengers due to the disruption of the network due to the seismic hazard scenarios.

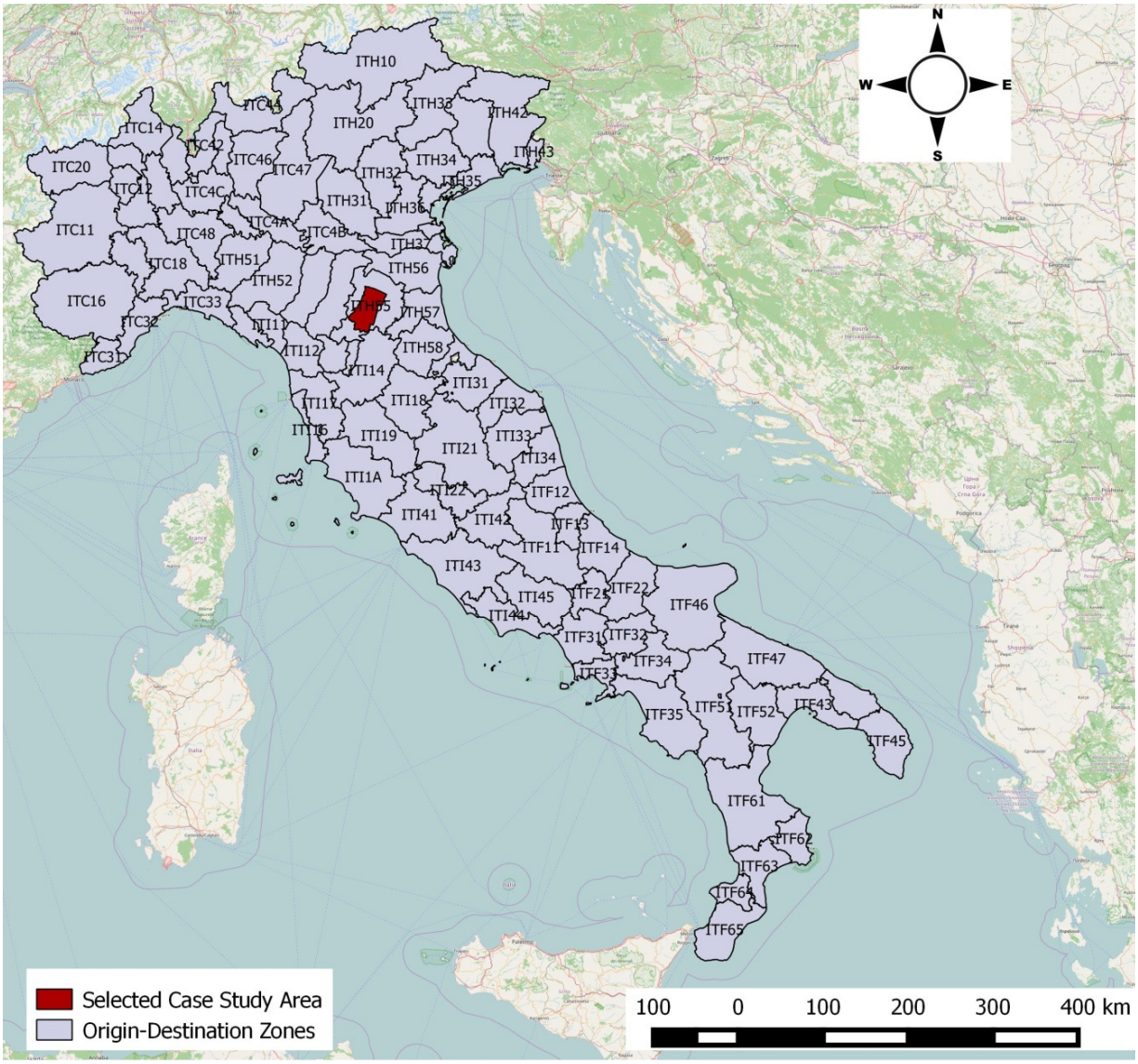

Figure 25: O-D zones for national traffic analysis

5.3.7 Economic Losses

The impact of the seismic hazard and the associated earthquake-triggered landslide cascading hazard were subsequently assessed in terms of the potential economic losses. To do so, the economic model developed by Medda and Wang (2016) was employed. This model considered O-D road passenger data in conjunction with Gross Domestic Product (GDP) data for the Italian NUTS3 regions (ETISPLUS, 2012) to establish the correlation between GDP and travel demand for Italy. Based on this regression analysis, Medda and Wang (2016) established Equation 2 to calculate the loss of GDP per capita (ΔGDP) for a specific O-D zone, *j*, where a is a constant equal to 0.0099 and ΔTr_{ij} is the change in travel demand for a passenger trip from O-D zone *i* to O-D zone *j*.

$$\Delta GDP_j = a \sum_i \Delta Tr_{ij} \quad \textbf{(2)}$$

O-D Zone ID	Italian NUTS3 region	O-D Zone ID	Italian NUTS3 region
ITC11	Torino	ITF64	Vibo Valentia
ITC12	Vercelli	ITF65	Reggio di Calabria
ITC13	Biella	ITH10	Balzano-Bozen
ITC14	Verbano-Cusio-Ossola	ITH20	Trento
ITC15	Novara	ITH31	Verona
ITC16	Cuneo	ITH32	Vicenza
ITC17	Asti	ITH33	Belluno
ITC18	Alessandria	ITH34	Treviso
ITC20	Valle d'Aosta/Vallée d'Aoste	ITH35	Venezia
ITC31	Imperia	ITH36	Padova
ITC32	Savona	ITH37	Rovigo
ITC33	Genova	ITH41	Podenone
ITC34	La Spezia	ITH42	Udine
ITC41	Varese	ITH43	Gorizia
ITC42	Corno	ITH44	Trieste
ITC43	Lecco	ITH51	Piacenza
ITC44	Sondio	ITH52	Parma
ITC46	Bergamo	ITH53	Reggio nell'Emilia
ITC47	Brescia	ITH54	Modena
ITC48	Pavia	ITH55	Bologna
ITC49	Lodi	ITH56	Ferra
ITC4A	Cremona	ITH57	Ravenna
ITC4B	Mantova	ITH58	Forli-Cesena
ITC4C	Milano	ITH59	Rimini
ITC4D	Monza e della Brianza	ITI11	Massa-Carrara
ITF11	L'Aquila	ITI12	Lucca
ITF12	Teramo	ITI13	Pistoia
ITF13	Pescara	ITI14	Firenze
ITF14	Chieti	ITI15	Prato
ITF21	Isernia	ITI16	Livorno
ITF22	Campobasso	ITI17	Pisa
ITF31	Caserta	ITI18	Arezzo
ITF32	Benevento	ITI19	Siena
ITF33	Napoli	ITI1A	Grosseto
ITF34	Avellino	ITI21	Perugia
ITF35	Salerno	ITI22	Terni
ITF43	Taranto	ITI31	Pesaro e Urbino
ITF44	Brindisi	ITI32	Ancona
ITF45	Lecce	ITI33	Macerata
ITF46	Foggia	ITI34	Ascoli Piceno
ITF47	Bari	ITI35	Fermo
ITF48	Barletta-Andria-Trani	ITI41	Viterbo
ITF51	Potenza	ITI42	Rieti
ITF52	Matera	ITI43	Roma
ITF61	Cosenza	ITI44	Latina
ITF62	Crotone	ITI45	Frosinone
ITF63	Catanzaro		

Table 11: O-D zones for national traffic analysis

The travel demand was assumed to have a linear elastic relationship with the change in travel time in the analysis and, therefore, Equation 2 was employed to determine the loss of GDP per capita for each O-D zone, where ΔTr_{ij} was equal to the cumulative change in travel time for that zone. Further information in relation to the economic loss modelling can be found in INFRARISK Deliverable 6.5 (Medda and Wang, 2016).

5.4 Risk Estimation

This section will describe the application of the 'Estimate risk' task in risk assessment process described by Hackl et al. (2016) to perform stress tests for the Italian case study. The methodologies and tools, as well as the format of the data employed at each stage of the analysis will be described. The stress tests performed considered low-probability, high consequence earthquake scenarios and their triggering effects in terms of landslide hazards for the selected case study area. The objective of the stress tests was to determine the associated risk and to ensure an acceptable level of risk. The risk to the network was considered in terms of the event probability and the associated direct and indirect consequences.

5.4.1 Methodology

Stress tests were performed for the selected Italian road network for a variety of low probability, high consequence seismic hazard scenarios based on the seismic hazard model described by Jiménez and García-Fernández (2016). These corresponded to a high activity seismicity model, a low attenuation ground motion model, and a fractile of extreme ground-motion values at the reference site equal to 0.90. For this combination of parameters, three hazard levels were considered: 10,000, 5,000 and 2,500 year return periods. These three extreme motion hazard deterministic 'scenarios', or GM-fields, were linked to a reference site that corresponded to a 'critical network element' that was identified using the 'betweenness centrality' method described by Medda and Taalab (2016). Four bridges were identified according to the betweenness centrality method, which comprise two adjacently located pairs of motorways bridges. These two locations are henceforth referred to as 'Critical Location 1' and 'Critical Location 2', as illustrated in Figure 26.

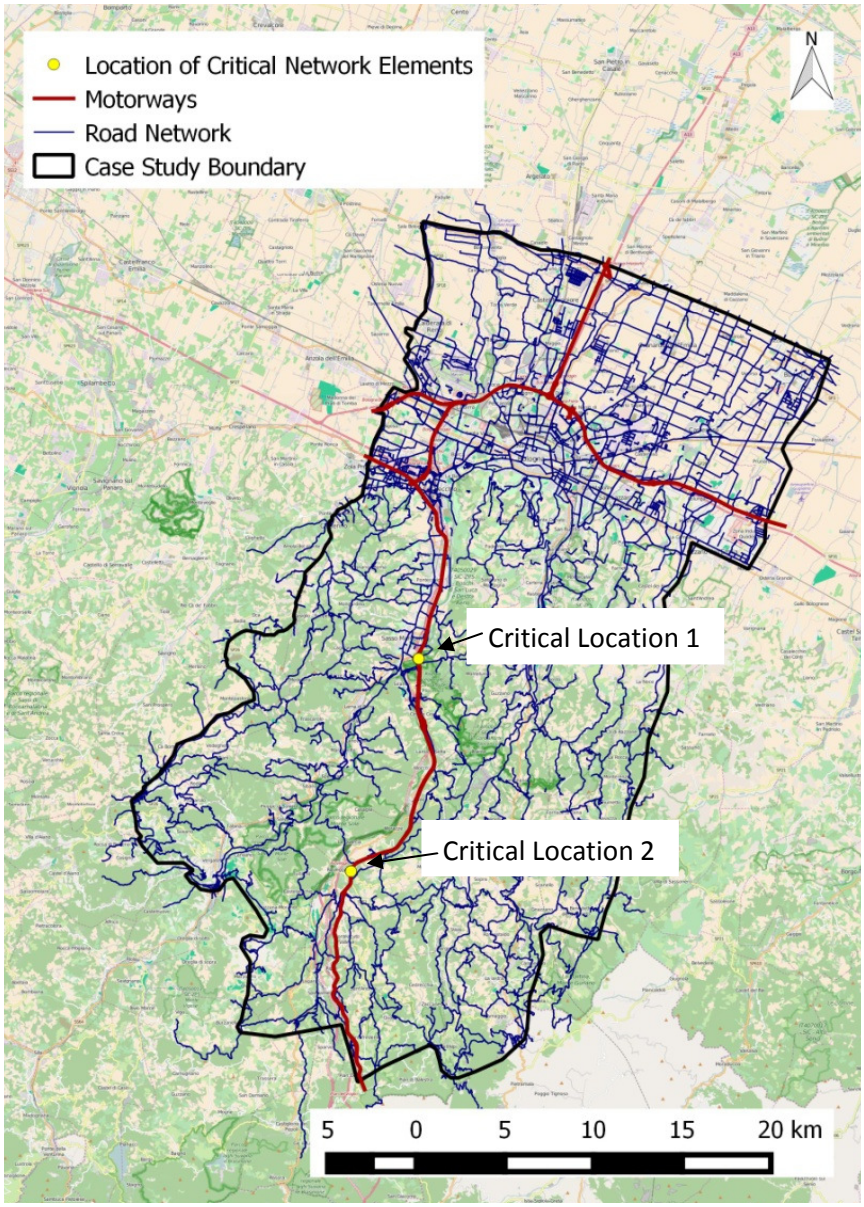

Figure 26: Location of critical network elements

The GM-fields developed by Jiménez and García-Fernández (2016) were subsequently linked to these critical locations, as shown in Figure 27 and Figure 28 for critical locations 1 and 2 respectively. To do so, the 100 km by 200 km GM-fields were geographically referenced based on the centre point of the hazard area, which was specified so as to correspond to the critical network element location. Each GM-field provided values of Peak Ground Acceleration (PGA) in table format at 1 km spacings. Therefore, the upper left-hand corner of each GM-field was geographically referenced at site coordinates 50 km West and 100 km North of the critical element location.

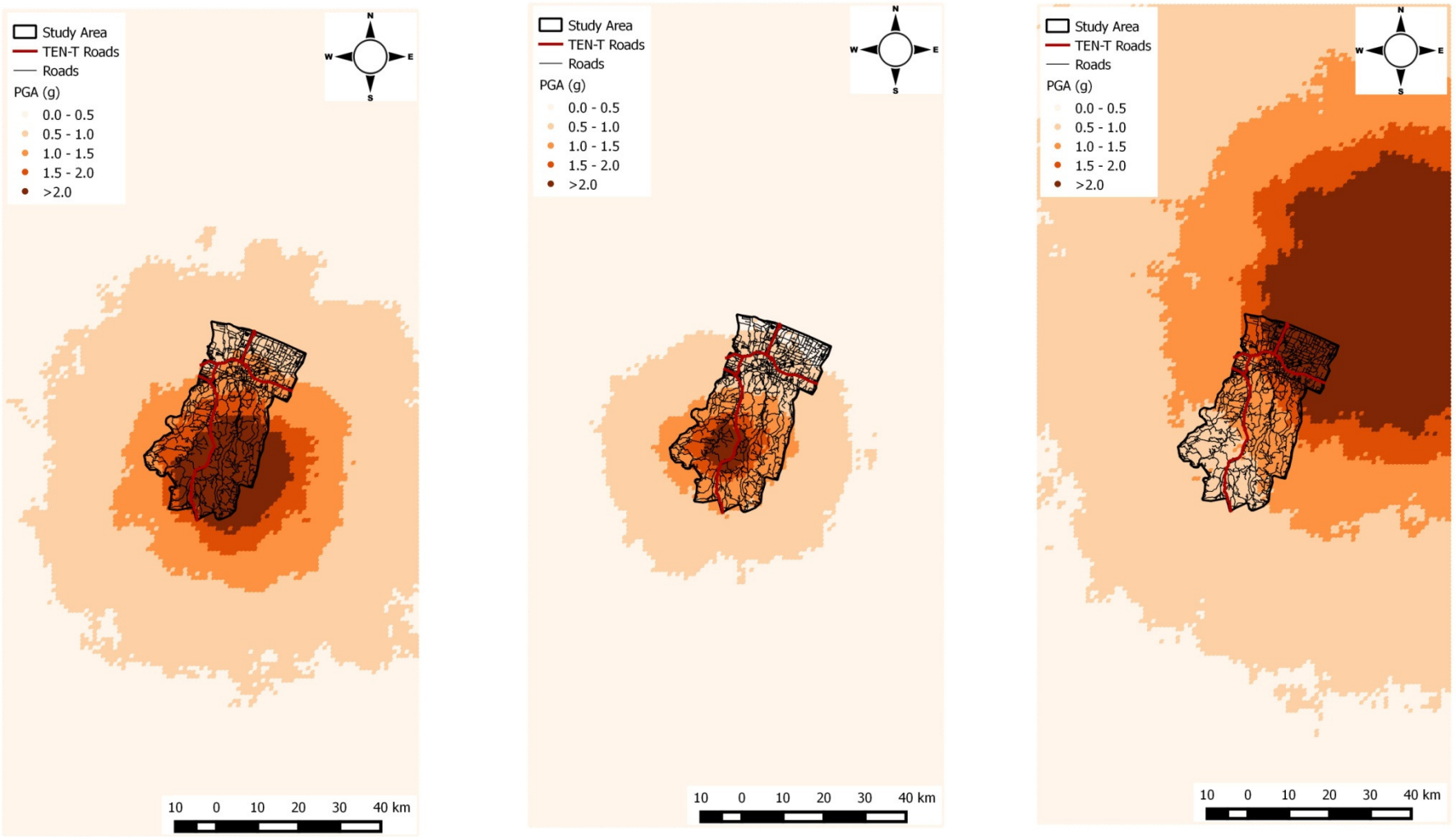

a) 10,000 year return period

b) 5,000 year return period

c) 2,500 year return period

Figure 27: GM field linked to critical location 1 (High activity seismicity model, low attenuation ground motion model, fractile = 0.90) (Note: This is 1 of 18 random fields applied)

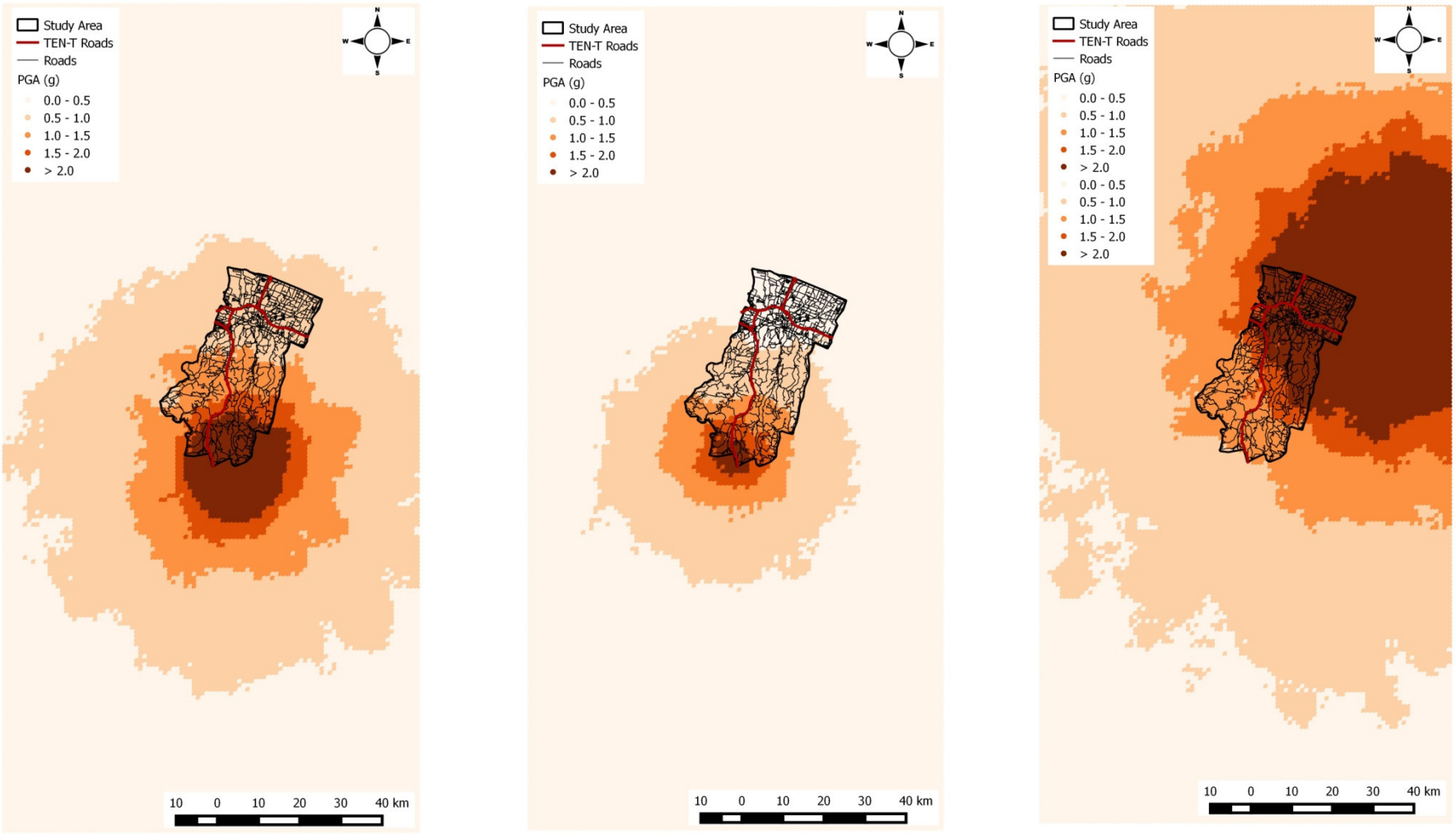

a) 10,000 year return period b) 5,000 year return period c) 2,500 year return period

Figure 28: GM field linked to critical location 2 (High activity seismicity model, low attenuation ground motion model, fractile = 0.90) (Note: This is 1 of 18 random fields applied)

The direct consequences to the road network were evaluated in terms of the physical damage due to the seismic hazard scenarios considered. There was uncertainty associated with the physical vulnerability of the individual network elements (bridges, tunnels and road sections) that was characterised according to the assigned fragility functions. Additionally, there was uncertainty associated with the seismic ground motion values at the location of each network element due to the 18 random fields that were applied to the GM-fields to account for spatial random variability. Therefore, a Monte Carlo simulation (MCS) method was employed as a sampling methodology to propagate these uncertainties within the analysis. Further information in relation to uncertainty quantification and MCS can be found in INFRARISK Deliverable 3.3 (D'Ayala and Gehl, 2015) and INFRARISK Deliverable 3.4 (D'Ayala and Gehl, 2015).

5.4.2 Software and Hardware

To perform stress tests for the selected Italian road network, the data that related to the various aspects of the risk assessment methodology, as described in Section 5.3, was stored in a Geographical Information System (GIS) platform. For the case study region, all data was geographical referenced using the 32N Universal Transverse Mercator (UTM) coordinate reference system, as appropriate for northern Italy. The MCS sampling was performed using Matlab software (MATLAB, 2013), whereby the relevant data was exported from GIS and was subsequently imported into Matlab. Furthermore, data processing in relation to the preparation of the necessary inputs for the NEXTA traffic analysis software, as well as post processing of the analysis results, was conducted using Matlab software.

The computation of the stress tests was performed using a 12 Core 3.50 GHz Intel Xeon desktop computer with 16,292 MB of memory, running on a 64bit operating system. For each stress test, the computational time required to perform approximately 100 MCS loops for the entire simulation workflow described in Section 5.4.3 was approximately 2 days.

5.4.3 Simulation Workflow

The various steps involved in performing the stress tests for the Italian case study, as well as their interactions, are illustrated for a portion of the case study road network in Figure 29. MCS sampling was performed to evaluate the potential losses due to the physical damage of the network bridges and tunnels to seismic ground motions and the physical damage for road sections due to earthquake-triggered landslides (see Figure 29a). To do so, the fragility function parameters that had been assigned to individual network elements were exported from the GIS platform in .csv file format and subsequently imported into Matlab. For each network element the following parameters were imported: the geographical coordinates of the structure, an identification number, the typology (for bridges and tunnels) and the associated fragility parameters (mean and dispersion values for each damage state considered). Additionally, the geographically referenced GM-field data was imported into Matlab.

For each simulation loop, one of the 18 random fields was applied to the GM-field under consideration and the PGA values associated with each network element (i.e. bridges, tunnels and road sections) were determined based on their geographical location. For each network element, the probability of reaching or exceeding the defined damage states based on the assigned fragility functions was subsequently determined based on the associated PGA value. For the use of median

fragility functions with their 16%-84% confidence bounds for the network bridges and tunnels, all three fragility functions (i.e. median, upper and lower confidence bounds) were sampled. To do so, a weighting of 0.452 was applied to the median fragility function, and weightings of 0.274 were applied to the upper and lower confidence bound fragility functions. These weightings were related to the probability densitities that corresponded to the 16^{th}, 50^{th} and 84^{th} percentiles.

Random damage sampling was subsequently performed by selecting a number falling between 0 and 1 at random. This number was then used to assign a unique damage state for the network element by identifying the most onerous damage state probability that was greater than the random number. This random sampling was repeated for all network elements to obtain the physical damage state of the entire road network, and this comprised a single MCS simulation loop (see Figure 29b).

Based on the assigned damage states for individual network elements, the associated repair costs and repair durations were assigned based on Table 7. Additionally, the associated functionality loss for each network element was assigned in terms of speed and lane capacity reduction, as outlined in Table 7. For each network link, as represented in the NEXTA traffic analysis software, the most critical functionality loss was adopted where two or more network elements were located along a particular link. The output of each MCS loop in terms of functionality loss for the overall network was subsequently imported into the NEXTA software to perform the traffic analysis; both at regional and national scales (see Figure 29c). To do so, the work zone scenario input file was used in NEXTA to define the location and characteristics of the functionality loss (see Taylor, 2013). To carry out multiple traffic analysis scenarios according to the ouput of the MCS sampling, the analyses were performed in a batch run. Further information in relation to running a NEXTA traffic analysis can be found in Appendix A of INFRARISK Deliverable 5.3 (Medda and Taalab, 2016).

To determine whether the number of MCS loops performed was sufficient, i.e. whether a stable estimation of the probabilistic distribution of the outcome had been constructed, the solution outputs were assessed in terms of their convergence, as described in Section 5.5.1.

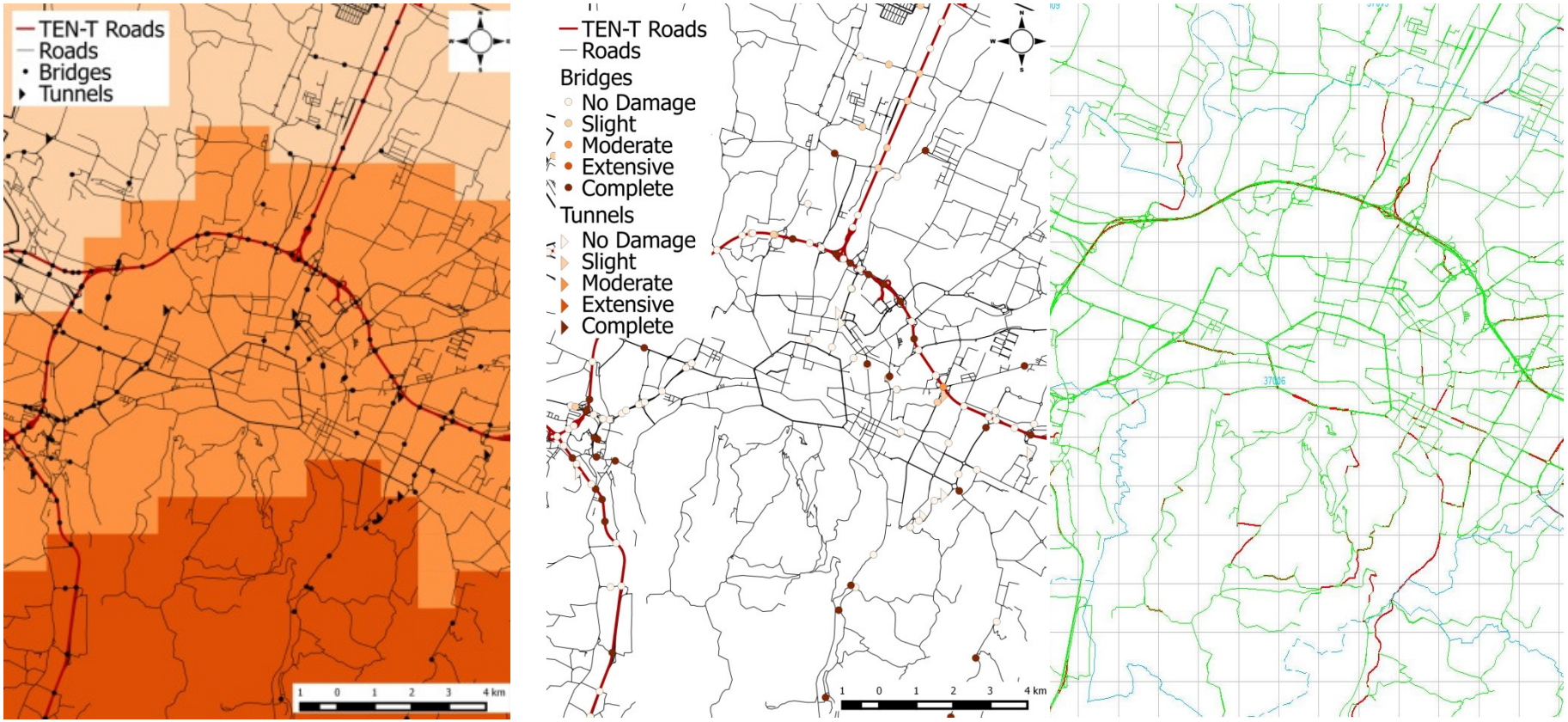

a) Seismic ground motions – PGA (*g*) b) Physical network damage c) Traffic disruption

Figure 29: Simulation workflow for single MCS simulation loop

5.5 Stress Test Results

In this section, the results of the various stress tests performed for the Italian case study road network are presented.

5.5.1 Solution Convergence

The outputs of the MCS sampling analysis were initially assessed to determine the number of simulation loops required to provide a stable probabilistic distribution of the solution output. To do so, a stress test that was performed for a GM-field that corresponded to a 10,000 year return period and that was linked to critical location 1 (see Figure 27a) and the percentage change in the coefficient of variation (COV) of the solution output was analysed as a function of the number of MCS loops performed. The solution output was considered stable for a convergence value of less than 1%.

Initially, the convergence of the total repair cost for the network was assessed. This was calculated for each MCS loop based on the summation of repair costs for the individual network elements (i.e. bridges, tunnels and road sections) and the convergence of the solution was subsequently calculated, as illustrated in Figure 30. Based on the total repair cost for the network, the solution converged to less than 1% after approximately 100 simulation loops. Since deterministic values were also adopted for the restoration duration values associated with the individual network elements, the results of the MCS sampling in terms of total (cumulative) repair duration for the network were identical to Figure 30.

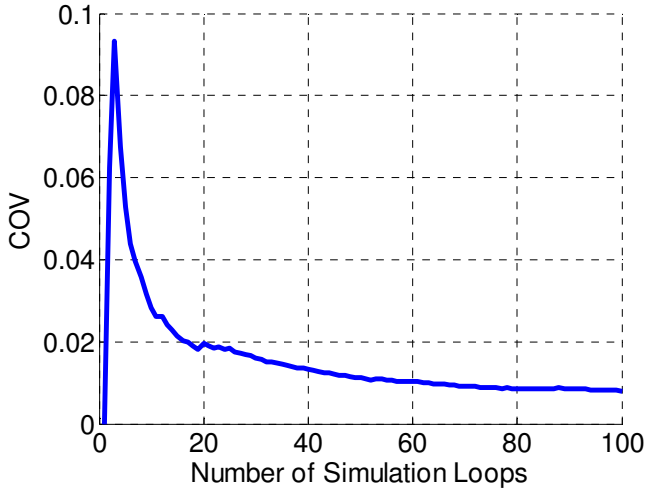

Figure 30: Convergence of MCS analysed in terms of total network repair cost

The convergence of the output of the traffic analysis was also assessed for each MCS loop according to the percentage increase in average journey time for the network. The solution output for the regional traffic analysis converged to less than 1% after approximately 100 MCS loops, as shown in Figure 31**a**. Furthermore, the solution output for the national traffic analysis in terms of the percentage increase in average journey time converged to less than 1% very rapidly (see Figure 31b).

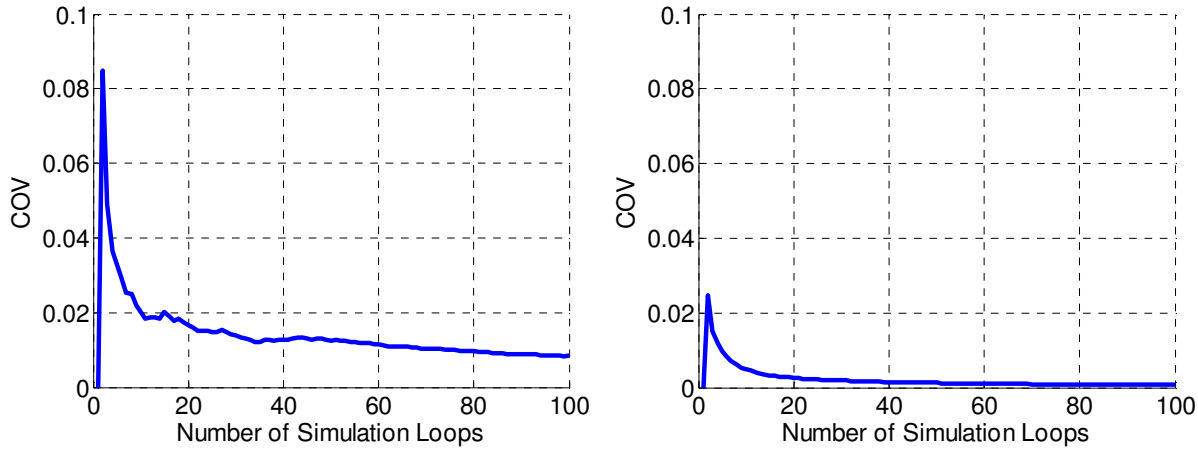

a) Regional traffic analysis b) National traffic analysis

Figure 31: Convergence of MCS analysed in terms of % increase in average journey time

5.5.2 Impact of Selected Fragility Functions

To evaluate the impact of the selected fragility functions for the bridges and tunnels along the case study road network, a comparison was made between the two methods employed to assign fragility functions to the network bridges and tunnels, as described in Section 5.3.4: 1) a combined fragility model and 2) the use of median fragility functions with their 16%-84% confidence bounds (CB). This comparison was conducted for the estimated consequences of the stress test that corresponded to a 10,000 year return period for the GM-field that was linked to critical location 1 (see Figure 27a).

A comparison of the Cumulative Distribution Functions (CDFs) for the results of the analyses in terms of the total repair cost for the network is illustrated in Figure 32. It is clearly shown that the distribution of network repair costs is greater where the median fragility functions with upper and lower bounds were assigned to the network bridges and tunnels than where the combined fragility functions were assigned. The difference is quite significant; the 50% probability value of network repair cost for the model where the median fragility functions with upper and lower confidence bounds were employed is appoximately €90 million greater than the 50% probability value for the model where combined fragility functions were employed. Furthermore, the distribution of values is greater for the model where median fragility functions with upper and lower confidence bounds were employed than for the model where combined fragility functions were employed. The CDFs clearly reflect the fact that the combined fragility function model resulted in fragility functions that had a significant dispersion (i.e. a flat slope).

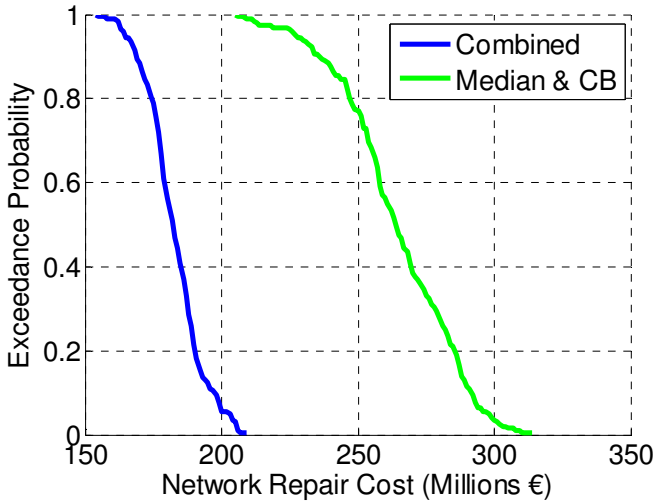

Figure 32: Comparison of CDF for total network repair cost for combined fragility functions and median fragility functions with upper and lower bounds (for network bridges and tunnels)

Additionally, the choice of fragility function model for the network bridges and tunnels impacted the results of the regional traffic analysis in terms of the percentage increase in average journey time, as shown in Figure 33a. However, the difference was not significant. For the results of the national traffic analysis, the choice of fragility function model did not impact the results in terms of the percentage increase in average journey time (see Figure 33b).

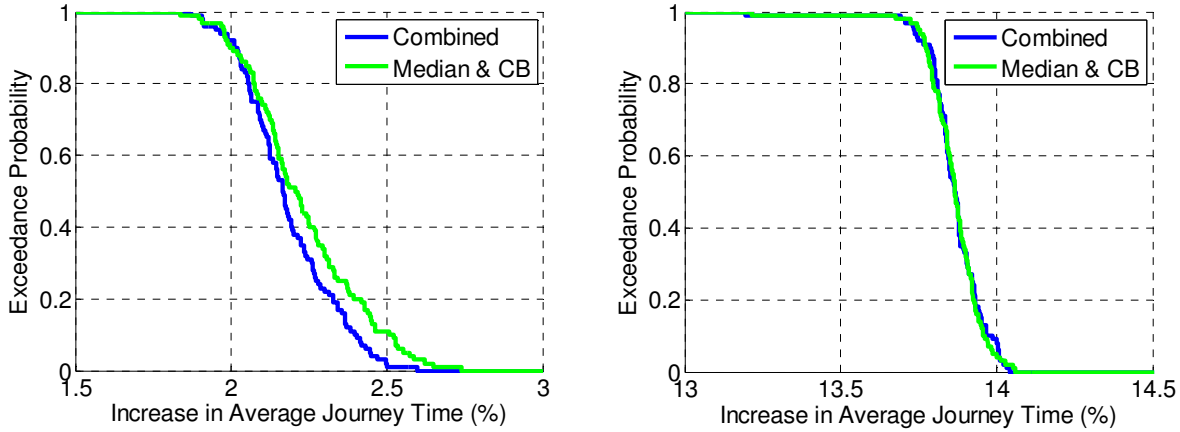

a) Regional traffic analysis

b) National traffic analysis

Figure 33: Comparison of CDF for percentage increase in average travel time for combined fragility functions and median fragility functions with upper and lower bounds (for network bridges and tunnels)

The choice of the median fragility functions with their 16%-84% confidence bounds generated more conservative results than the combined fragility model. Furthermore, the use of median fragility functions with confidence bounds allows for a clear decomposition of the total standard deviation into the two uncertainty sources; the slope of each curve represents the inherent dispersion due to

the fragility derivation procedure (e.g. record-to-record variability, bridge modelling uncertainties), while the gap between the confidence bounds is an expression of the variability between the different fragility models from the literature (i.e. model-related uncertainties). Consequently, the use of median fragility functions with confidence bounds was adopted for the network bridges and tunnels for the stress tests performed for the Italian case study road network.

5.5.3 Direct Consequences

The consequences of the seismic hazard scenario and the associated cascading landslide effects were analysed in terms of the total cost of network repairs due to the low probability, high consequence events considered. These consequences were deemed to be directly attributable to the road infrastructure owner or manager, i.e. direct consequences. Figure 34a illustrates the CDF of the total network repair costs for the GM-fields linked to critical location 1 (see Figure 26) for the various return periods considered. The results for the 5000 and 2500 year return periods are similar; the total cost of repairs for the network were estimated to be at least €200 million and the 50% probability value was approximately €265 million. The total network repair costs for the 2500 year return period seismic hazard event were significantly greater; the minimum cost was €300 million and the 50% probability value was approximately €365 million.

For the GM-fields linked to critical location 2, the results for the 2500 year return period are also most critical (see Figure 34b); the total network repair costs are estimated to exceed €375 million, while the 50% probability value is approximately €430 million. Overall the potential consequences in terms of the total cost of network repairs are more onerous for critical location 2 than critical location 1.

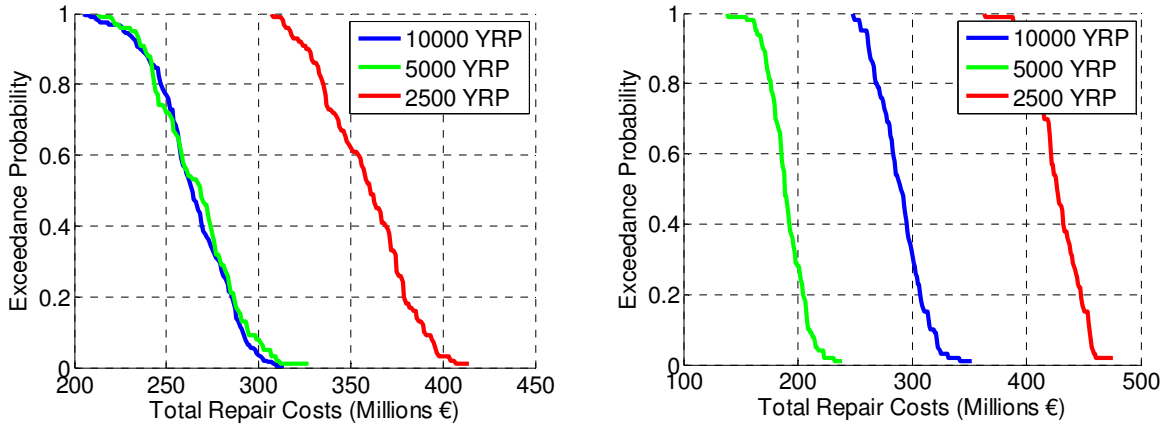

a) GM field linked to critical location 1 b) GM field linked to critical location 2

Figure 34: Total network repair costs

The breakdown of repair costs according to the network element type (i.e. bridges, tunnels and road sections) considered in the analysis is presented in Figure 35. For all stress tests conducted, the consequences in terms of network repair costs due to damage induced in road pavements due to earthquake-triggered landslides is relatively low compared to the repair costs associated with network bridges and tunnels. The repair costs associated with the network bridges is greatest for the

stress test scenarios that correspond to a 2,500 year return period (see Figure 35c and Figure 35f) as this seismic scenario relates to an event where the earthquake epicentre is situated to the north of the selected study area (see Figure 27 and Figure 28), where a large number of bridges are located in the vicinity of Bologna city centre (see Figure 14).

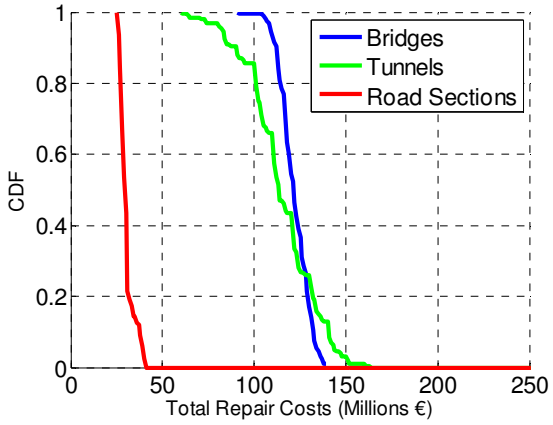

a) GM field linked to critical location 1 – 10,000 year return period

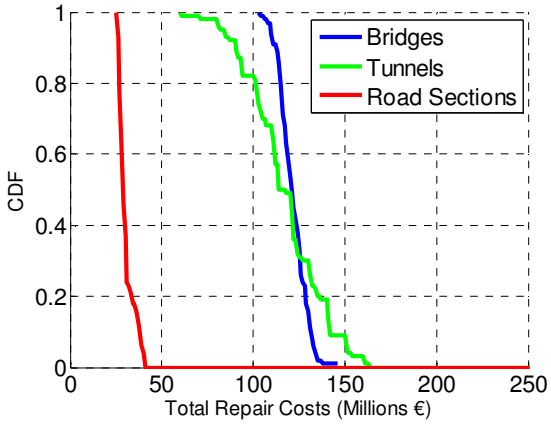

b) GM field linked to critical location 1 – 5,000 year return period

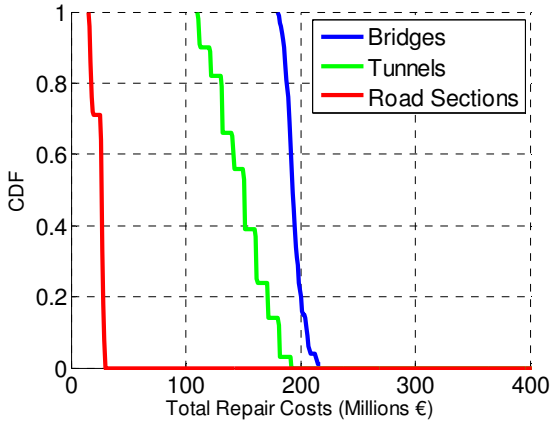

c) GM field linked to critical location 1 – 2,500 year return period

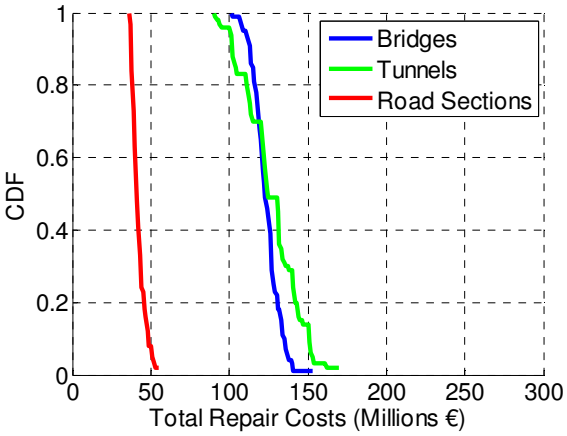

d) GM field linked to critical location 2 – 10,000 year return period

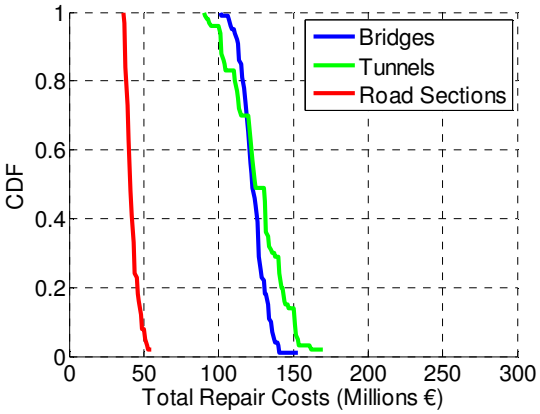

e) GM field linked to critical location 2 – 5,000 year return period

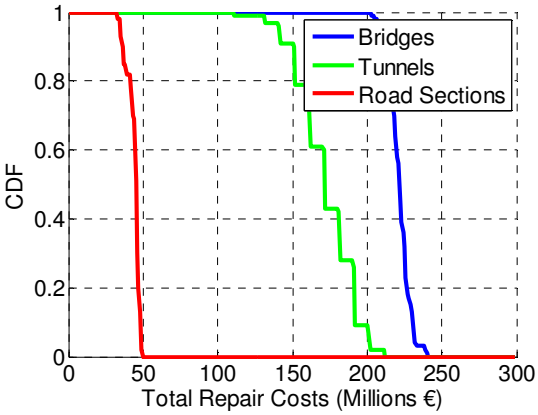

f) GM field linked to critical location 2 – 2,500 year return period

Figure 35: Network repair costs

The total cumulative network repair time was also calculated for each of the stress tests performed. The network repair time was classified as a direct consequence of the hazard scenarios since this parameter is considered to be of direct concern to the infrastructure manager. However, the repair time is also related to the indirect consequences since this will influence the duration of the restoration period and, consequently, the length of time for which road passengers will experience travel delays.

Figure 36 illustrates the results of the stress tests performed. The total cumulative network repair time was greatest for the seismic hazard scenario that was linked to critical location 1 and corresponded to a 2500 year return period, which corresponded to a 50% probability value of 118 years. The duration of the actual restoration period for the network will depend of course on the number of work crews available and the sequence in which network elements are restored. Further information in relation to restoration interventions can be found in INFRARISK Deliverable 4.2 (Hackl et al., 2016).

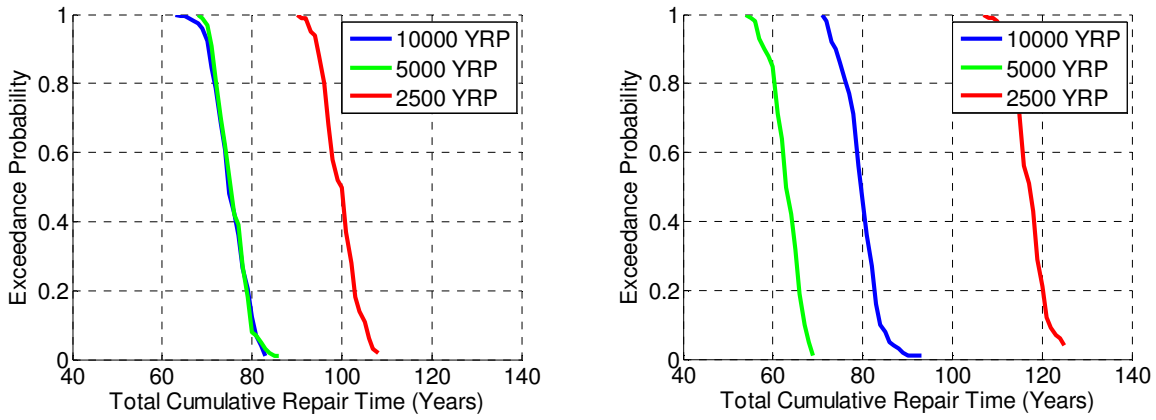

a) GM field linked to critical location 1 b) GM field linked to critical location 2

Figure 36: Total cumulative network repair time

5.5.4 Indirect Consequences

The indirect consequences refer to those additional costs incurred as a result of the hazard scenario, aside from those directly attributed to the infrastructure manager or owner. For the stress tests performed, these were assessed according to the travel disruption, both at regional and national levels (see Section 5.3.6), as well as the economic losses associated with passenger travel disruption at national level.

5.5.4.1 Disruption for road passengers at regional level

To determine the increase in journey times for road passengers at regional level, the results of traffic analyses performed for damaged network scenarios (based on the output of the MCS analysis) to the results of a traffic analysis performed for an 'undamaged' network, where the traffic demand remained constant.

The results of the regional traffic analyses are presented in Figure 37 in terms of the increase in average journey time for the network. This refers to the increase in the mean journey duration

based on all the journeys simulated in the traffic analysis for the time period of 07:15 to 09:15, as described in Section 5.3.6.1. The percentage increases in average journey time for all stress tests performed were similar: the 50% probability value ranged between 2.2% and 2.3%.

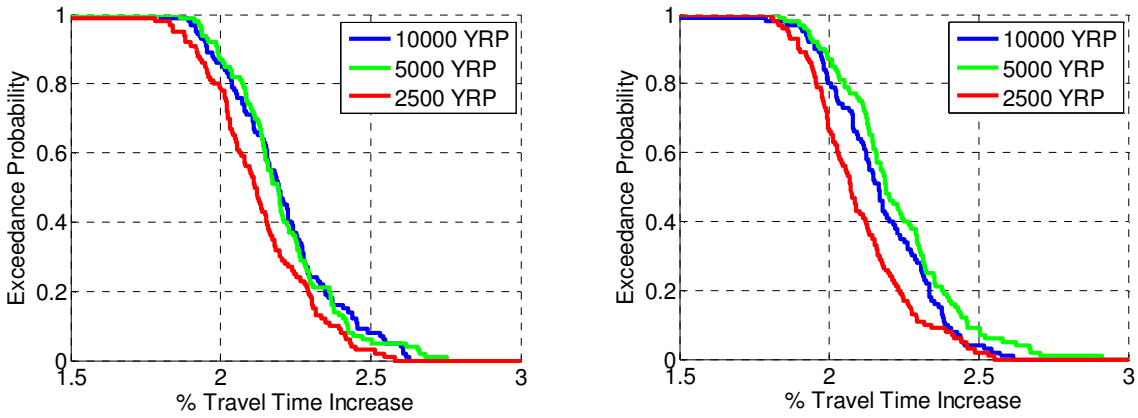

a) GM field linked to critical location 1 b) GM field linked to critical location 2

Figure 37: Percentage increase in average journey time for regional traffic analysis

The potential for passenger travel disruption was also assessed according to the potential for passenger travel delays by analysing the percentage change in journey time for individual origin-destination (O-D) pairs (see Figure 23 for O-D zones at regional level). Initially the impact in terms of travel disruption was assessed for the O-D pair with the greatest travel demand (i.e. the greatest number of passenger trips travelling between a pair of O-D zones), which is shown in Figure 38, where 4266 passenger trips occur between these two zones each morning between 07:15 and 09:15. The results for all scenarios analysed were similar (see Figure 39), showing a 50% probability that a travel time increase of 1.25% would be encountered for passengers travelling between Bologna and the neighbouring San Lazzaro di Savena zones.

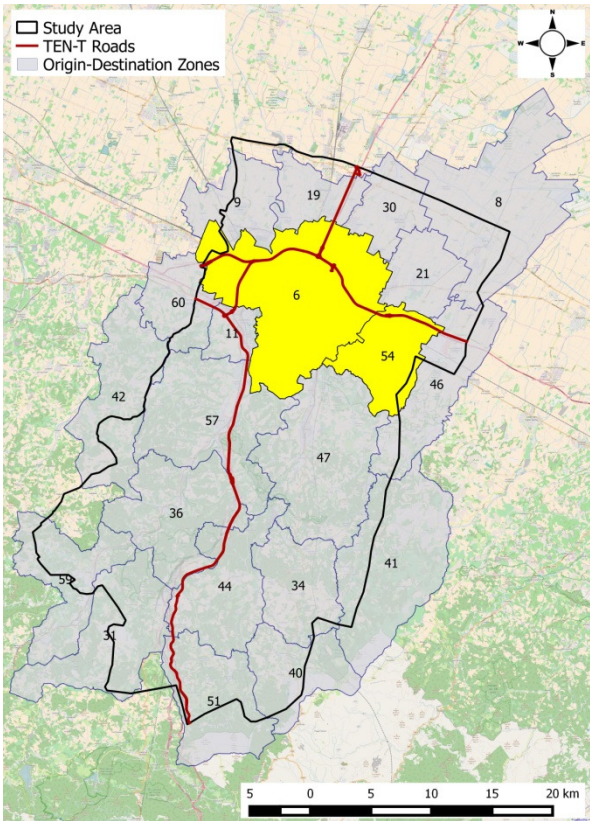

Figure 38: Regional O-D pair with greatest daily travel demand

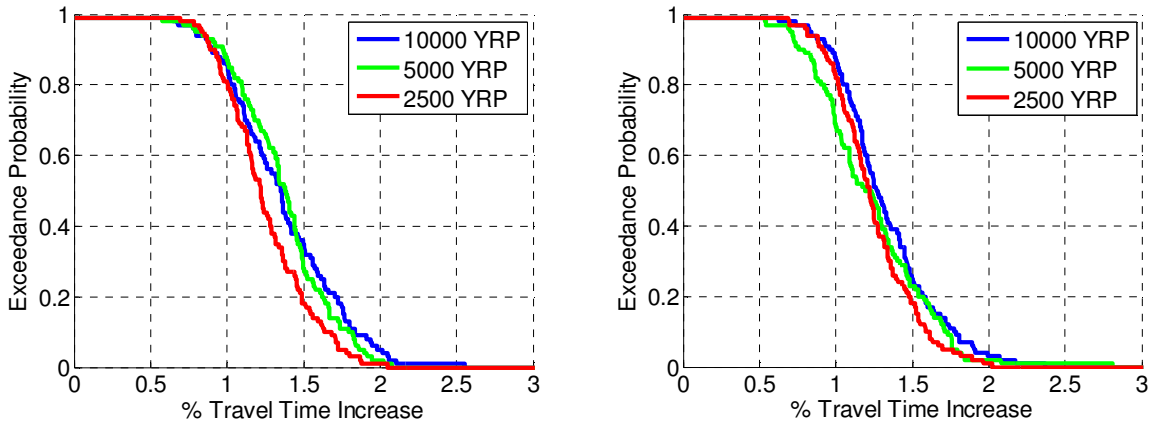

a) GM field linked to critical location 1 b) GM field linked to critical location 2

Figure 39: Percentage increase in journey time for O-D pair in regional traffic analysis with greatest travel demand

The greatest increase in travel times was predicted for passengers travelling between the O-D zones of Monzuno and Budrio (see Figure 40). This demonstrates the network impacts due to the earthquake and earthquake-triggered landslide hazards since passengers travelling between these O-D zones would generally travel via the TEN-T motorway as the shortest path. However, due to the damage caused to the TEN-T roads, passengers travelling between Monzuno and Budrio would be required to travel along other routes that result in travel time increases of at least 25%, whereby the

50% probability value for all hazard scenarios considered was approximately equal to 37% (see Figure 41).

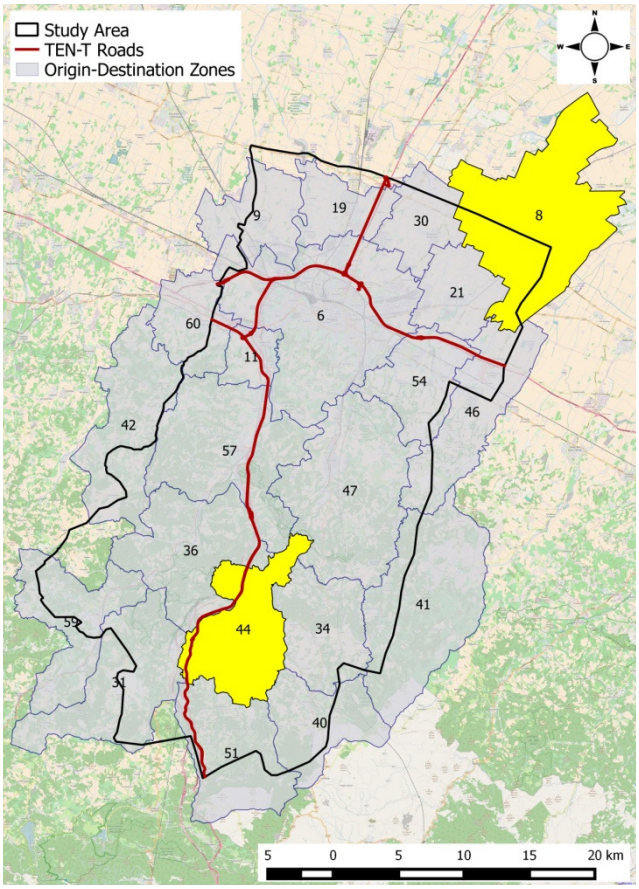

Figure 40: Regional O-D pair with largest increase in travel time

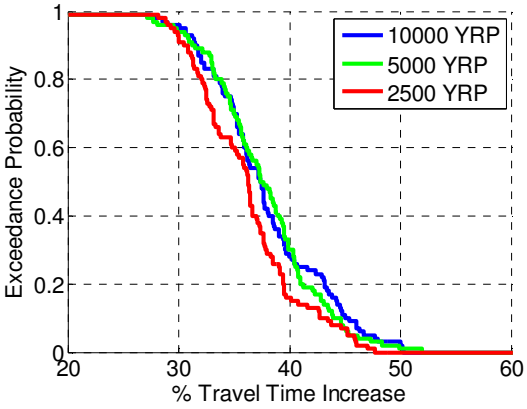

c) GM field linked to critical location 1

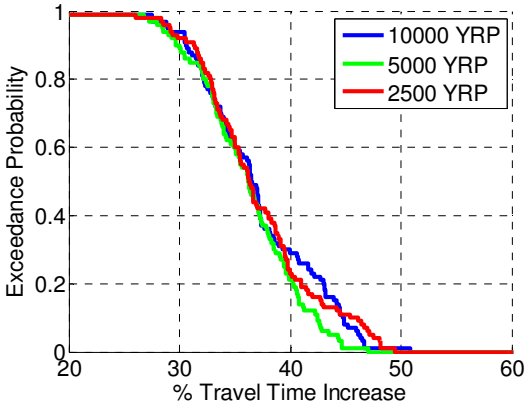

d) GM field linked to critical location 2

Figure 41: O-D pair in regional traffic analysis with greatest travel time increase

5.5.4.2 Disruption for road passengers at national level

To determine the increase in journey times for road passengers at national level, the results of traffic analyses performed for damaged network scenarios (based on the output of the MCS analysis) were compared to the results of a traffic analysis performed for an 'undamaged' network, where the traffic demand remained constant. The results of the national traffic analysis are presented in Figure 42 in terms of the increase in average journey time for the network. This refers to the increase in the mean journey duration based on all the journeys simulated in the traffic analysis, as described in Section 5.3.6.2. The results of all stress tests were very similar; the percentage increase in average journey time ranged between approximately 13% and 14%, whereby the 50% probability value corresponded to approximately 13.8%.

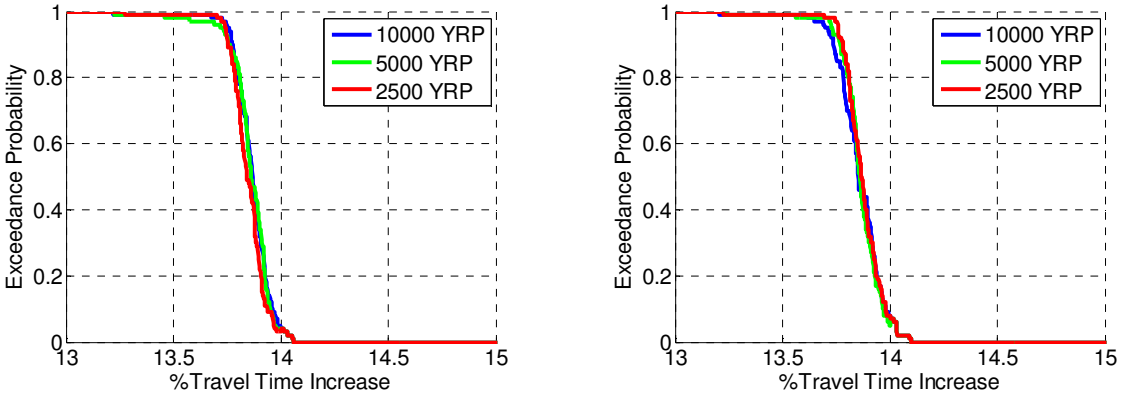

a) GM field linked to critical location 1 b) GM field linked to critical location 2

Figure 42: Percentage increase in average journey time for national traffic analysis

The potential for travel disruption at national scale was also assessed by analysing the percentage change in passenger journey times for individual origin-destination (O-D) pairs (see Figure 25). Initially the impact in terms of travel disruption was assessed for the O-D pair with the greatest travel demand (i.e. the greatest number of passenger trips travelling between a pair of O-D zones), which is shown in Figure 44 (highlighted in yellow), where almost 37,000 passenger vehicle trips between the provinces of Caserta and Napoli occur in the network per hour. The results for all stress tests were almost identical, showing a 50% probability that a travel time increase of 10% would be encountered for passengers travelling between Caserta and Napoli (see Figure 44). Interestingly, these are neighbouring O-D zones that are not located along a route that would be directly impacted (in terms of physical damage) by the hazard scenarios considered. As such, the travel time increases are a result of increased traffic volumes caused by traffic diversions arising from the network disruption in the case study area.

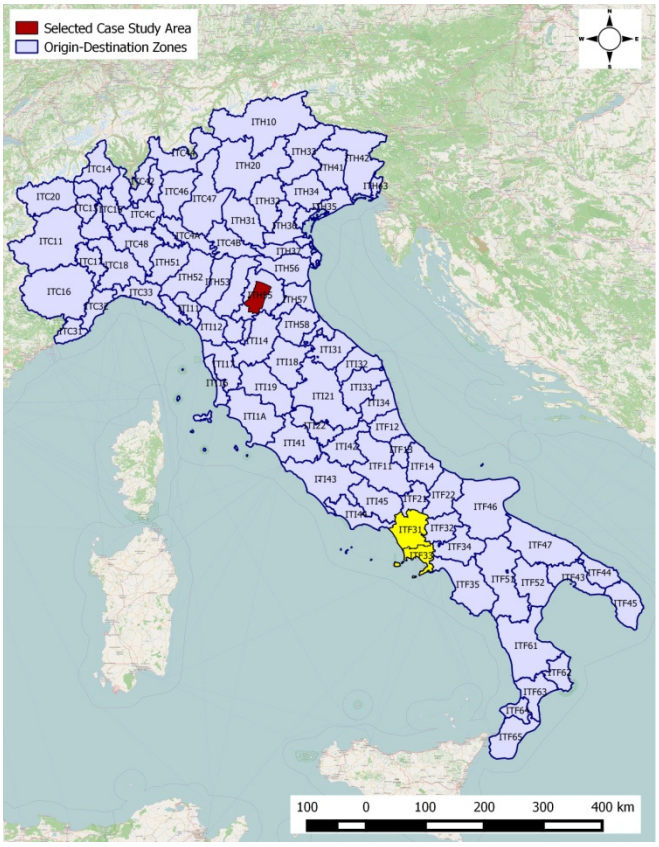

Figure 43: National O-D pair with greatest daily travel demand

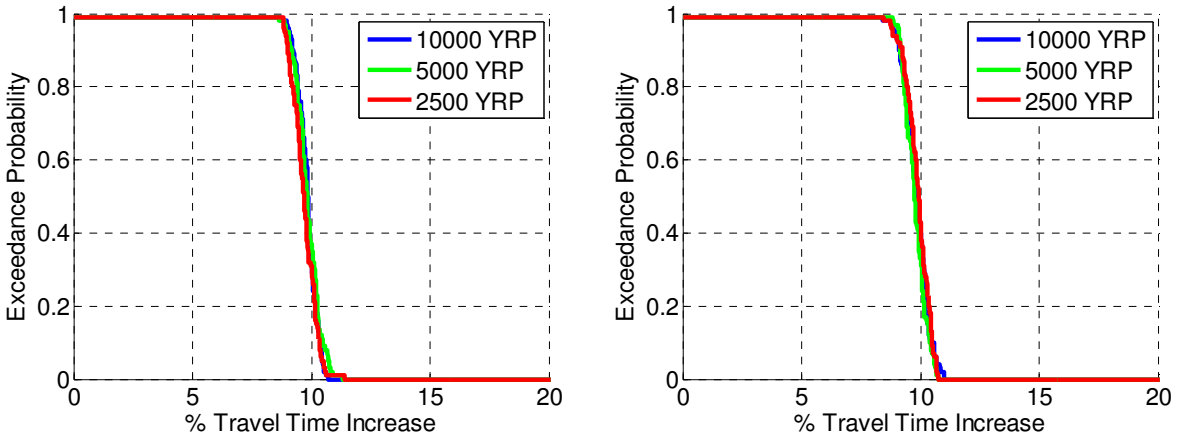

a) GM field linked to critical location 1 b) GM field linked to critical location 2

Figure 44: Percentage increase in journey time for O-D pair in national traffic analysis with greatest travel demand

The most significant travel time increases due to the stress tests performed for the Bologna case study area were for passenger trips between O-D zones located in North West Italy in the vicinity of the city of Milan. The significant travel time increases were due to the increased traffic volumes along this portion of the road network as a result of the diverted traffic due to the disruption caused in the Bologna case study area. For example, for the O-D zones of Verbano-Cusio-Ossola and Cremona (see Figure 45), the 50% probability values of percentage increase in travel time

corresponded to approximately 100%, as shown in Figure 46, and travel time increases of at least 80% were predicted.

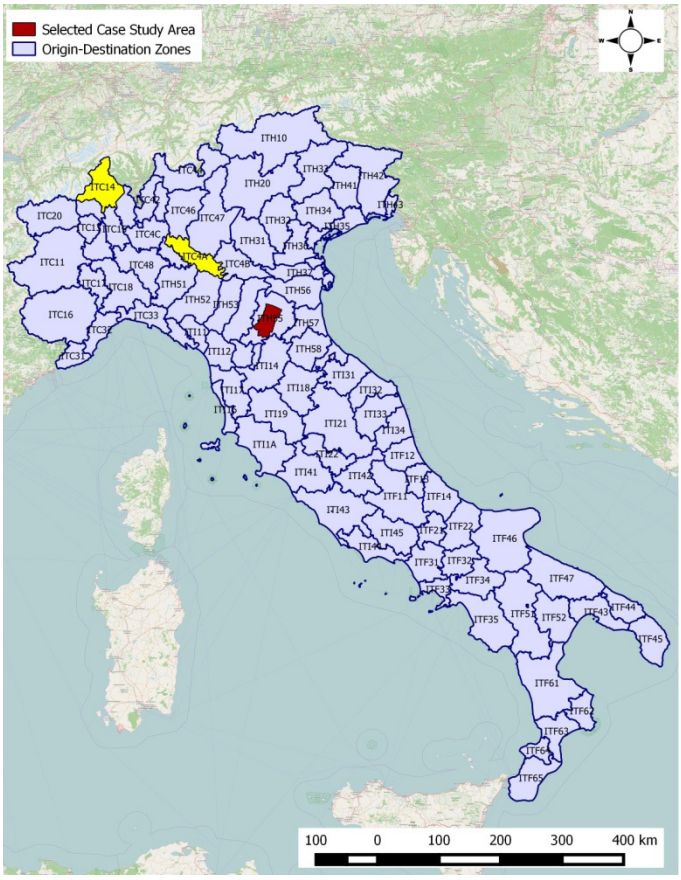

Figure 45: Verbano-Cusio-Ossola and Cremona national O-D zones

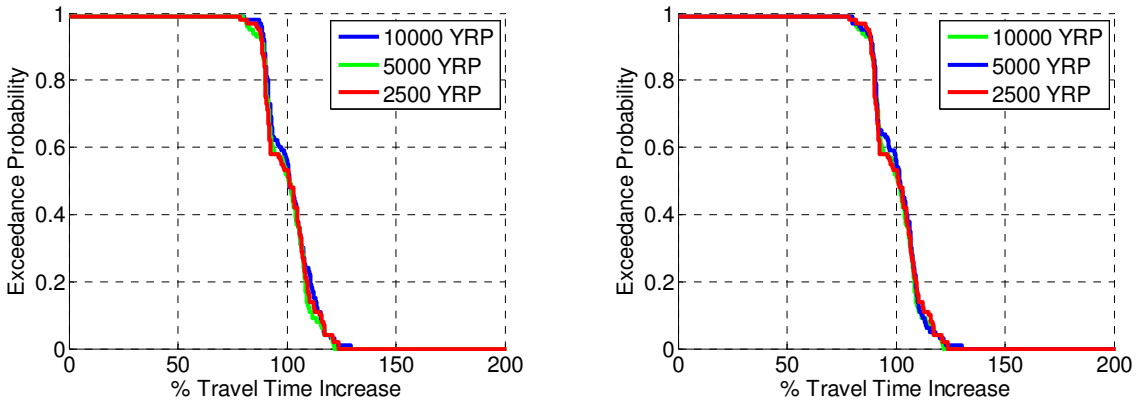

a) GM field linked to critical location 1 b) GM field linked to critical location 2

Figure 46: Travel time increase for passenger trips between Verbano-Cusio-Ossola and Cremona national O-D zones

Consequently, the loss of GDP per capita (ΔGDP) for the O-D zones in this region were significant. The losses were most significant for the O-D zone of Milano (ITC4C), as shown in Figure 47, where

the 50% probability value for all stress tests performed corresponded to approximately €17,800 (46% of the GDP per capita for this province).

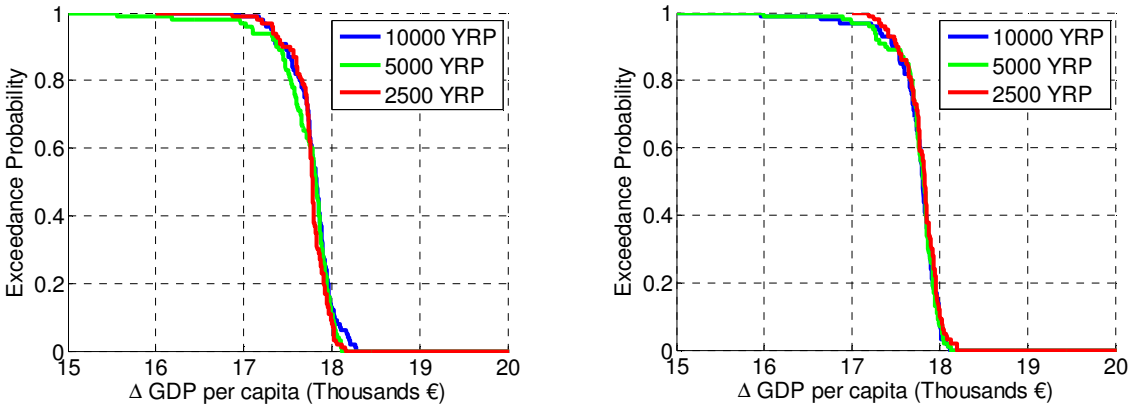

a) GM field linked to critical location 1 b) GM field linked to critical location 2

Figure 47: Economic losses for Milano national O-D zone

The 50% probability values of GDP per capita losses for all of the national O-D zones are shown in Figure 48. The O-D zones in the vicinity of the city of Milan had the greatest losses in terms of GDP per capita (greater than €6000). In addition, the O-D zone of Bologna had significant losses that correspond to 20% of the GDP per capita for this province. For the majority of O-D zones in Northern Italy the 50% probability values of GDP per capita losses were at least €3000. Similar losses were evident for the O-D zones in the vicinity of the city of Naples. These results highlight the complex road network effects due to the seismic hazard scenarios considered and demonstrated that the indirect consequences for other Italian regions in terms of economic losses were significant.

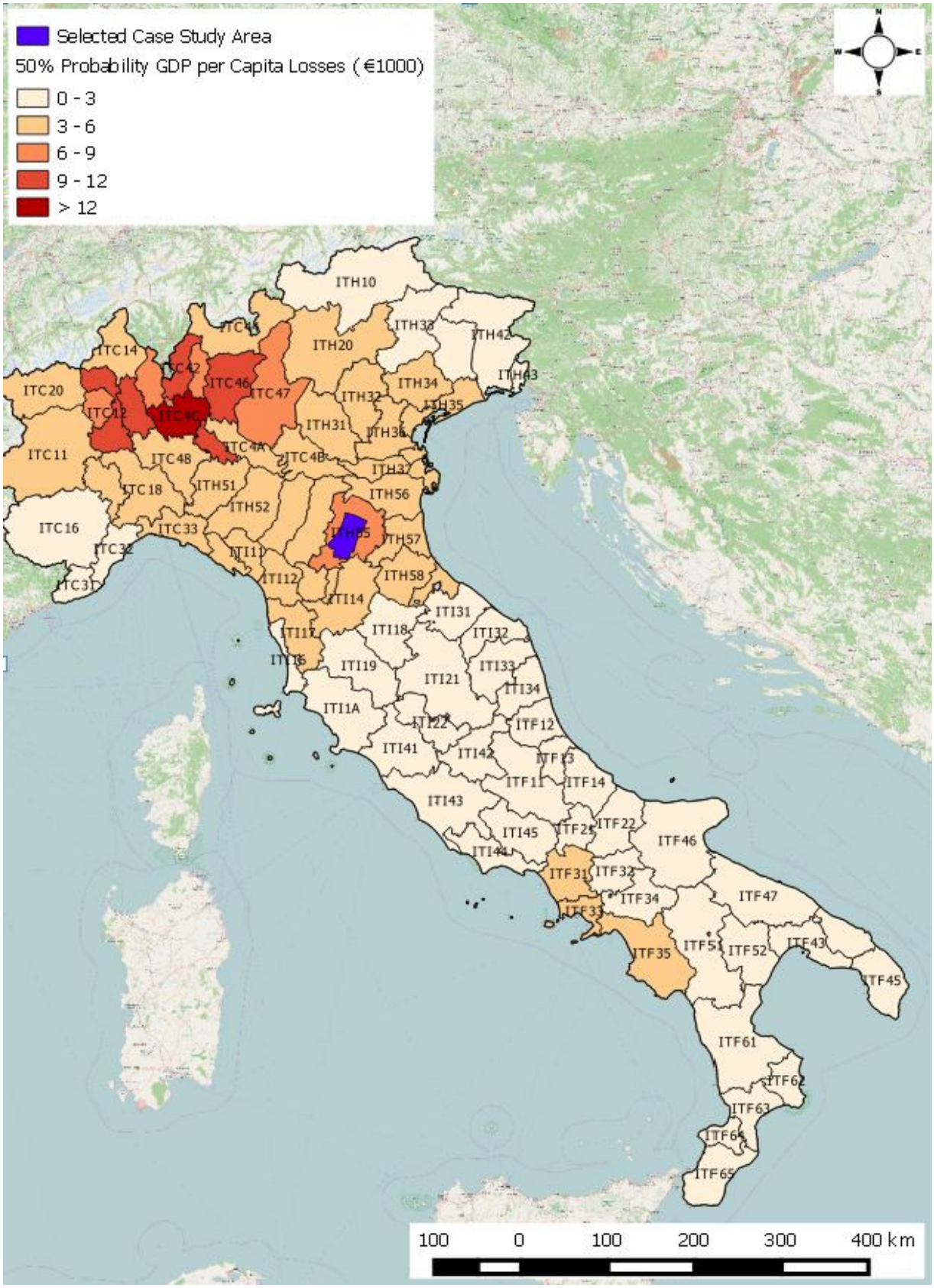

Figure 48: Economic losses per O-D zone at national level in terms of GDP per capita

5.6 Stress Test Outcome

The results of the stress tests performed for the Italian case study have been presented in terms of the direct and indirect consequences, as described in Sections 5.5.3 and 5.5.4. This was deemed to be an appropriate means by which to present the results of the stress tests described herein since just three return periods were considered in terms of the seismic hazard. The analysis of supplementary stress tests based on additional return periods would facilitate the presentation of the associated risk, such as the annualised risk, as described by Hackl et al. (2016).

The goal of the stress test framework applied to the Italian case study was to determine whether or not the potential losses were deemed to be acceptable (see van Gelder and van Erp, 2016). In reality, stress tests are performed based upon evaluation criteria, e.g. total monetary losses. As such, the results of the stress tests performed for the Italian case study were analysed based on the criteria outlined in Table 12.

Evaluation Criteria	Threshold
Total repair cost	€300 million
Maximum increase in travel time per region	50%
Maximum GDP per capita loss per region	€16,000

Table 12: Evaluation criteria employed to assess the outcome of the stress tests for Italian case study

Figure 49 illustrates the results of the stress tests performed according to the 'total repair cost' evaluation criterion. For the seismic GM field linked to critical location 1 (Figure 49a), the upper distribution tails of two of the stress tests exceeded the threshold value and one stress test demonstrated with certainty that the threshold value in terms of total repair costs would be exceeded. For the seismic GM field linked to critical location 2 (Figure 49b), one of the stress tests demonstrated that the threshold value would definitely not be exceeded, another stress test demonstrated that there was a 28% probability that the threshold value would be exceeded, and the third stress test demonstrated that the threshold would most certainly be exceeded.

The outcome of probabilistic stress tests will depend on the risk acceptability of the infrastructure owner or manager. However, in this case since the stress tests that correspond to a 2,500 year return period both demonstrate with certainty that the 'total repair cost' threshold will be exceeded, the stress tests have failed, i.e. the potential losses are deemed to be unacceptable. At this point the infrastructure owner/manager may decide to analyse parts of the network in greater detail to reduce the uncertainty associated with the risk estimate, i.e. obtain more accurate structural information or repair cost estimates for specific structures along the network. Otherwise the infrastructure owner/manager may decide to implement intervention measures to mitigate against these potential losses according to the third task of the general risk assessment process proposed by Hackl et al. (2016). To do so, the decision theory proposed by van Gelder and van Erp (2016) has the potential to be used to determine the optimal intervention strategy for the network.

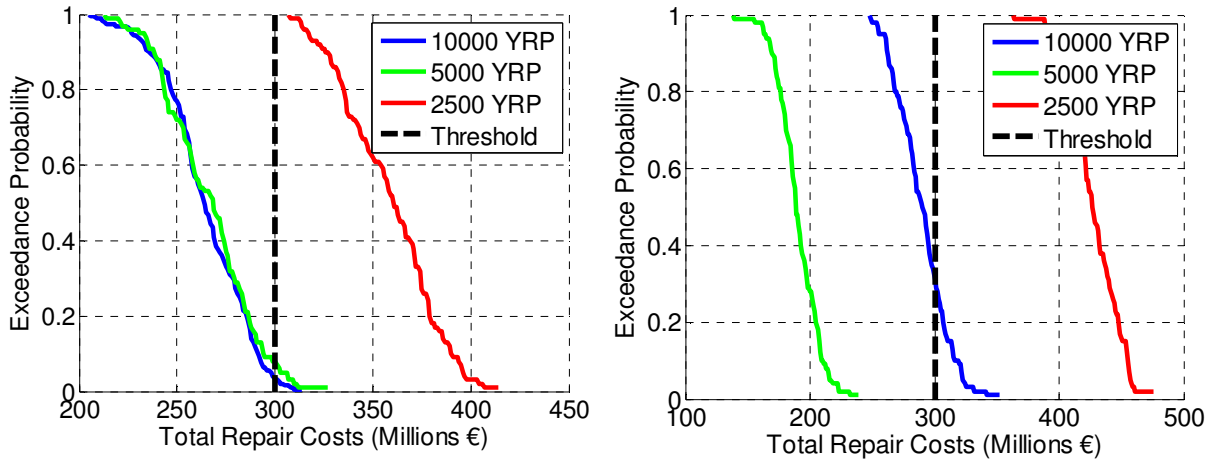

a) GM field linked to critical location 1 b) GM field linked to critical location 2

Figure 49: Stress test results: total network repair costs

To evaluate the outcome of the stress tests according to the 'maximum increase in travel time' evaluation criterion, the results of the traffic analyses were compared to the imposed thresholds. To do so, the results of both the regional and national traffic analysis were analysed in terms of the O-D pair with the greatest increase in travel time. Figure 50 illustrates that all stress tests predicted that the maximum increase in travel time at regional level would not exceed the threshold value (with approximately 99% certainty).

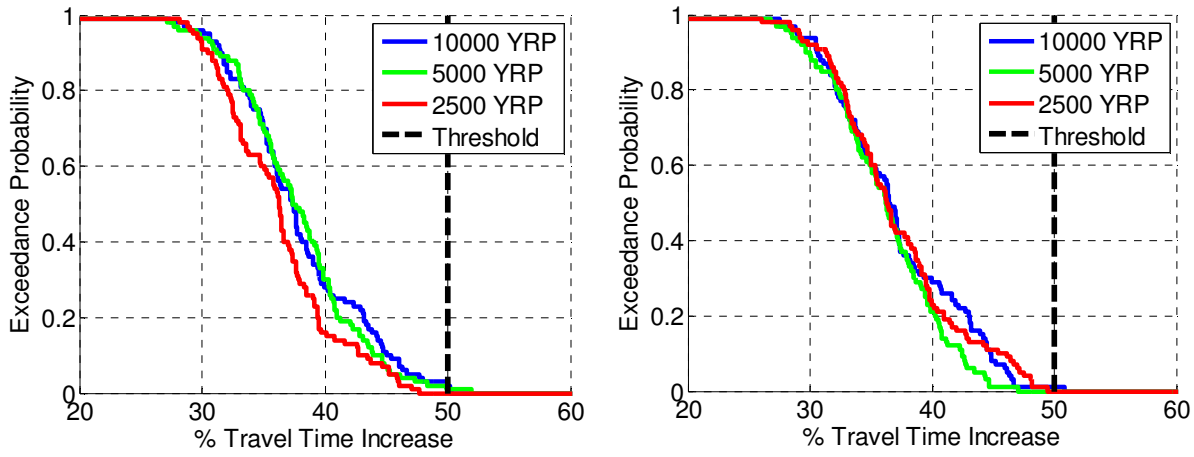

a) GM field linked to critical location 1 b) GM field linked to critical location 2

Figure 50: Stress test results: max. increase in travel time at regional level

However, the results of the stress tests in terms of the maximum travel time increase at national level demonstrated that the threshold value would most certainly be exceeded (see Figure 51). As such, the stress tests performed failed in terms of the 'maximum increase in travel time' evaluation criterion. Therefore, the infrastructure manager/owner may decide to conduct an intervention programme to reduce the overall network travel time increases by strengthening specific network

structures or adding redundancy to the network. Again, the decision making theory proposed by van Gelder and van Erp (2016) could be employed to determine the optimal strategy in terms of prioritisation of works.

These results demonstrate the importance of considering the wider impacts of the seismic hazards for distributed transport networks since the effects were most significant at the scale of the national road network rather than for the regional roads that were directly impacted by the natural hazard occurrence.

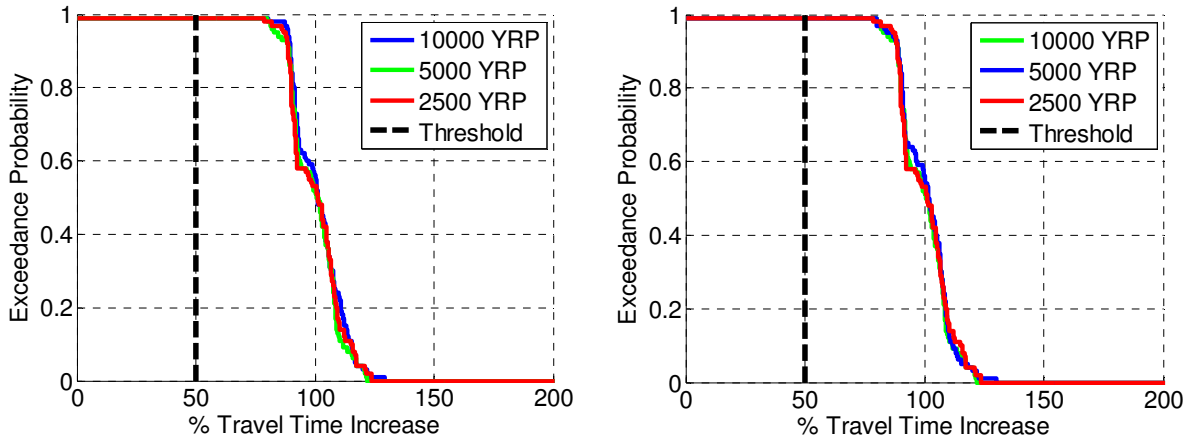

a) GM field linked to critical location 1 b) GM field linked to critical location 2

Figure 51: Stress test results: maximum increase in travel time at national level

Finally, the outcomes of the stress tests performed were evaluated according to the maximum GDP per capita loss per region. Figure 52 illustrates with 99% certainty that all stress tests predicted that the imposed threshold would be exceeded. As such, mitigation measures would be required for the outcome of the stress tests to be acceptable.

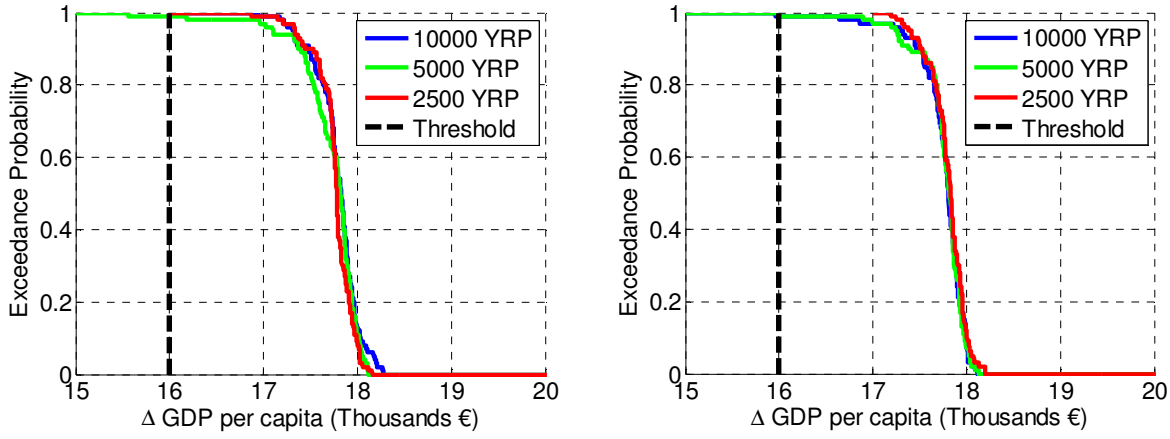

a) GM field linked to critical location 1 b) GM field linked to critical location 2

Figure 52: Stress test evaluation: max. GDP per capita loss

5.7 Discussion

The Italian case study described herein has demonstrated the systematic application of the methodologies that have been developed within the INFRARISK project. These were to perform stress tests for a critical road network due to low probability, high consequence seismic hazard scenarios according to the overarching risk assessment methodology proposed by Hackl et al. (2016).

The stress tests considered the structural vulnerability of individual network elements (i.e. bridges, tunnels and sections of roadway) to seismic ground motions and damage induced by earthquake-triggered landslides. The consequences were assessed according to the network repair costs and the total time required to conduct the network repairs (i.e. the direct consequences), as well as the increase in travel times for road passengers and the associated ecnomic losses (i.e. the indirect consequences).

The analysis was performed in modular format so that further complexity could be employed at various stages depending on the overall objective or focus of the stress tests. For example, the stress tests for the Italian case study could be extended to consider various restoration sequences in terms of infrastructure repair activities and the associated impacts of various strategies in terms of accumulated losses following the natural hazard occurrence. Similarly, economic loss modelling could be further improved by considering the non-linear relationship between travel demand and travel time delay that generally occurs following a natural hazard event.

The stress tests performed for the Italian case were considered to be reliable since the structural characteristics of individual network elements were explicitly considered in the analysis. Furthermore, the traffic modelling was based on origin-destination passenger data specific to the region, which further contributed to the reliability of the stress tests. However, the stress tests would further benefit from more precise estimates of the cost and duration of repairs associated with individual network elements, perhaps based on an expert survey (see D'Ayala and Gehl, 2015).

A limited number of stress tests was performed for the Italian case study. This raises the question that many infrastructure managers/owners will be faced with; whether or not the number of stress tests is sufficient. The results of the stress tests described herein differed significantly in terms of the indirect consequences (i.e. total network repair cost and duration). However, the results of the stress tests in terms of the indirect consequences did not vary significantly. As such, the sufficiency of the number of stress tests is related to the evaluation of the results.

For the Italian case study specifically, the number of stress tests performed was deemed to be sufficient in terms of the indirect consequences. However, further stress tests would be beneficial in the evaluation of the direct consequences. To do so, additional ‘critical locations’ along the network could be considered, to which the seismic GM fields would be linked. To do so would require significant computional resources and would benefit from a more efficient damage sampling algorithm, such as the Probability Sort algorithm proposed by van Gelder and van Erp (2016).

The stress tests performed for the Italian case study considered existing scenarios, i.e. based on the existing structural condition of the road network and the current network demand. However, the applied stress test framework can also be applied to consider the impact of a network intervention program. For example, the stress test framework could be used to determine the potential losses for

the Italian case study if strengthening measures were implemented for all of the concrete, simply supported, multi-span bridges along the TEN-T motorway in this region. Based on such stress tests, the decision-making protocol proposed by van Gelder and van Erp (2016) could subsequently be employed to determine the optimal intervention programme for the road network. In addition, the stress test framework has the potential to consider future scenarios; for example, stress tests could be performed for a future scenario whereby the network traffic is substantially greater.

6.0 CROATIAN RAIL NETWORK

This section will describe the application of the 'Conduct Risk Assessment' phase of the overarching risk assessment methodology described by Hackl et al. (2016) that was used to perform stress tests for the Croatian rail network case study. The 'Conduct Risk Assessment' phase comprises five main tasks: 1) set up risk assessment, 2) determine approach, 3) define system, iv) estimate risk and v) evaluate risk, which will be described for the Croatian case study in the following sections.

6.1 Risk Assessment

The objective of the stress tests for the Croatian case study was to determine the potential losses due to the impact of low probability, high consequence flood hazard scenarios on the national rail network. As part of the 'set up risk assessment' task in the risk assessment process, it was decided that the impacts would be analysed in terms of both the direct and indirect consequences. Direct consequences refer to the costs associated with the flood occurrence that are considered directly attributable to the rail infrastructure owner or manager. Indirect consequences refer to the additional losses encountered as a result of the rail network disruption.

As there is generally a large degree of uncertainty associated with the occurrence of low probability, flood hazard scenarios, as well as the response of existing rail elements to such events, a risk assessment approach that considered and accounted for these uncertainties was adopted for the stress tests.

6.2 Approach

Due to the large scale of the rail network examined and the complexity associated with the prediction of flood hazard scenarios and the vulnerability estimation for rail network elements due to such events, it was decided to perform stress tests for the selected Croatian rail network according to a two stage approach. Initially, a qualitative assessment of the rail network was performed according to an Objective Ranking Tool method to assess the risk to the network at a relatively high level of abstraction. A more detailed quantitative assessment was subsequently performed for the network according to a series of modules, as defined by Hackl et al. (2016).

6.3 Spatial Boundaries

The spatial boundaries of the Croatian rail network are illustrated in Figure 53. This covers an area of approximately 35,000 km^2 and consists of approximately 800 km of rail; including rail lines along the Mediterranean corridor of the TEN-T network (see Section 4.2).

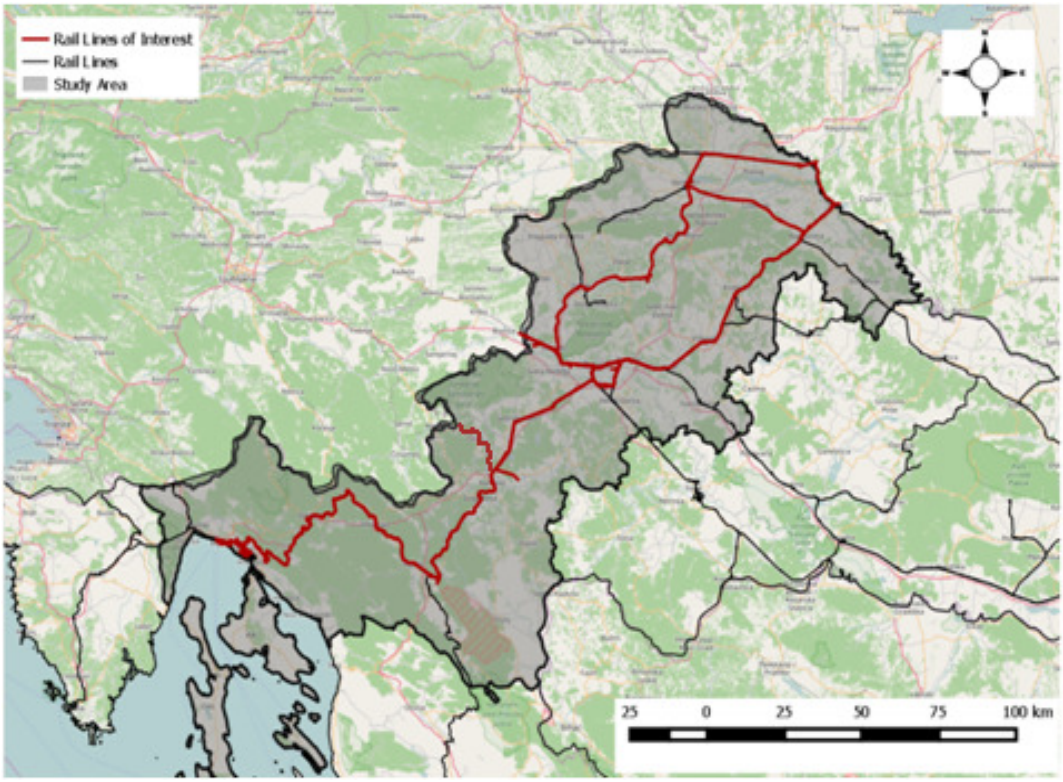

Figure 53: Selected Croatian rail lines

6.4 Network Vulnerability

The susceptibility of the selected Croatian rail network to floods was assessed according to the vulnerability of individual sections of rail track to rainfall-triggered landslides and to inundation, and the vulnerability of the network bridges to scour, as outlined in Table 13. These were considered as 'infrastructure events', i.e. an event that is a change in infrastructure condition that may lead to a change in infrastructure use or a change in human behaviour, as described by Hackl et al. (2016).

Network Element	Hazard
Rail Sections	Rainfall-triggered landslides
Bridges	Flood-induced scour
Rail Sections	Inundation

Table 13: Network elements and associated hazards for Croatian case study

6.5 Objective Ranking Tool (ORT)

An ORT application was developed for the Croatian rail network case study. The ORT is a web-based multi-user application that can be used for decision making, making comparisons between alternatives or for ranking processes, which is based on the theoretical principles of similarity judgment, the use of a Delphi panel and Analytic Hierarchy Processing (AHP). Detailed information in relation to the ORT can be found in Appendix B.4 of INFRARISK Deliverable 4.2 (Hackl et al., 2016). The aim of the ORT application for the Croatian case study was to efficiently and effectively assess the risk to the selected rail network due to extreme flood hazard scenarios, where the objective was

to prioritise parts of the network to trigger a more detailed quantitative assessment as part of overall stress tests for the network.

The first step of the ORT for the Croatian rail network consisted of a Delphi panel, which brought together a group of relevant experts to determine the following: 1) the criteria to be used to rank individual rail sections, 2) the relative weighting of these criteria that would be used in the similarity judgement formula, 3) whether each ranking criterion would be substitutive (i.e. 0 or 1) or additive (i.e. between 0 and 1), 4) whether or not mitigation measures can be taken for each criterion (i.e. yes or no). Seven ranking criteria were selected in total and it was decided within this Delphi panel to focus upon three main failure criteria for elements of the rail network due to flooding: 1) the potential for track inundation due to flooding, 2) the potential for blockages/damage to the rail track due to rainfall triggered landslides, 3) the potential for damage to the rail network due to bridge scour. It was decided to conduct a separate ORT analysis for the rail network for each of the three aforementioned criteria, as shown in Figure 54, whereby the seven ranking criteria were considered for each.

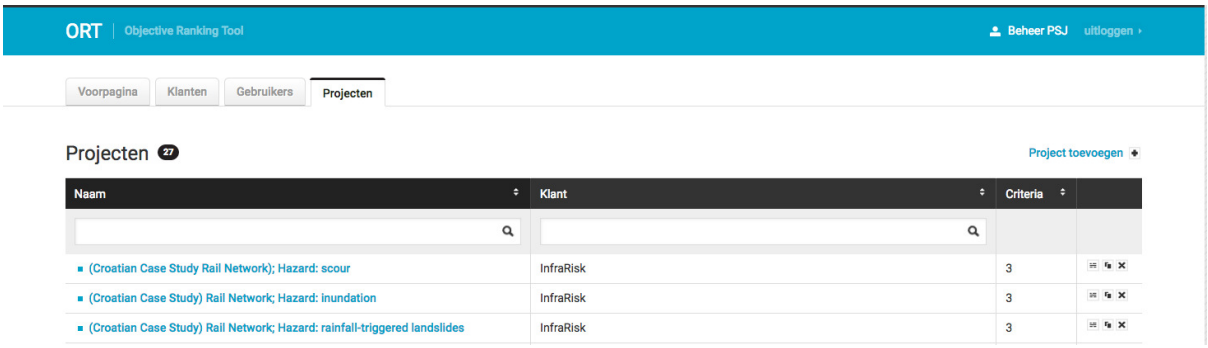

Figure 54: ORT analyses conducted for Croatian rail network

Based on this list of ranking criteria, the next step of the ORT involved the application of similarity judgement to determine the relative weighting percentages of the individual ranking criteria. To do so, each member of the Delphi panel applied the principles of similarity judgement individually using an online AHP tool (www.bpmsg.com). The overall relative weighting percentages of the individual ranking criteria are shown in Figure 55.

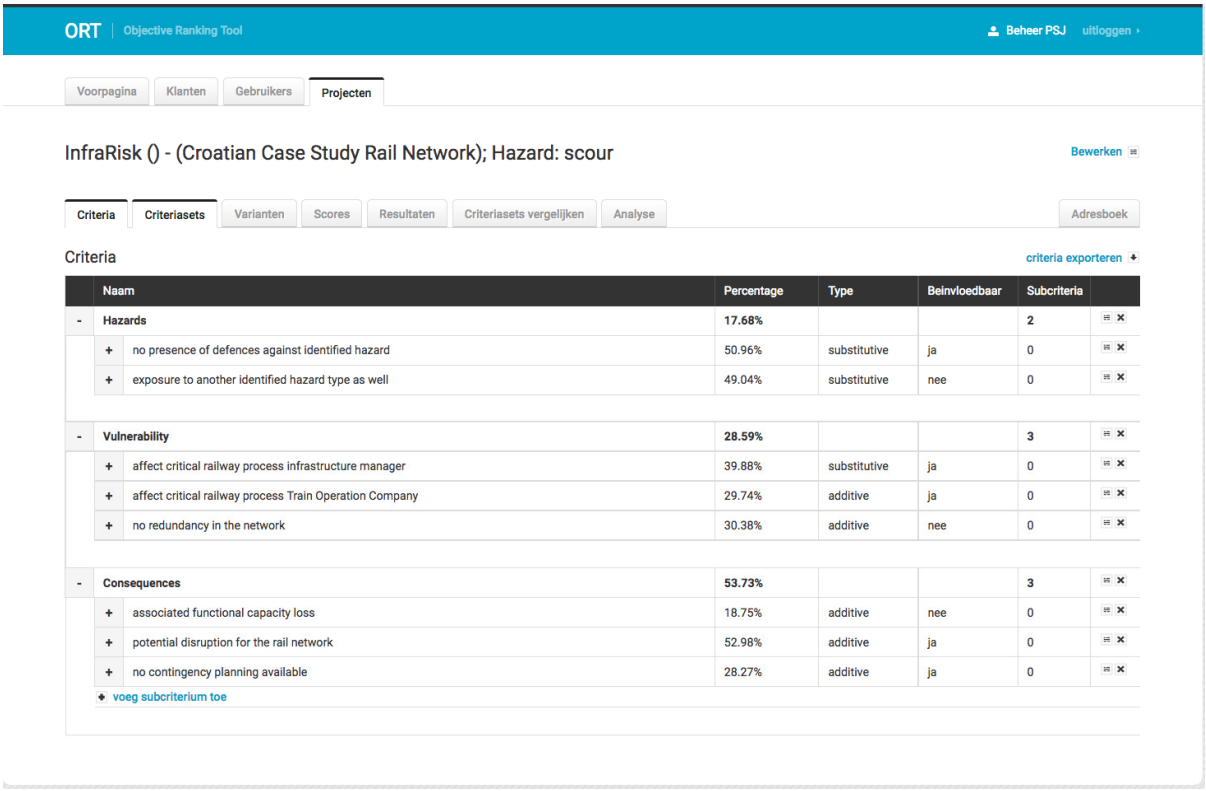

Figure 55: ORT ranking criteria

The Delphi panel also determined the most appropriate way to divide the rail network into individual rail 'sections' (i.e. regularised track lengths, between train stations, between network elements), which would be ranked according to the selected criteria. Ultimately, it was decided that the best approach for the ORT application in this instance was to define individual rail 'sections' as sections of rail between the official train stations along the network. Figure 56 illustrates a selection of the rail sections listed in the ORT application.

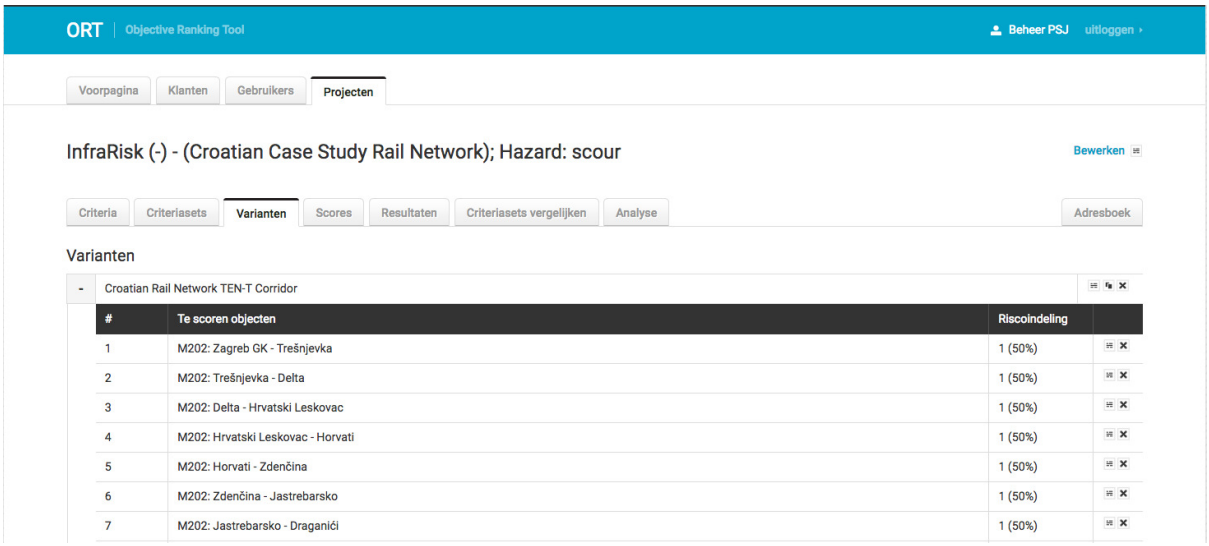

Figure 56: Partial view of ORT application showing list of rail sections

6.5.1 ORT Ranking Process

Based on the selected ranking criteria, all rail sections were scored based on the definition of 'substitutive' or 'additive' criteria, as shown in Figure 57 for the analysis due to the potential for bridge scour. For the ORT ranking process, quantitative data is preferable. However, in cases where this is not available, participants are encouraged to consider qualitative data.

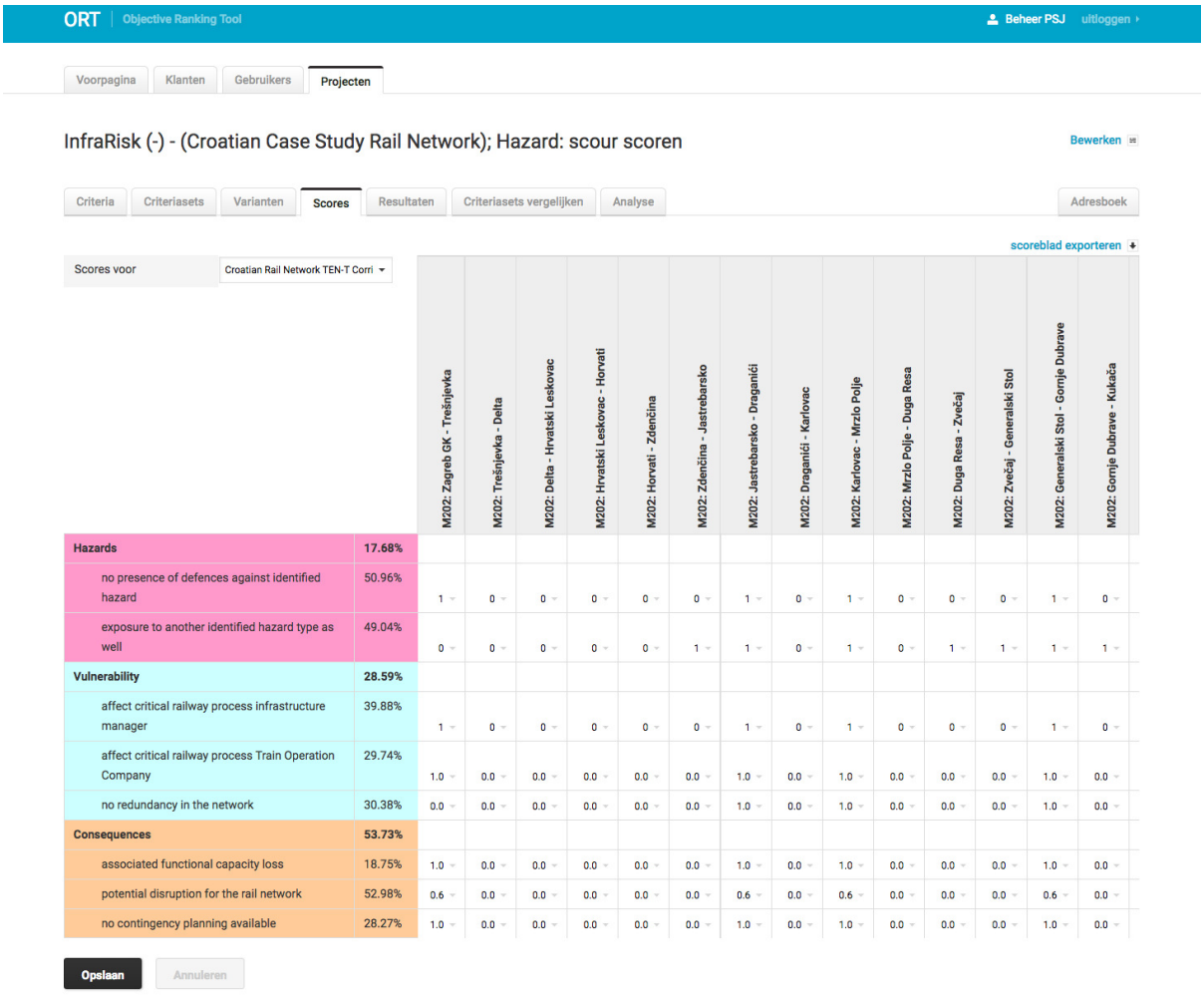

Figure 57: Partial view of ORT application showing ranking of individual rail sections due to the potential for scour

For the Croatian case study, the geographically referenced data outlined in Table 14 was available. Additionally, limited information was available via visual inspection using Google Street View. As such, the available data for the Croatian case study consisted of a combination of quantitative and qualitative data. Certain information was completely unavailable. For example, foundation information for rail bridges along the network, which is useful in determining the susceptibility of existing bridges to flood-induced scour. Croatian Railways (HZ Infrastruktura) were contacted in an attempt to obtain more information about the rail network. Unfortunately however, nobody was available. However, general information obtained from the 2016 Network Statement produced by Croatian Railways was also considered during the ranking process. If was decided that where data was completely unavailable, rail sections were to be equally scored.

	Data information	Data format
Hazards	Probability of flooding (very high, high, moderate, low)	Polygon shapefile
	Flood water depth corresponding to a 1000 year return period	Raster file (10x10m resolution)
	Hydrological network	Polyline shapefile
	Presence of flood defences	Polygon shapefile
	Susceptibility to landslides (very low, low, moderate, high, very high)	Raster file (10x10m resolution)
Vulnerability	Geographical location of rail network	Polyline shapefile
	Geographical location of rail bridges and tunnels	Point shapefile
	Elevation information for train stations	Point shapefile

Table 14: GIS data employed to rank rail sections for ORT application

For each of the three ORT analyses, the scoring of individual rail sections was conducted. Low probability, extreme flood hazard events were considered and, therefore, a 1000 year return period flood hazard map was considered for the analysis due to inundation. For the ORT analyses due to rainfall-triggered landslides and scour, hazard maps were unfortunately not available for a given return period. Consequently, the ranking process was based on the available information and the judgement of the relevant expert. For landslides, the rail sections were deemed to be vulnerable to rainfall-triggered landslides based on the landslide susceptibility map and the geographical location of the rail section under consideration. For the assessment of the vulnerability of rail sections to scour, this was based on limited information on the location of rail bridges and the number and location of bridge piers.

To rank the rail sections according to the 'Vulnerability' criteria, 'critical railway processes' for the infrastructure manager were deemed to include the following: maintenance and reconstruction of rail network elements (e.g. bridges, tunnels, rail track, and embankments), traffic management and railway signalling. Meanwhile 'critical railway processes' for the train operation company included the processes for running trains (locomotives and wagons) for passengers and freight transport. Where rail sections were deemed to have their critical railway processes impacted by the hazard, a score of '1' was assigned. Where alternative rail routes were possible, which could lead to possible re-routing of the train, a score of 0.5 was assigned to the rail section. Finally, for the 'no redundancy in the network' ranking criterion, rail sections that did not have any redundancy available were assigned a score of '1'. For the majority of the rail lines, network redundancy was not present. Information from the Network Statement for the Croatian rail network in relation to the operational conditions of different rail lines, which can be used to identify possible re-routing options, was also used for this ranking criterion.

To rank the individual rail sections according to the 'Consequences' ranking criterion, the functional capacity loss was deemed to be equal to '1' where the hazard was present and no redundancy of the network was available. For the case of rainfall-triggered landslides and double rail tracks, it was assumed that the landslide would impact a single rail track only and, therefore, a score of '0.5' was assigned to rail sections in this case. To rank the rail sections according to the 'potential disruption for the rail network' ranking criterion, the ranking score was related to the duration of the

functionality loss of the rail section. For example, if the functionality loss duration was considered to range between 0 and 3 days, a score of '0.3' was assigned. If the functionality loss duration was considered to last between 3 days and 2 weeks, a score of '0.6' was assigned. Finally, is the functionality loss duration was expected to last more than 2 months, a score of '1' was assigned. For the 'no contingency planning available' criterion, no information could be found in the Network Statement for the rail network in relation to dedicated contingency plans. Consequently, a score of '1' was assigned to each rail section.

6.5.2 ORT Results

Based on the scoring of the individual rail sections, the ORT analysis was subsequently conducted (further information in relation to the calculation for the ORT analysis can be founded in Appendix B of Hackl et al., 2016). Figure 58 shows the ORT results for the ten rail sections with the highest overall scores. The total score for each rail section was calculated based on the results of the individual analyses conducted for the three hazards considered (i.e. inundation, rainfall-triggered landslides, bridge scour). The total score was based on partial dependencies since the three hazards considered are asymptotically dependent as their occurrence is related to a single source event, i.e. rainfall. Due to the scale of the analysis, the three hazards are considered to be only partially dependant since geographically specific characteristics such as the terrain topography, properties of the hydrological network, etc. may introduce local effects.

ORT Results

	Reference railway section	M202 Generalski Stol - Gornje Dubrave	M201 Koprivnica DG - Botovo	M201 Botovo - Drnje	M201 Lepavina - Križevci	M201 Vrbovec - Dugo Selo	M202 Ogulinski Hreljin - Gomirje	M202 Gomirje - Vrbovsko	M202 Vrbovsko - Moravice	M202 Lokve - Fužine	M202 Zdenčina - Jastrebarsko
Total score	1.0000	0.9312	0.9312	0.9312	0.9312	0.9312	0.7830	0.7830	0.7830	0.7830	0.7746
Inundation	1	0.8893	0.8893	0.8893	0.8893	0.8893	0	0	0	0	0.8893
Rainfall-Triggered Landslides	1	0.9396	0.9396	0.9396	0.9396	0.9396	0.9396	0.9396	0.9396	0.9396	0.9396
Scour	1	0.9396	0.9396	0.9396	0.9396	0.9396	0.9396	0.9396	0.9396	0.9396	0

Figure 58: Partial view of ORT application showing the ten highest ranked rail sections

The highest scored rail sections consisted of one section along the M202 route from Rijeka to Zagreb, and four rail sections along the M101 route from Koprivnica to Dugo Selo. These rail sections were exposed to all three hazards. For the remaining rail sections, 17 were exposed to two of the hazards and 19 sections were exposed to a single hazard.

6.5.3 ORT Summary

The objective of the ORT application for the Croatian rail network case study was to determine the locations along the network where the risk due to extreme flood scenarios is most significant. The ORT analysis is intended to act as an initial qualitative approach to risk assessment, which employs limited resources. This facilitates the prioritisation of resources for a more detailed quantitative risk assessment of limited parts of the network, as will be described in Sections 0 to 6.9 for the Croatian case study. A proof of concept application of the ORT has been demonstrated for the Croatian rail network. This application could be further enhanced through the availability of additional data or through the participation of the infrastructure manager (Croatian Railways) in the Delphi panel.

6.6 System Definition for Quantitative Risk Assessment

This section describes the hazards, infrastructure and consequences that were modelled for the Croatian case study rail network. For each, the selected boundaries (spatial and temporal), events, scenarios, relationships and models are described.

This section describes the overall 'system', which refers to the following:

- Definition of the flood hazard.
- Definition of the rail network infrastructure and the vulnerability of this infrastructure to the hazards considered.
- Definition of the potential losses in terms of physical repair works.
- Definition of the potential functionality loss of the rail network.
- Definition of the potential disruption for rail network transport.

The spatial boundaries for the network were described previously in Section 6.3 and the means by which the network vulnerability was assessed is presented in Section 6.4. However, further details in relation to the network vulnerability assessment are provided in Sections 6.6.3 to 6.6.6.

6.6.1 Flood Hazard Model

This section presents the methodology that was employed to derive predicted values of rainfall, river discharge and water depth for extreme, low probability flood hazard scenarios since the network vulnerability was assessed according to these flooding mechanisms (see Section 6.4). Historical rainfall and river data was obtained from the Croatian Hydrological and Meteorological Department for data stations in close proximity to the selected rail lines of interest. The following precipitation information was obtained for the meteorological stations: monthly and yearly maximum values of precipitation amount (mm) and their corresponding durations (min) for the period 2000 to 2014. In terms of river data, the following information was obtained for the hydrological stations: daily maximum values of water level (cm) and river discharge (m^3/s) for the period 1990 to 2014. To estimate the flood hazard associated with the rail network, a statistical approach was adopted by fitting annual maxima to extreme value distributions, and extrapolating them to extreme quantile levels, as described in the following sections.

6.6.1.1 Extreme rainfall scenarios

To model extreme rainfall scenarios, a statistical approach was adopted based on the historical rainfall data available whereby extreme value distributions were fitted to various rainfall intensity values to calculate the duration of rainfall for a given rainfall intensity value. Figure 59 illustrates a fitted Generalised Extreme Value (GEV) distribution to the rainfall data for rainfall intensities of 10, 15 and 20 mm/hr, which were extrapolated for return periods of 200, 500 and 1000 years. To consider the associated uncertainty, a probability distribution was assigned to the estimated values of rainfall duration for the rainfall intensities of 10, 15 and 20 mm/hr. A lognormal distribution was adopted to consider lack of symmetry and to prohibit negative rainfall durations, whereby the mean value of the distribution was adopted from the extrapolation analysis. To calculate the standard deviation of the lognormal distribution, a constant coefficient of variation (COV) equal to 10% was assumed. A summary of the mean and standard deviations values for the rainfall duration estimates

for rainfall intensities of 10, 15 and 20 mm/hr that corresponded to various return periods is presented in Table 15.

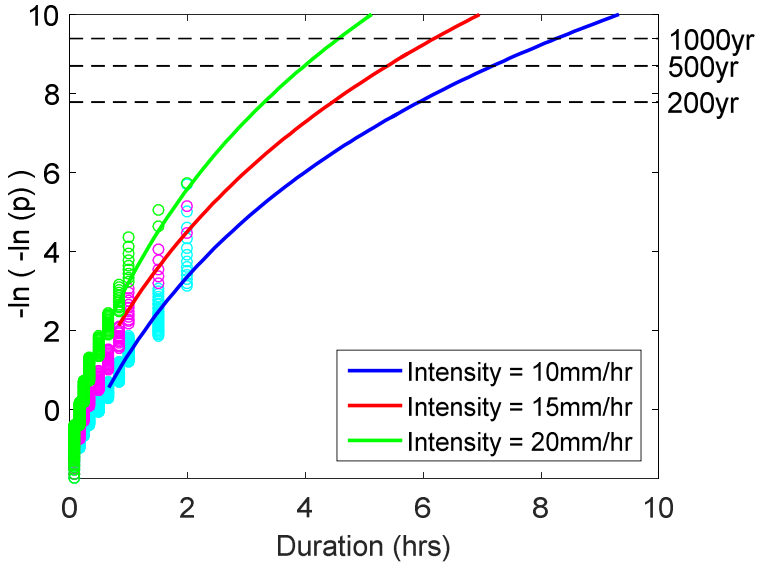

Figure 59: GEV distribution fit to historical rainfall intensity data

Rainfall Intensity	Rainfall Duration Distribution Parameters (minutes)		
	200 year return period	500 year return period	1000 year return period
10 mm/hr	μ = 5.967, σ = 0.859	μ = 7.167, σ = 1.075	μ = 8.267, σ = 1.240
15 mm/hr	μ = 4.433, σ = 0.665	μ = 5.433, σ = 0.815	μ = 6.233, σ = 0.935
20 mm/hr	μ = 3.350, σ = 0.503	μ = 3.950, σ = 0.593	μ = 4.550, σ = 0.683

Table 15: Mean and standard deviations of lognormal distributions for rainfall duration values for a given rainfall intensity value

6.6.1.2 Extreme river discharge scenarios and associated water depths

To determine extreme values of river discharge, a statistical approach was also adopted based on the available historical data whereby extreme value distributions were fitted to the river discharge data. To do so, the river discharge from a specific hydrological station was analysed and the maximum discharge values per annum were identified. The data was analysed per year to ensure a homogeneous dataset that filtered out possible seasonal influences.

Based on the annual maximum river discharge values, a Generalised Extreme Value (GEV) distribution was fitted to the data, as shown in Figure 60. Using the fitted GEV distribution, an extrapolation was subsequently carried out to calculate the discharge level associated with specific return periods (see Figure 60). To account for the uncertainty in the extrapolation process, confidence intervals were calculated (see Figure 60) using a maximum likelihood method via the

Fisher matrix. Therefore, the extrapolation process provided an estimate of the characteristic discharge value associated with a given return period at a particular location, along with upper and lower bound values. An optimisation routine was subsequently employed to fit a lognormal distribution, where the mean value corresponded to the mean characteristic value that was obtained according to the GEV extrapolation and the upper and lower bound values corresponded to the 2.5th and 97.5th percentile values, respectively.

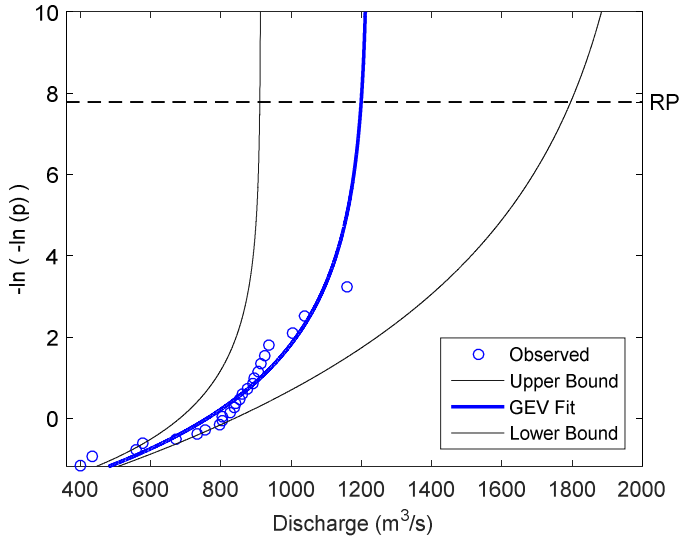

Figure 60: GEV distribution fit to historical river discharge data

The water depths associated with the extreme river discharge scenarios identified in Figure 60 were also identified. This was based on a correlation analysis that considered river discharge values associated with a given hydrological station and the associated water depths in the same river. To perform the analysis, a statistical approach was also adopted, as outlined in Figure 61.

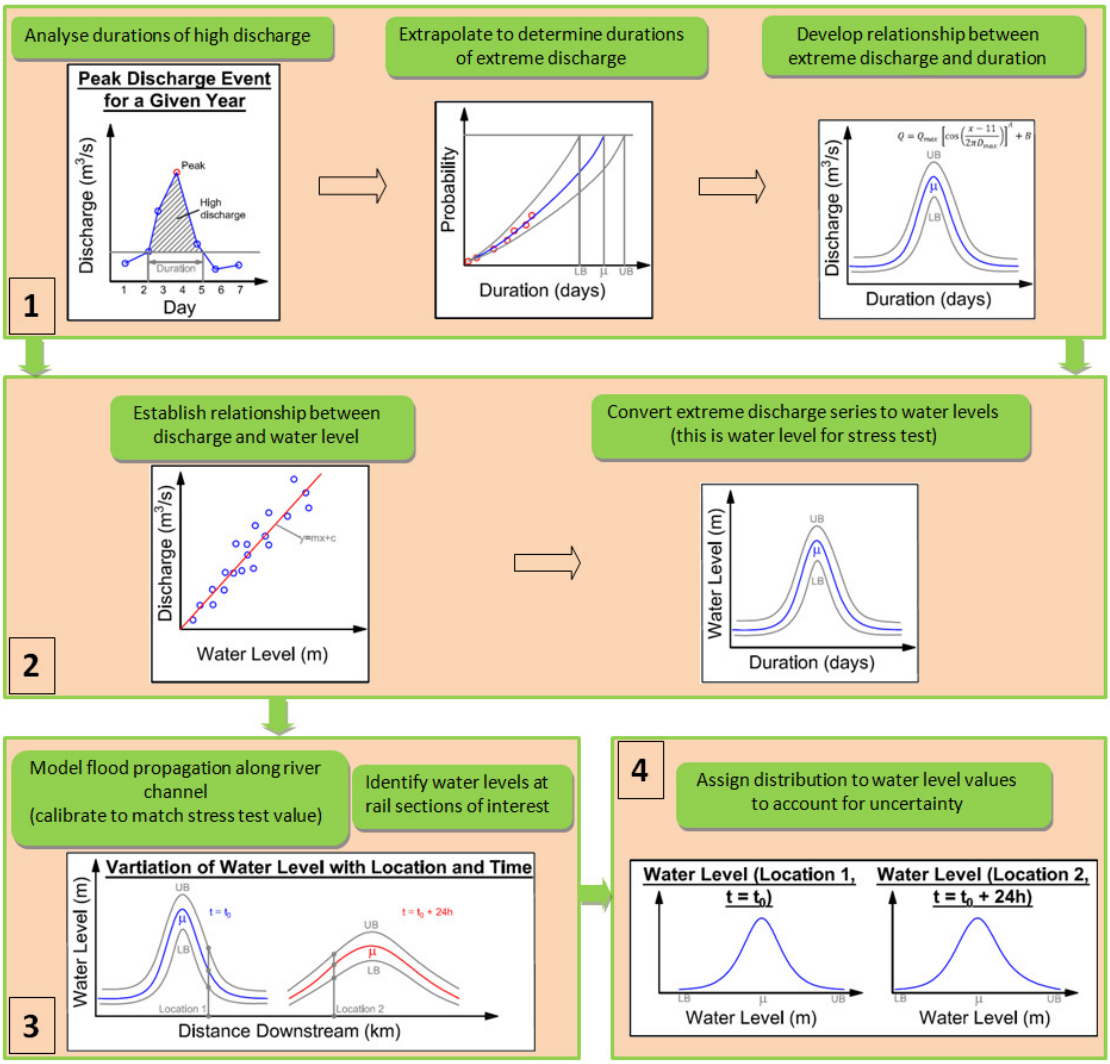

Figure 61: Methodology employed to establish relationship between extreme river discharge values and associated water depths downstream

The methodology employed consisted of four steps. In the first step (see Figure 61), the peak yearly river discharge values were analysed to establish the relationship between high discharge values and the duration for which these values occurred during a flood event. To do so, the 25 years of river discharge data for a given hydrological station was analysed to establish the measured discharge values for 10 days prior to and 10 days following the date of the peak river discharge value occurrence per annum. This data was subsequently plotted as a hydrograph for each of the 25 years, as shown in Figure 62, where the mean hydrograph is also shown.

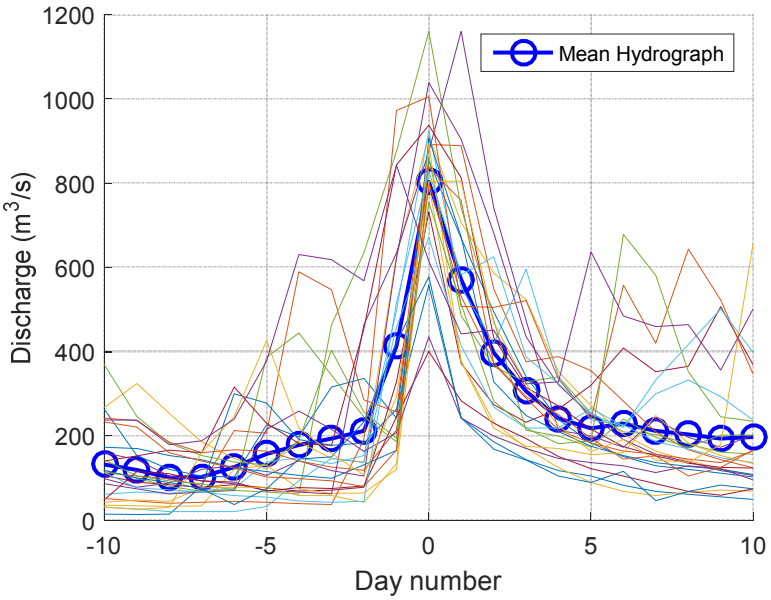

Figure 62: River discharge values for 10 days prior to and 10 days following the date of the peak river discharge per annum

The data was subsequently analysed to determine the number of days for which the discharge values were greater than twice the average daily value for the period of 10 days prior to and 10 days following the date of the peak discharge. This measure was used to establish the duration of each of the 25 annual peak river discharge value scenarios. The dependency between the maximum river discharge values and their corresponding durations was subsequently analysed according to a correlation analysis, as shown in Figure 63 and a low correlation was shown. This established that the discharge values and the durations were independent parameters and, therefore, the joint distribution of the discharge values and the duration of these values was determined by multiplying the independent distributions for these parameters.

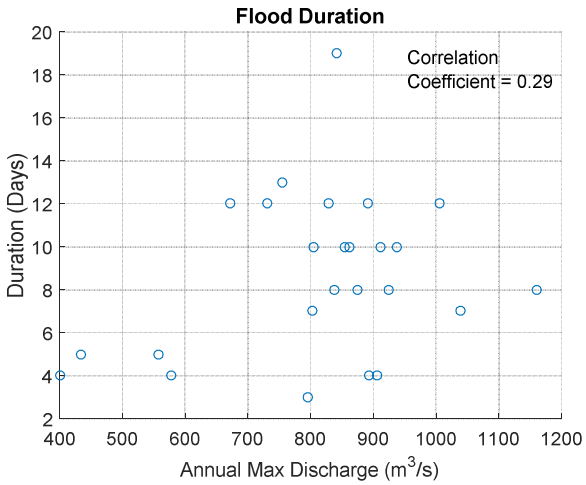

Figure 63: Correlation analysis between extreme river discharge value and duration of extreme discharge value

Furthermore, an extrapolation was subsequently conducted to determine the duration of the peak river discharge values for various return periods (see Figure 64). In this case it was found that a Normal distribution was most representative of the data. Lower and upper bound values were also calculated to provide a measure of the associated uncertainty.

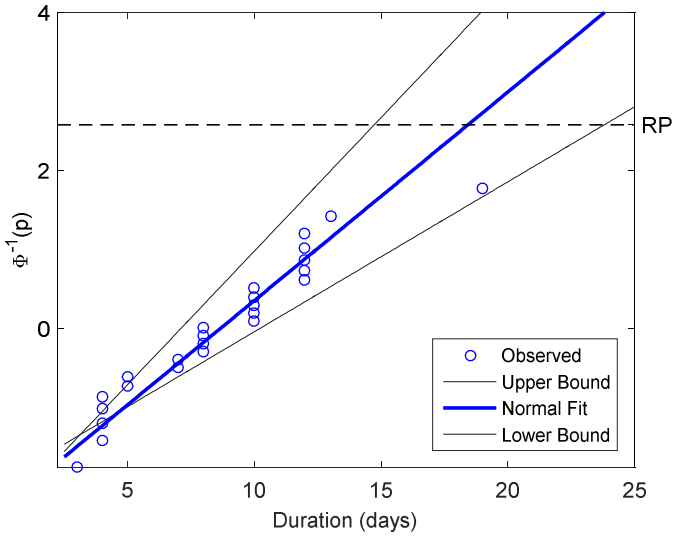

Figure 64: Normal distribution fit to duration of peak river discharge data ('RP' = Return Period)

Equation 3 was subsequently employed to determine the river discharge values for the 10 days prior to and the 10 days following the extreme river discharge value that corresponded to a given return period, where Q represents the river discharge value (in m^3/s), D_{max} represents the characteristic duration of the peak discharge value (in days) calculated during the extrapolation process, A and B are constants that are determined from the measured river discharge data using a least squares method, and x represents the day that the river discharge value is evaluated. Note that the peak discharge value is assumed to occur on day 0, where the analysis timescale includes 10 days before the peak and 10 days after the peak.

$$Q = Q_{max}\left[cos\left(\frac{x-11}{2\pi D_{max}}\right)\right]^{A} + B \qquad \textbf{(3)}$$

Figure 65 presents the calculated discharge values based on Equation 3 where upper and lower bounds were included to account for the associated uncertainty. These were calculated from the 15% and 85% percentile river discharge values and the 15% and 85% percentile duration values, where the variable distributions were multiplied as they were considered to be independent parameters (see Figure 63). It is noted that this plot does not specifically represent a best fit to the observed data; rather it represents the best fit of the model described by Equation 3 to the data. This results in a best fit of the shape of the discharge series, with the vertical shift from the observed data resulting from the fact that the model represents the extreme discharge series of an extreme event (e.g. a 200 year discharge series). The predicted flood waves follow a typical cosine function shape, i.e. the water level rises from a starting water level to a maximum water level and then back to the starting water level again. For simplicity a symmetrical shape was assumed, although in reality flood waves usually show an asymmetric (hysteresis) shape because the rising limb is generally steeper than the falling limb (see D'Ayala and Gehl (2014)).

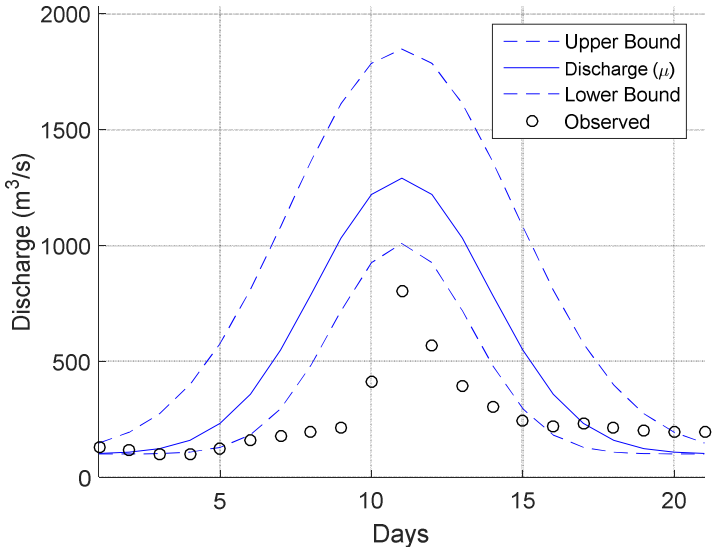

Figure 65: Discharge values as a function of time for extreme river discharge scenario

Step 2 of the methodology involved the determination of the relationship between river discharge values and the water depths (see Figure 61) based on the historical data. A simplified linear relationship was assumed between the value of river discharge at a specific location and the water depth at the same location, as shown in Figure 66. Figure 67 shows the discharge series from Figure 65 after it has been converted to a flood wave in terms of water levels, using the linear relationship shown in Figure 66.

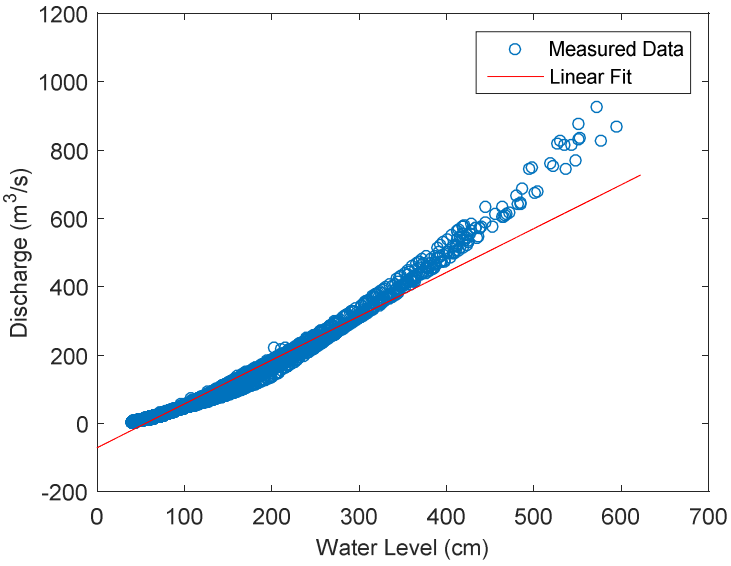

Figure 66: Linear fit to water level versus discharge measurements

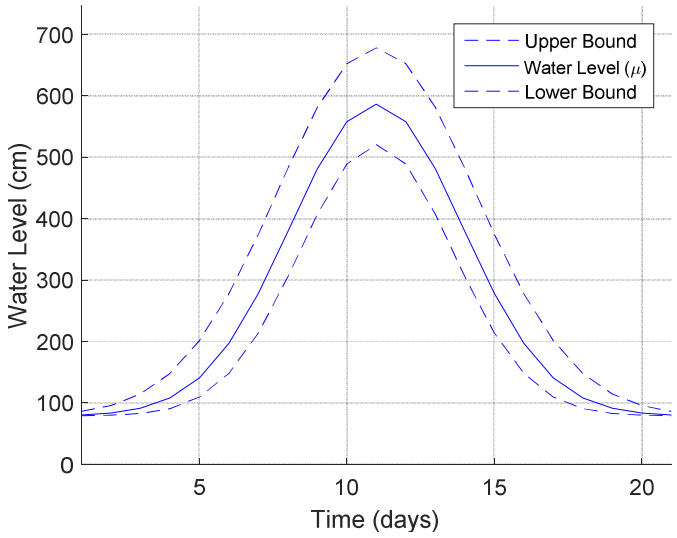

Figure 67: Predicted flood wave in terms of water levels

Step 3 of the methodology employed a linear hydrodynamic model to represent the propagation of the flood wave downstream that could be used to determine water depths at specific locations (see Figure 61). To do so, a relatively straightforward approach was adopted since it was not feasible to conduct detailed hydraulic modelling due to data limitations. Furthermore, more complex hydraulic modelling approaches are highly computationally expensive.

As such, a linear hydrodynamic model was adopted to predict the propagation of the flood wave (i.e. the movement of river water downstream). In this model, the river bed cross section was simplified as a prismatic box, with a flow carrying width, B_s, and a storage width at the water level, B, a constant slope, i, and a constant roughness coefficient, c_f. This model was employed to predict the propagated speed of the flood wave to be estimated downstream. Additionally, the model was used to determine the diffusion coefficient t, which describes how the flood wave flattens out while moving downstream.

Based on the assumed linear relationship between river discharge and water levels, the propagation speed at the location of the maximum water level, c, was calculated according to Equation 4, where R is the hydraulic radius, equal to the maximum water depth in case of a prismatic shape of the river bed. The diffusion coefficient, K, was calculated according to Equation 5, where U_e is calculated according to Equation 6.

$$c = \frac{\frac{3}{2}B_S}{B}\sqrt{gRi/c_f} \quad \textbf{(4)}$$

$$K = \frac{Q}{2iB} = \frac{dB_S U_e}{2iB} \quad \textbf{(5)}$$

$$U_e = \sqrt{gRi/c_f} \quad \textbf{(6)}$$

The flood wave downstream was described in time, t, and space, x, according to Equation 7, where a_0 is the minimum water level, P is a calibration constant that was specified to ensure that the water level $a(x,t)$ had dropped to half its height at time t, at location $x = 0$ (according to Equation 8, where $t_{0.5}$ is the time taken for the flood height to drop to half of its peak value).

$$a(x,t) = a_0 + \frac{P}{2\sqrt{\pi K t}} e^{-\frac{x^2}{4Kt}} \quad \textbf{(7)}$$

The equation for $a(x,t)$ is developed to show the propagation of a sudden peak flood at t=0 with a total volume of P. This allows the height of the flood wave to be calculated at various locations along the river at different points in time as the water dissipates after the occurrence of the flood event. It is noted that in the above equation, for t=0, the theoretical water level would be infinity.

To calibrate Equation 7 to ensure that the flood wave height was equal to the extreme flood height for the chosen return period (i.e. the maximum water level calculated by converting the discharge series to water levels using the linear relationship between discharge and water level), the value of t_0 (at x = 0 m) was calculated. Equation 8 was subsequently employed to calculate the water height at any distance, x, from the hydrological station downstream at any point in time after t_0.

$$P = \left(\frac{a_{max}}{2} - a_0\right) * 2\sqrt{\pi K * 4t_{0.5} * 24 * 3600} \quad \textbf{(8)}$$

Figure 68 presented the propagated flood wave downstream at various points in time after the occurrence of a flood for a specific return period, as calculated according to Equation 8. To account for the associated uncertainty in terms of the water depth, the upper and lower confidence bounds that corresponded to the 5th and 95thpercentile of the distribution were considered.

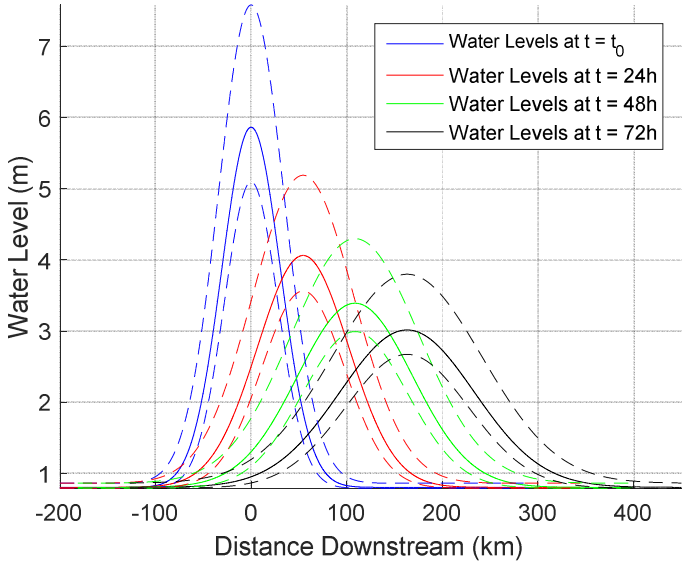

Figure 68: Propagation of flood wave over space and time

The final step of the methodology, step 4, involved determining a suitable distribution to represent the associated uncertainty in terms of the water depth. As part of this process, upper and lower confidence bounds corresponding to the 2.5th and 97.5th percentile of the distribution were considered with a normal distribution typically being adopted.

6.6.1.3 Climate change effects

Climate change has led to the increased frequency and intensity of meteorological events (IPCC, 2014). Several scientific models have been developed to quantify the increase in severity and frequency of such events (Beniston et al., 2007). However, such modelling approaches require significant data inputs and calibration. Therefore, specific modelling of the impact of climate change on rainfall durations, as well as river discharge values and the associated river water depth was not conducted for the Croatian case study. However, the potential impacts of climate change were considered in relation to the return periods analysed for the stress tests described herein.

6.6.2 Network Vulnerability: Rainfall-Triggered Landslides

There are two main geological regions in Croatia that result in two distinct ground failure mechanisms in two regions, as shown in Figure 69. For the western part of Croatia along the Adriatic Sea, the predominant ground failure mechanism consists of rockfalls. For the north eastern Croatian region known as Continental Croatia, the predominant ground failure mechanism consists of landslides, which were the focus of the stress tests performed for the Croatian rail network.

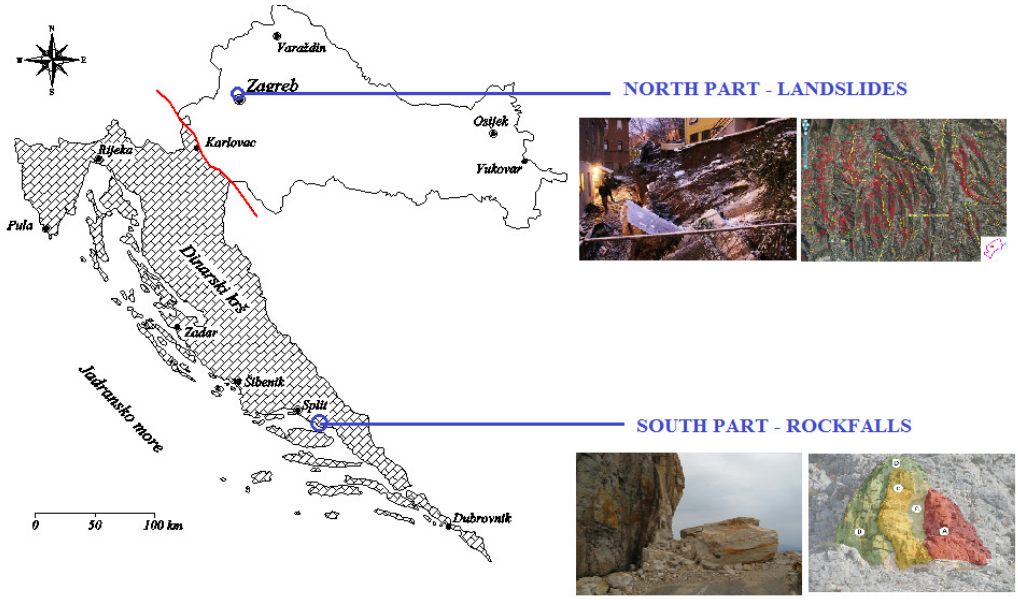

Figure 69: Two predominant ground failure mechanisms in Croatia (Librić et al., 2014)

To characterise the vulnerability of the rail network to rainfall-triggered landslides, fragility functions were employed for specific sections of rail track along the case study rail network in the north eastern region of Croatia that were located adjacent to cuttings or embankments. Since fragility functions for infrastructure earthworks due to rainfall-triggered landslides are not commonly available, a similar methodology to that described in INFRARISK Deliverable 3.2 (D'Ayala and Gehl, 2015) was employed for the development of fragility functions for sections of rail track due to shallow rainfall-induced landslides. This methodology was used to calculate the probability of a slope (i.e. cutting or embankment) reaching or exceeding a pre-defined damage state in terms of the adjacent section of rail track as a function of a measure of intensity of the rainfall loading.

The development of fragility functions for transport infrastructure earthworks described by D'Ayala and Gehl (2015) is based on unsaturated soil mechanics theory to determine the effect of rainfall

infiltration on the stability analysis of slopes in terms of a translational (planar) shallow landslide failure mechanism assumming an infinite slope model (see D'Ayala and Gehl, 2014). In the context of the INFRARISK project, shallow landslides are those that have a small depth relative to their length and a wetting front depth of less than 2m (D'Ayala and Gehl, 2014). To determine the response of a slope to a rainfall event, a seepage analysis may be performed to predict slope behaviour under reduced suction due to the wetting front that develops in the slope. However, since limited data was available in relation to specfic embankments or cuttings along the Croatian rail network, a simplified relationship between rainfall and suction was established based on the literature rather than conducting a seepage analysis, which did not account for site specific geological conditions.

For the Croatian case study, the rainfall event was considered in terms of the rainfall duration, *D*, for a given rainfall intensity value, *I*. Figure 70 illustrates this relationship between rainfall duration and the depth of the wetting front that was established based on research conducted by Zhang et al. (2011) for a similar topography to that of the current case study. This relationship is described by Equation 9 where S is the matric suction, γ_{m} is the unit weight of water, Z is the depth to the point of interest in the slope and d is the wetting front depth.

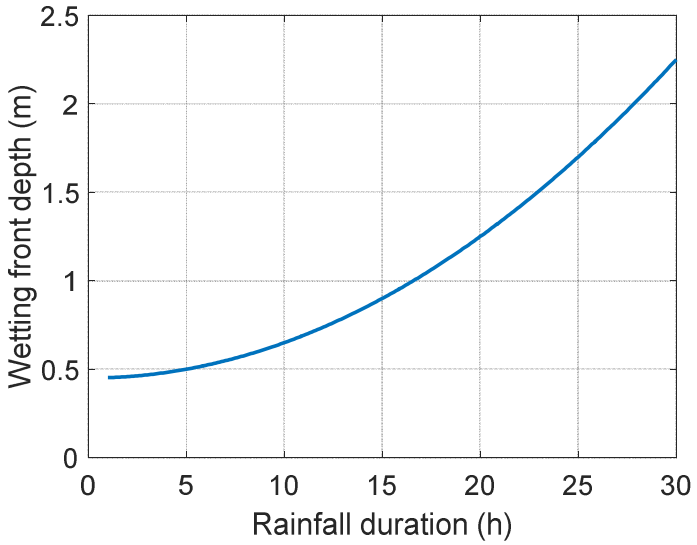

Figure 70: Relationship between rainfall duration and wetting front depth

$$S = \gamma_m(Z - d) \qquad \textbf{(9)}$$

The damage states defined for the fragility functions considered the landslide depth, i.e. the amount of soil material deposited since this measure enabled the functionality loss of the adjacent rail section to be determined. For the Croatian case study, a 1m clearance was assumed between the base of the slope and the adjacent rail track in all cases, as illustrated in Figure 71, where α is the angle of the slope. The damage states were subsequently defined in terms of distance that the landslide material extended beyond the base of the slope (see Table 16) based on the damage definitions outlined by D'Ayala and Gehl (2015). Since the wetting front will most likely have progressed to a certain distance from the failure plane prior to rainfall reaching the intensities investigated, the distances from the failure plane to the wetting front for failure planes of 1.0m, 1.75 and 2.5m were assumed to be 0.5m, 1.0m and 1.5m, respectively.

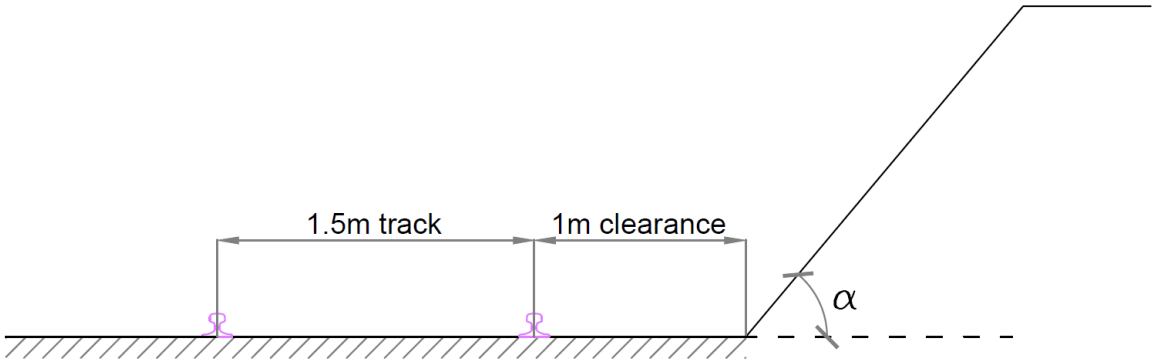

Figure 71: Assumed geometry for the development of rainfall-triggered landslides

Damage State	Damage Description	Landslide Depth (m)
1: Low	Minor slip, eroded surface, not affecting track elements.	1.00
2: Medium	Significant embankment material loss, not affecting track elements.	1.75
3: High	Deeper slide, significant embankment material loss affecting track elements.	2.50

Table 16: Damage states for rail sections due to rainfall-triggered landslides

Fragility functions were developed for four slopes that were identified along the Croatian rail network. To develop fragility functions for these slopes, a typology was initially developed for each of the slope locations, as outlined in Table 17. A reliability analysis was performed to consider the uncertainty associated with the geotechnical parameters for the site soil properties of the slope, as outlined in Table 18. The mean values of the geotechnical parameters were adopted based on the expert opinion for the soil properties of this region (European Commission and the European Soil Bureau Network, 2004). Coefficients of Variation (COV) values were adopted from the literature (Sivakumar et al., 2005; Phoon and Kulwahy, 1999).

Category	Location			
	A	B	C	D
Network type and level	Rail	Rail	Rail	Rail
Object type	Embankment	Embankment	Embankment	Embankment
Geometry (slope angle)	20°	30°	50°	60°

Table 17: Earthworks typology for locations identified as vulnerable to rainfall-triggered landslides

Geotechnical parameter	Mean	COV
Cohesion, c' (kPa)	5	0.1
Friction angle, ϕ' (°)	30	0.21
Unit weight, γ (kg/m^2)	19	0.9

Table 18: Geotechnical parameters for locations identified as vulnerable to rainfall-triggered landslides

For the Croatian case study, fragility functions were developed due to rainfall-triggered landslides for three rainfall intensity values; 10mm/h, 15mm/h and 20mm/h as illustrated in Figure 72, Figure 73 and Figure 74, respectively. Fragility functions were developed for each of the slope locations considered and for the three damage states. Further information in relation to the location and description of the slopes analysed is presented in Section 6.7.1 and Appendix B.

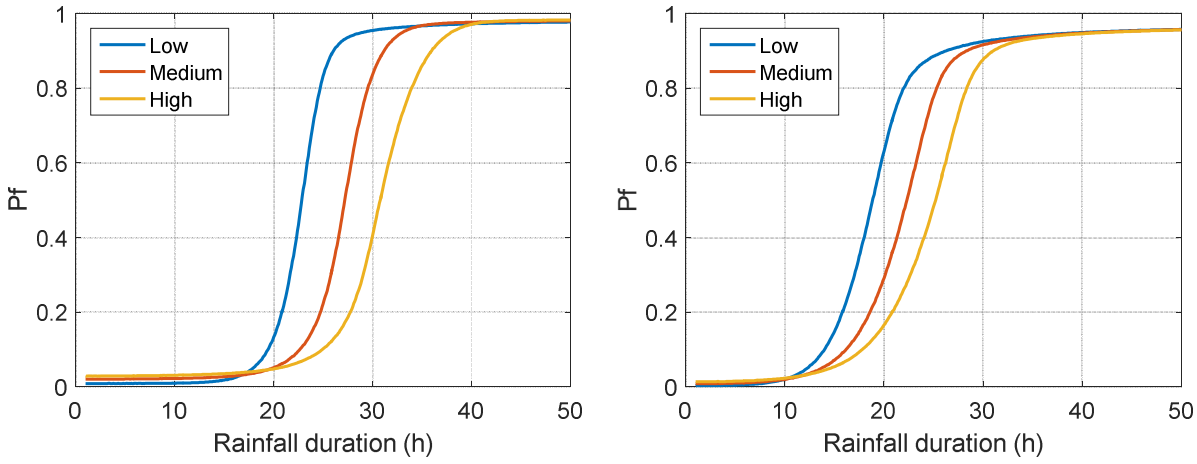

a) Slope location A

b) Slope location B

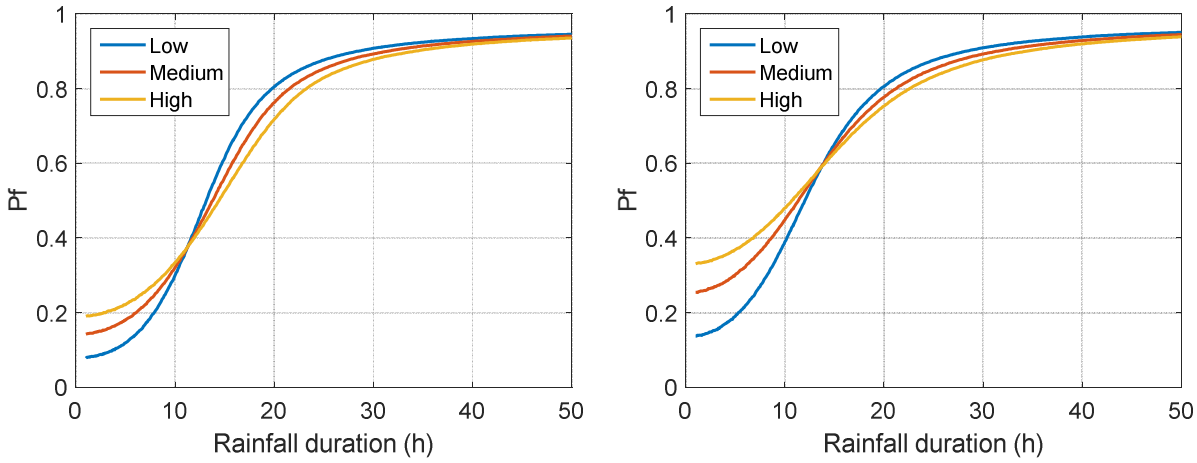

c) Slope location C

d) Slope location D

Figure 72: Fragility functions for rainfall Intensity of 10 mm/h

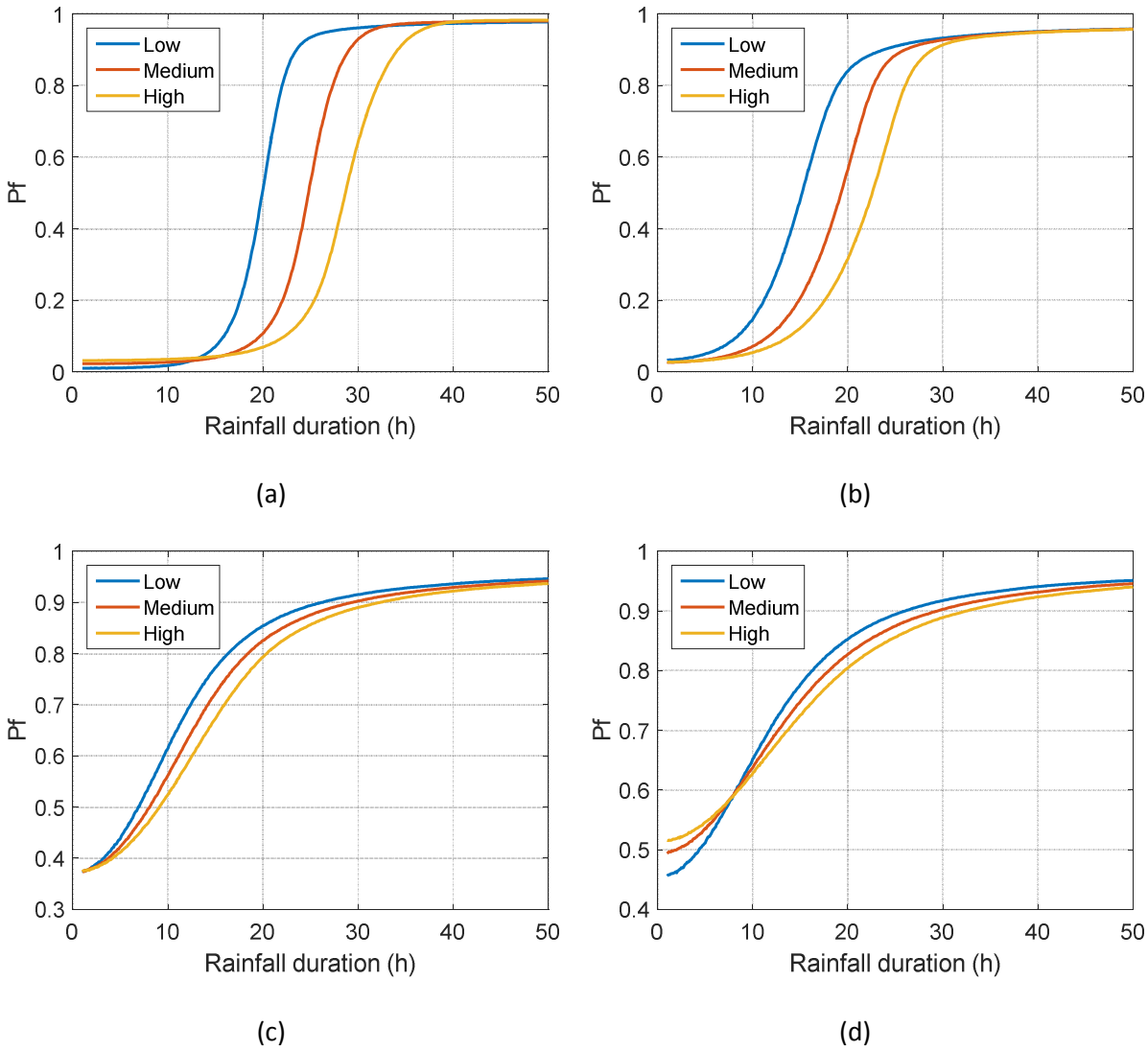

Figure 73: Fragility functions for rainfall Intensity of 15 mm/hr for (a) $\phi' = 20^o$, (b) $\phi' = 30^o$, (c) $\phi' = 50^o$, (d) $\phi' = 60^o$

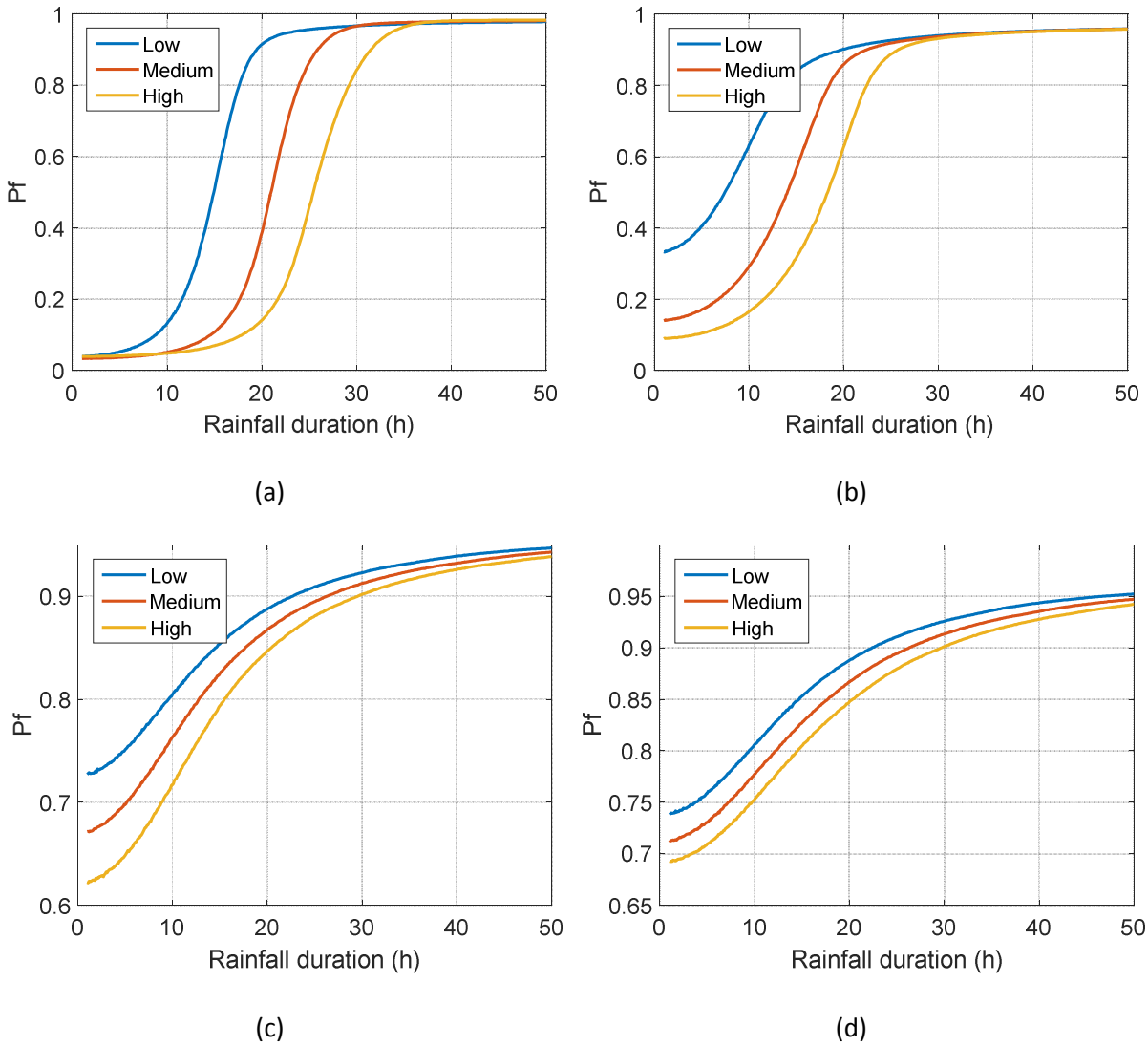

Figure 74: Fragility functions for rainfall Intensity of 20 mm/hr for (a) $\phi' = 20^o$, (b) $\phi' = 30^o$, (c) $\phi' = 50^o$, (d) $\phi' = 60^o$

6.6.3 Network Vulnerability: Bridge Scour

One of the three vulnerability aspects of the Croatian rail network considered in the analysis was the potential for bridge scour due to an extreme, low probability flood hazard scenarios (see Section 6.4). The 'Kupa Karlovac' bridge was identified as a bridge along the rail network that is potentially susceptible to scour due to the fact that it includes a pier located in the River Kupa, as shown in Figure 75 and Figure 76. This bridge is located along on the rail line connecting Zagreb and Rijeka and is of significant importance for international rail transport. Further details of the Kupa Karlovac bridge can be found in Appendix B. There was a hydrological data station located upstream from the bridge, that provided daily maximum values of water flow (m^3/s) that were extrapolated to extreme quantile levels for various return periods according to the flood hazard model described in Section 0.

Figure 75: Kupa Karlovac rail bridge (Google Street View Image)

Figure 76: Kupa Karlovac rail bridge (Google Satellite Image)

6.6.3.1 Scour analysis

The calculation of the total scour for the Kupa Karlovac bridge considered three components: 1) general scour, 2) contraction scour, and 3) local scour, as described by D'Ayala and Gehl (2014). To calculate the total scour for the bridge, a hydraulic model of the Kupa River in the vicinity of the bridge was generated using HEC-RAS software (HEC-RAS 4.1.0) based on cross section data for the River Kupa, geometric data for the Kupa Karlovac bridge and the adjacent road bridge, as well as assumed hydraulic parameters. Detailed information in relation to hydraulic modelling for scour analysis is described in INFRARISK Deliverable 3.1 (D'Ayala and Gehl, 2014).

Terrain information regarding the river bed of the Kupa River was obtained from a Digital Elevation Model (DEM) for Croatia and cross section information for the river bed of the Kupa River that was available at the location of the Brodarci and Karlovac hydrological data stations, as shown in Figure 77. The hydrological model was generated in HEC-RAS based on this topographical information, where river cross sections were specified at 10m intervals.

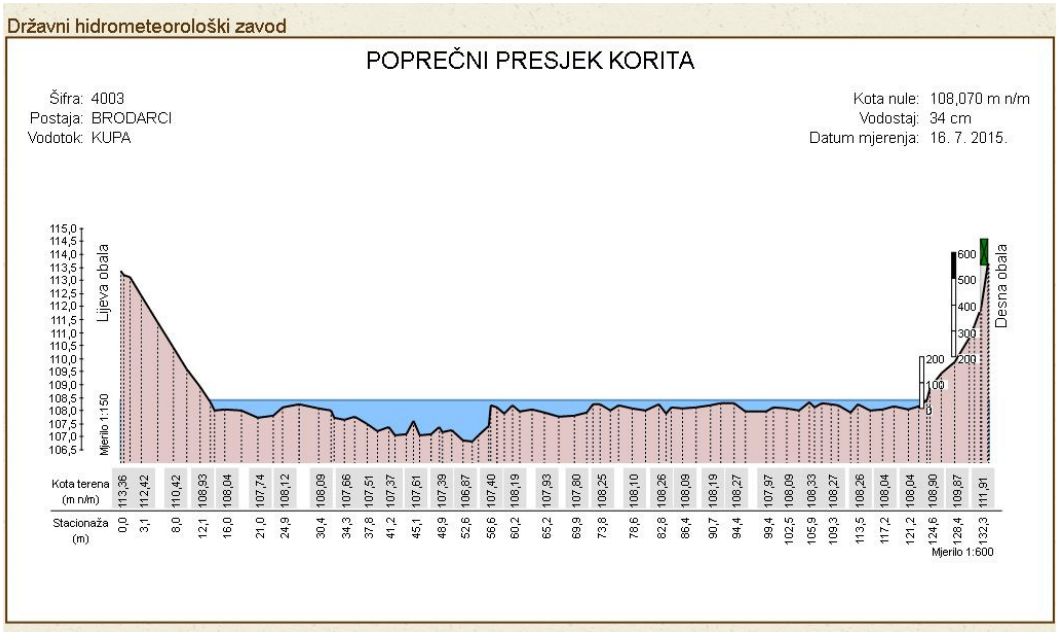

a) Brodarci hydrological station

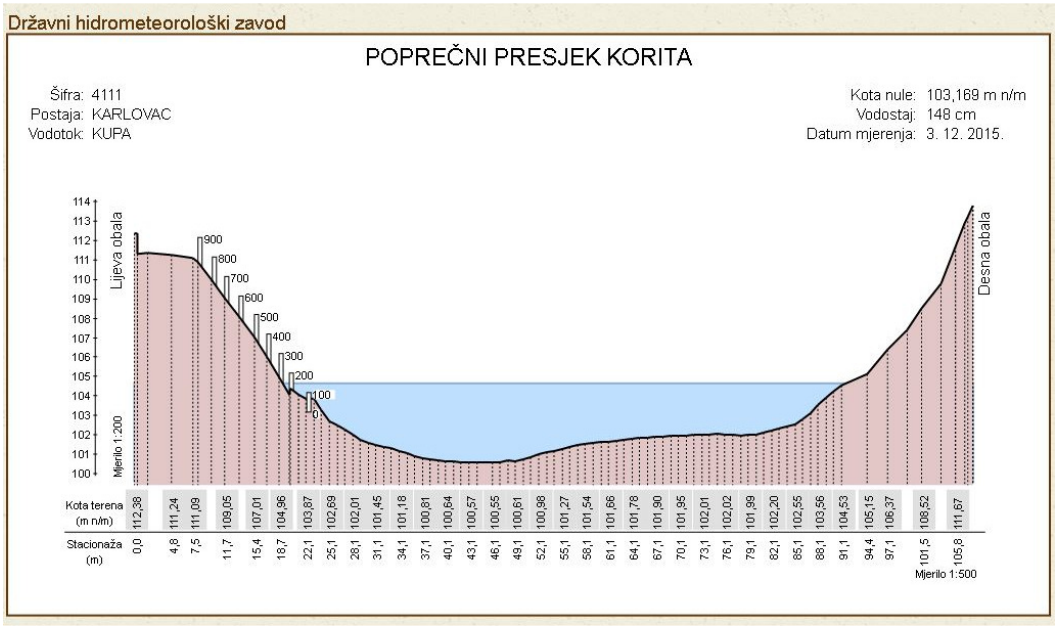

b) Karlovac hydrological station

Figure 77: Cross sections of River Kupa (http://hidro.dhz.hr/)

The geometry of the Kupa Karlovac bridge was obtained from Croatian Railways (HZ Infrastruktura, 2013) and is described in Appendix B. This was modelled in the HEC-RAS hydrological model since structures such as bridges and culverts cause an energy loss in terms of the river discharge.

Additionally, the road bridge located 27m downstream of the railway bridge was included in the hydrological model since any existing structures (e.g. bridges, culverts, levees) can also impact the river flow. The geometry for the road bridge was estimated based on a visual inspection using Google Street View.

Information regarding the granulometry of the river bed was also needed for the hydrological model to estimate the scour values as a function of the river discharge. Granulometric data was obtained for the River Kupa from a sediment study of Croatia (Bekic and Oskorus, 2012), as shown in Figure 78. The parameters needed to characterise the bed material were the median diameter of bed material, D_{50}, and the 95th percentile grain diameter, D_{95}. Values of 2.5mm and 8.0mm were adopted for D_{50} and D_{95}, respectively based on this data source.

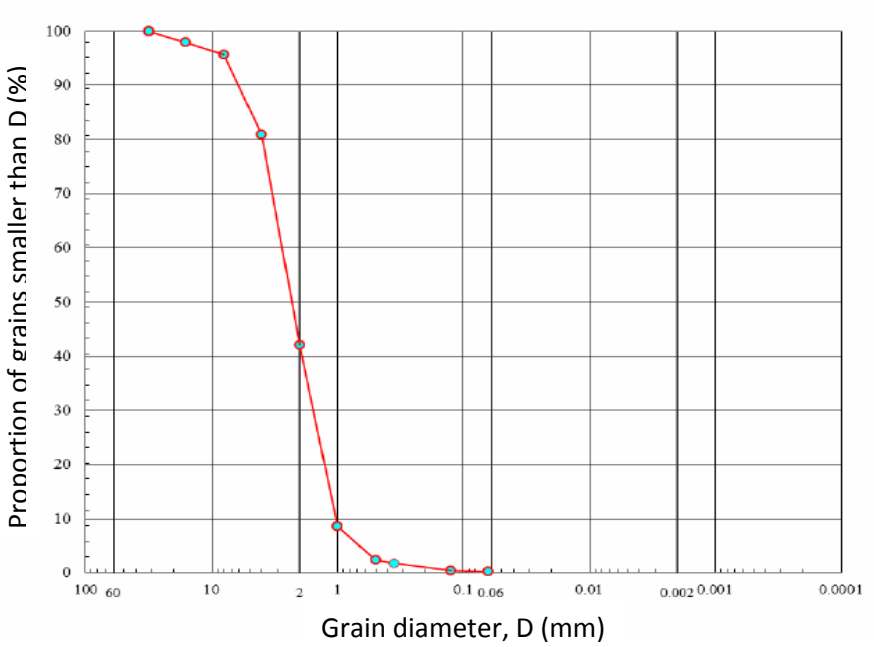

Figure 78: River Kupa granulometry information (Bekic and Oskorus, 2012)

Since the goal of the scour calculation was to facilitate the development of fragility functions for the Kupa Karlovac bridge, the scour analysis was performed for values of river discharge for the River Kupa that varied between 50 m^3/s and 1950 m^3/s at 50 m^3/s intervals, as illustrated in Figure 79, where the water surface is shown for different values of river discharge. Figure 80 provides a three-dimensional view of the HEC-RAS hydrological model. The results of the scour analysis are presented in Table 19, which are illustrated in Figure 81 for a river discharge value equal to 1050 m^3/s. Notably the hydrological model did not model any scour protections at the piers of the bridge.

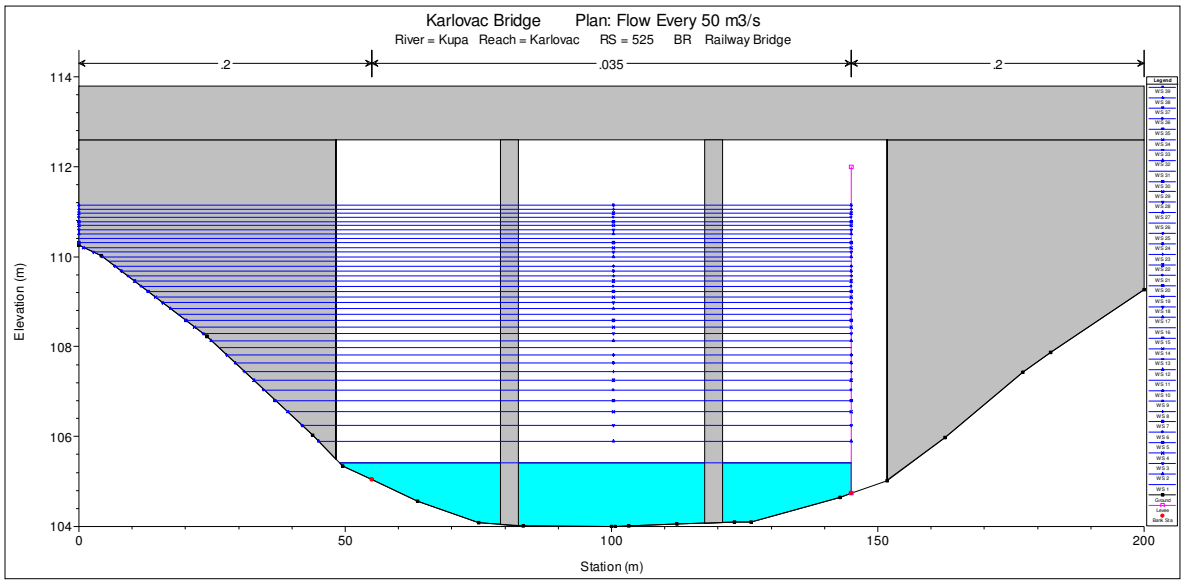

Figure 79: HEC-RAS hydrological model used to simulate various river discharge values for the River Kupa in the vicinity of the Kupa Karlovac bridge

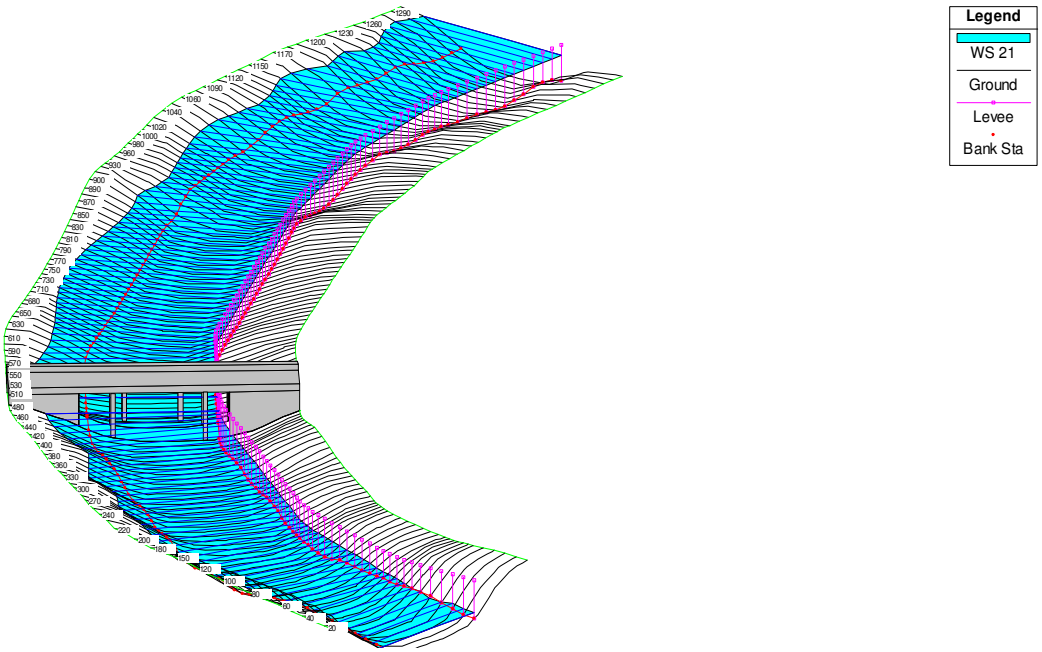

Figure 80: View from downstream of HEC-RAS hydrological model for the Kupa Karlovac bridge

Flow	Abutment South (m)			Pier South (m)			Pier North (m)		
(m^3/s)	A	B	C	A	B	C	A	B	C
50	0.00	0.09	0.09	2.49	0.35	2.84	2.46	0.35	2.81
100	0.42	0.10	0.52	3.00	0.66	3.66	2.97	0.66	3.63
150	0.72	0.19	0.91	3.36	0.92	4.28	3.33	0.92	4.25
200	1.01	0.26	1.27	3.64	1.14	4.78	3.61	1.14	4.75
250	1.28	0.32	1.61	3.87	1.37	5.24	3.84	1.37	5.21
300	1.53	0.39	1.92	4.07	1.55	5.62	4.04	1.55	5.59
350	1.76	0.44	2.20	4.46	1.75	6.21	4.43	1.75	6.18
400	1.97	0.49	2.46	4.63	1.97	6.60	4.60	1.97	6.57
450	2.18	0.53	2.71	4.80	2.17	6.97	4.77	2.17	6.94
500	2.39	0.58	2.97	4.55	2.33	6.88	4.52	2.33	6.85
550	2.58	0.62	3.20	4.67	2.51	7.18	4.65	2.51	7.16
600	2.76	0.66	3.42	4.79	2.66	7.45	4.77	2.66	7.43
650	2.92	0.70	3.62	4.91	2.85	7.76	4.89	2.85	7.74
700	3.10	0.73	3.83	5.02	3.06	8.08	5.00	3.06	8.06
750	3.26	0.77	4.03	5.13	3.22	8.35	5.11	3.22	8.33
800	3.42	0.80	4.22	5.23	3.40	8.63	5.21	3.40	8.61
850	3.58	0.84	4.42	5.32	3.53	8.85	5.30	3.53	8.83
900	3.74	0.87	4.61	5.42	3.68	9.10	5.40	3.68	9.08
950	3.90	0.90	4.80	5.52	3.87	9.39	5.50	3.87	9.37
1000	4.04	0.93	4.97	5.60	4.03	9.63	5.58	4.03	9.61
1050	4.17	0.96	5.13	5.58	4.18	9.76	5.66	4.18	9.84
1100	4.32	0.99	5.31	5.76	4.35	10.11	5.74	4.35	10.09
1150	4.45	1.02	5.47	5.84	4.50	10.34	5.83	4.50	10.33
1200	4.59	1.05	5.64	5.93	4.64	10.57	5.91	4.64	10.55
1250	4.73	1.09	5.82	6.00	4.77	10.77	5.98	4.77	10.75
1300	4.86	1.27	6.13	6.07	4.94	11.01	6.05	4.94	10.99
1350	5.00	1.43	6.43	6.15	5.11	11.26	6.13	5.11	11.24
1400	5.13	1.54	6.67	6.21	5.22	11.43	6.20	5.22	11.42
1450	5.26	1.72	6.98	6.28	5.39	11.67	6.26	5.39	11.65
1500	5.45	1.86	7.31	6.35	5.53	11.88	6.33	5.53	11.86
1550	5.67	2.00	7.67	6.42	5.67	12.10	6.41	5.67	12.09
1600	5.86	2.14	8.00	6.49	5.82	12.31	6.47	5.82	12.29
1650	6.06	2.29	8.35	6.55	5.97	12.52	6.53	5.97	12.50
1700	6.25	2.40	8.65	6.62	6.08	12.70	6.60	6.08	12.68
1750	6.44	2.55	8.99	6.68	6.23	12.91	6.67	6.23	12.90
1800	6.63	2.70	9.33	6.74	6.38	13.12	6.72	6.38	13.10
1850	6.81	2.82	9.63	6.81	6.50	13.31	6.79	6.50	13.29
1900	6.99	2.96	9.95	6.86	6.64	13.50	6.84	6.64	13.48
1950	7.17	3.08	10.25	6.93	6.75	13.68	6.91	6.75	13.66

Table 19: Calculated scour depths as a function of the river flow rate (A = local & contraction scour, B = general scour, C = total scour)

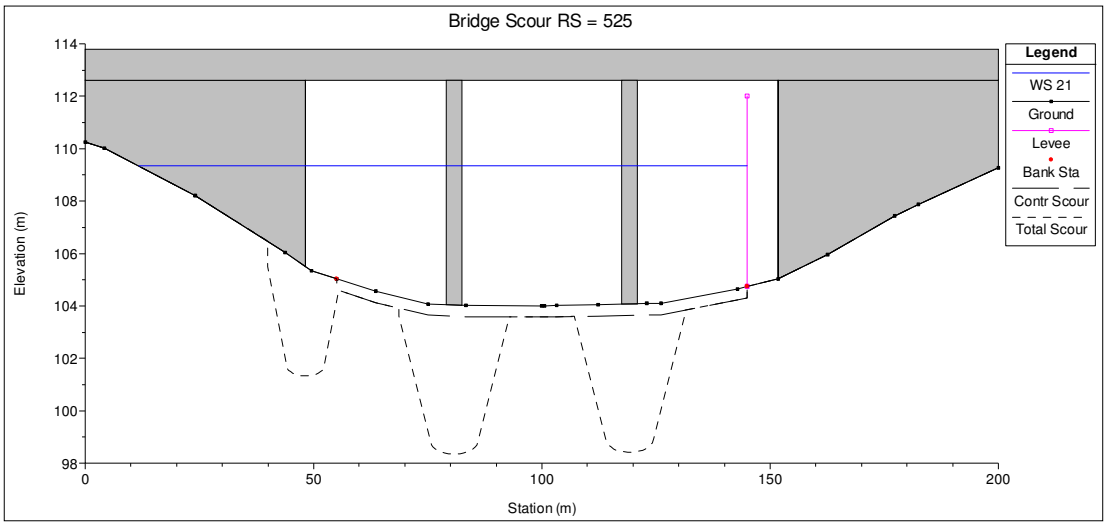

Figure 81: Calculated scour depths at the Kupa Karlovac bridge according to the HEC-RAS hydrological model (corresponding to 1050 m^3/s)

6.6.3.2 Determination of corresponding bridge damage states

The Kupa Karlovac bridge was subsequently assessed in terms of the potential for damage due to scour. Geotechnical and structural failure of the piles were considered. Since the length of piles for the bridge was unknown, the expected pile lengths were estimated and this was used in conjunction with the results of the scour analysis to determine the potential bridge damage. Damage states were defined for the bridge and fragility functions were subsequently developed for each damage state as a function of river discharge, which was the selected intensity measure to evaluate the associated hazard (i.e. scour).

To calculate the loading on the bridge foundations, the dead load and imposed load were initially estimated. The dead load was estimated based on the available structural drawings for the bridge. The imposed load was estimated using the LM71 and SW/0 load models in Eurocode 1 (CEN, 2010). A conservative alpha factor of 1.33 was applied in the imposed load calculations and a dynamic amplification factor of 1.06 was calculated and applied. Table 20 and Table 21 summarise the loading estimates for the bridge.

Element	Vertical Dead Load (kN) – Unfactored		
	Superstructure	Substructure	Total
Pier North	1201	6212	7413
Pier South	1201	6212	7413
Abutment South	368	8698	9066

Table 20: Estimated dead loading for Kupa Karlovac bridge

Element	Imposed Load (kN)		
	LM71	SW/0	Critical Case
Pier North	5391	4774	5391
Pier South	5391	4774	5391
Abutment South	2360	2263	2360

Table 21: Estimated imposed loading for Kupa Karlovac bridge

Information provided by Croatian Railways in relation to the Kupa Karlovac bridge indicated that the foundations consisted of 70 timber piles per pier and 60 timber piles per abutment (HZ Infrastruktura, 2013). However, the length of the piles was unknown. To estimate the pile lengths, calculations were performed to determine the pile lengths that would be required in order to comply with current design practice and the uncertainty associated with the length of the piles was incorporated in the analysis by considering three cases: 1) a minimum pile length required to meet current design standards, 2) an expected pile length, which provides 20% excess capacity, 3) a maximum pile length, which provides 40% excess capacity. The range of calculated pile lengths for the bridge are provided in Table 22.

Element	Minimum	Expected	Maximum
Abutment South	6.1 m	7.3 m	8.5 m
Pier North & South	5.9 m	7.1 m	8.3 m

Table 22: Estimated pile lengths for Kupa Karlovac bridge

The damage states for the railway bridge due to scour were defined based on expert judgement within the project consortium. Descriptions of the three damage states considered are presented in Table 23. Fragility functions were subsequently developed for the bridge to provide the probability of reaching or exceeding each damage state as a function of the magnitude of river discharge, which was related to the depth of scour and the bridge, as described in Section 6.6.3.1.

Damage State	Name	Description
1	Limit train speed during repair works	It is assumed that speed restrictions will be applied as soon as any significant scour damage is identified. Noticeable scour is taken as 1 m depth (± 0.5 m). This damage state is not based on any structural capacity checks.
2	Total interruption of the traffic during repair works	As the scour depth increases, this damage state is reached. It occurs once there is no longer capacity to support the imposed load, without dynamic amplification.
3	Total collapse of the structure	Collapse occurs when the piles no longer have capacity to support the unfactored dead load.

Table 23: Damage states defined for rail bridges due to scour

Two types of failure were considered for the piled foundations of the bridge due to scour; geotechnical failure and structural failure. For analysing the potential for a geotechnical failure of the piles, failure was assumed to occur when the scour depth extended beyond the depth of the base of the bridge pier or abutment, resulting in exposure of the piles and a corresponding reduction in skin friction and, consequently, overall pile capacity. The potential for structural failure of the bridge piles was assumed to occur when exposure of the piles occurred due to scour, where the potential for buckling failure (i.e. the critical failure mode) of the piles is present. To consider the potential for buckling of the bridge piles due to scour, Euler's formula for column buckling was employed, as outlined in Equation 10, where P_{cr} is the critical axial force which will cause pile to buckle, E is the modulus of elasticity of the timber piles, I is the second moment of area of the pile, L is the unsupported length of the pile and K is the effective length factor for the pile.

$$P_{cr} = \frac{\pi^2 EI}{(KL)^2} \qquad \textbf{(10)}$$

For the analysis, the piles were assumed to consist of a uniform diameter along their length. However, the methodology employed has the potential to be extended to consider piles that consist of a variable cross section (Davidson et al., 2011). Furthermore, a conservative deterministic estimate of the modulus of elasticity, $E = 8.3 \times 10^6$ kN/m^2 was assumed for the piles since the source of the timber that was used to construct the piles was unknown (Collin, 2002; Davidson, et al., 2011). In addition, a deterministic value of the depth to fixity below the scour depth equal to 2 m for the bridge piles was assumed (Davidson et al., 2011; Tomlinson and Woodward, 2014), as illustrated in Figure 82.

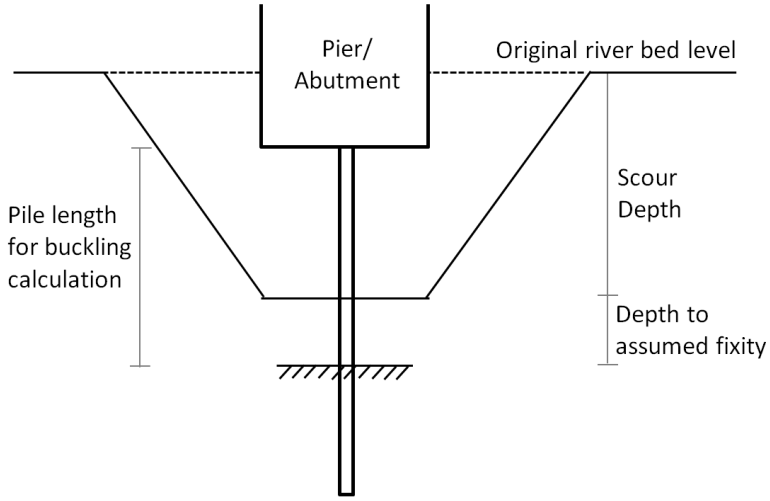

Figure 82: Pile length used for buckling calculation

Figure 83 demonstrates the reduction of the pile load capacity with increasing depth of scour and, consequently, exposed pile length, whereby the critical buckling load reduces rapidly as the exposed pile length increases. The transition between the damage states, with respect to structural failure, occurs when the piles buckle under the loads described in Table 23.

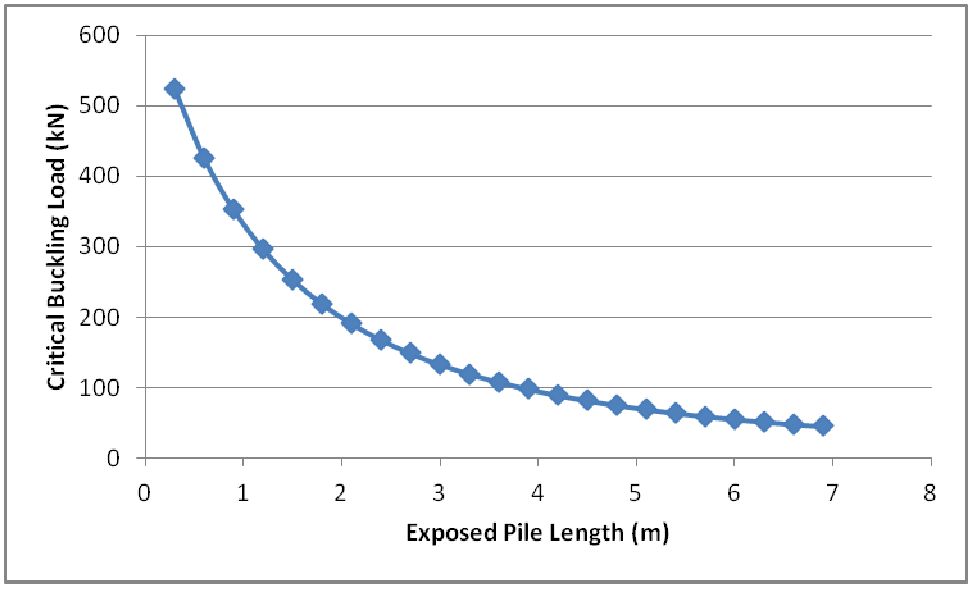

Figure 83: Critical buckling load for exposed piles of Kupa Karlovac bridge due to scour

6.6.3.3 Development of fragility functions

The critical scour depths for each damage state for Abutment South and the piers of the Kupa Karlovac rail bridge are presented in Table 24 and Table 25. In all cases, the critical scour depth for Damage States 2 and 3 was governed by geotechnical failure rather than structural failure.

Assumed Pile Length	Scour Depth		
	Damage State 1	Damage State 2	Damage State 3
Minimum	0.5 m	5.10 m	7.25 m
Expected	1.0 m	6.33 m	8.47 m
Maximum	1.5 m	7.54 m	9.69 m

Table 24: Scour depths for Abutment South of the Kupa Karlovac bridge that correspond to each damage state considered

Assumed Pile Length	Scour Depth		
	Damage State 1	Damage State 2	Damage State 3
Minimum	0.5 m	2.49 m	5.42 m
Expected	1.0 m	3.67 m	6.60 m
Maximum	1.5 m	4.85 m	7.78 m

Table 25: Scour depths for Piers North and South of the Kupa Karlovac bridge that correspond to each damage state considered

Based on the analysis described in Sections 6.6.3.1 and 6.6.3.2, fragility functions were subsequently developed for the bridge by firstly determining the river discharge values associated with each scour depth (see Table 19). A normal distribution was subsequently fitted to the data, where it was assumed that the minimum pile length corresponded to the 5th percentile of the distribution, the expected pile length corresponded to the mean and the maximum length corresponded to the 95th

percentile value. To plot the fragility functions for each damage state, the CDF of the distribution was subsequently generated, as shown in Figure 84. The fragility functions for damages states 2 and 3 were more critical for the bridge piers than the abutment due to their exposed location in the riverbed.

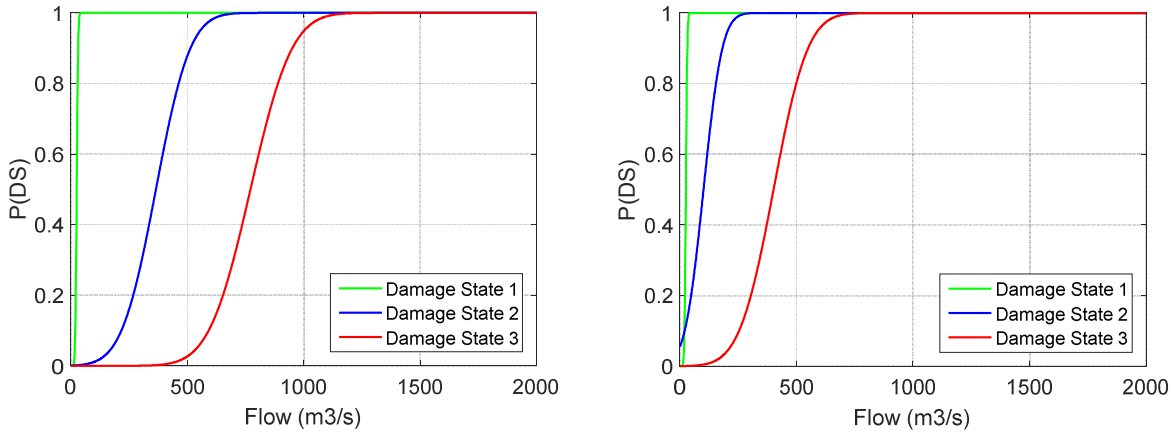

a) Abutment South b) Piers North & South

Figure 84: Fragility functions for the Kupa Karlovac bridge due to scour

The fragility functions presented in Figure 84 for the Kupa Karlovac bridge demonstrate a high probability that the various damage states will be reached or exceeded for relatively low values of river discharge. This is due to the fact that no bridge scour protections were considered in the analysis. Since bridge scour protections were evident for this bridge based on a visual inspection, the impact of their presence on the development of fragility functions for the rail bridge was subsequently considered.

The scour protection measures for the Kupa Karlovac bridge were assumed to withstand river discharge values for a 500 year flood event. As such, the fragility functions presented in Figure 84 were shifted to the right to account for their presence. To adopt a conservative approach, which accounted for the possible deterioration of the bridge scour protections, the lower bound 500-year river discharge value was considered (see Section 6.6.1.1). The fragility functions presented in Figure 84 were subsequently shifted to this value, as shown in Figure 85 for the bridge piers.

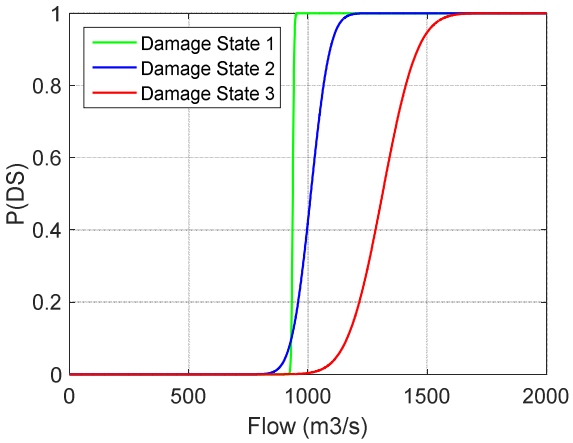

Figure 85: Fragility functions for Piers North & South of Kupa Karlovac bridge where scour protections were considered

Since it was not possible to model the bridge scour protection measures in the hydrological model described in Section 6.6.3.1, a relatively simple approach was adopted herein to account for their presence. However, the presence of bridge scour protection measures may not only shift the fragility functions but may also impact their slope (i.e. the dispersion values). More advanced hydrological modelling could be employed to obtain more accurate fragility functions that account for bridge scour protection measures. However, such an approach was not conducted herein.

Many assumptions were made in order to perform the scour analysis. There is uncertainty associated with each of these assumptions. However, for the purposes of simplifying this analysis, only the uncertainty associated with the pile length was considered when generating the fragility functions. In a detailed analysis, the uncertainty associated with all the assumptions could be considered. The following are some of the parameters which were assumed in this analysis but which have uncertainty associated with them:

- Pile length;
- Depth of pier/abutment below river bed (depth where piles begin);
- Level of scour protection;
- Pile diameter;
- Pile modulus of elasticity;
- Buckling is the critical structural failure mode;
- Soil properties;
- Dead load;
- River bed profile;
- Embedded pile depth required for fixity;
- Granulometry for scour analysis.

6.6.4 Network Vulnerability: Track Inundation

The vulnerability of the Croatian case study rail network to extreme, low probability flood events was also considered in terms of the potential for inundation of rail track sections. To do so, the potential for inundation of the rail track was assessed for two categories of topography: 1) inundation of track sections located on embankments (Figure 86), 2) inundation of track sections location in cuttings or at grade (Figure 87).

Figure 86: Rail track on embankment

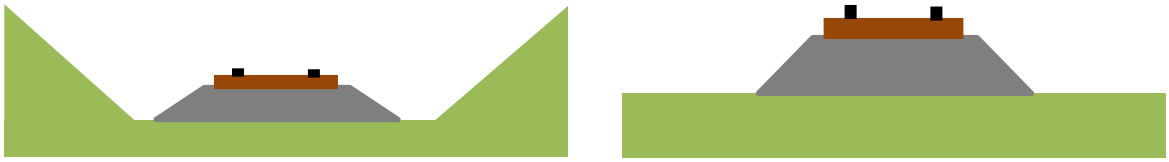

a) Cutting b) At grade

Figure 87: Rail track in cutting or at grade

To assess the potential for track inundation, the three damage states defined in Table 23 were considered and were modified to determine the associated maximum permissible train axle weights for each damage state, as presented in Table 26. Unfortunately, access to axle load data for the Croatian rail network was not available. As such, it was assumed that passenger trains would be prohibited when Damage States 1 and 2 have been reached. Furthermore, it was assumed that freight trains would be prohibited when Damage States 1 to 3 are reached.

Damage State	Name	Effect on functionality
0	Normal operation	None
1	Limited disruption	80 km/h speed limit and/or a 20 tonne axle weight limit.
2	Severe disruption	30 km/h speed restriction and/or a 15 tonne axle weight limit.
3	Closure	All functionality has been lost.

Table 26: Definition of damage states for sections of rail track due to inundation

Expert opinion was subsequently employed to determine the inundation depths associated with each damage state for sections of rail track. For each damage state, the minimum, expected and maximum inundation depth was defined. This information was then used to develop the fragility functions, in the same manner as described in Section 0. Table 27 and Table 28 present the minimum, expected and maximum values of inundation depth corresponding to the various damage states considered for rail tracks on embankments and rail tracks in cuttings or at grade, respectively.

Damage State	Name	Flood depth in relation to embankment height (bottom of ballast)		
		Minimum	Expected (Average)	Maximum
0	Normal operation	0%	25%	50%
1	Limited disruption	50%	75%	90%
2	Severe disruption	75%	90%	100%
3	Closure	100%	At rail level	Above rail level

Table 27: Inundation depth for each damage state for tracks on embankments

Damage State	Name	Flood depth in relation to embankment height (bottom of ballast)		
		Minimum	Expected (Average)	Maximum
0	Normal operation	No water on track	At underside of ballast (approx. 500mm below rail level)	At top of sleeper (approx. 150mm below rail level)
1	Limited disruption	At underside of sleeper (approx. 300mm below rail level)	At top of sleeper (approx. 150mm below rail level)	100mm below rail level
2	Severe disruption	100mm below rail level	25mm below rail level	At rail level
3	Closure	50mm below rail level	At rail level	Above rail level

Table 28: Inundation depth for each damage state for tracks at grade or in cuttings

For rail track on embankments, Table 27 shows the flood levels in terms of the height of the embankment, h_1, (see Figure 86), whilst the height of the top of the rail above the top of the embankment, h_2, was assumed to be equal to 0.5 m. Notably, the fact that flood water may possibly saturate the embankment material, leading to embankment failure upon recession of the flood water was also considered in Table 27.

The fragility functions that were developed based on expert judgement are presented in Figure 88. For demonstrative purposes, an embankment height, h_1, equal to 3m was assumed herein for rail tracks located on embankments (Figure 88a). However, for the stress tests performed for the Croatian rail network described in Section 6.7, fragility functions were developed for sections of rail track located on embankments using estimates of the height, h_1, of each embankment, based on visual inspection from Google Street View.

The lognormal distribution is used to generate the fragility functions. An optimisation routine is used to fit distributions where the objective is that the minimum corresponds to the 5th percentile, the expected value corresponds to the mode of the distribution and the maximum equals the 95th percentile. It also inverts the lognormal distribution to negative and translates it as the water level value can be less than or greater than zero. It should be noted that the optimisation routine cannot always achieve this objective perfectly but reasonably good fits are achieved.

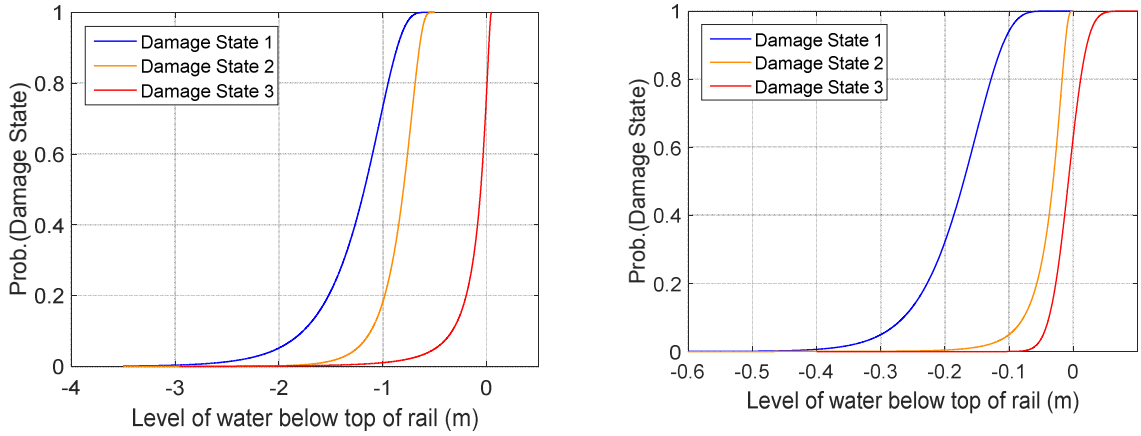

a) Rail track on embankment b) Rail track in cutting or at grade

Figure 88: Fragility functions for sections of rail track due to inundation

6.6.5 Functionality Loss

Based on expert opinion, distributions of intervention cost were determined for each damage state. Normal distributions were used, with mean and standard deviations. In addition, various levels of functionality loss were associated with each of the damage states. Table 29 summarises the costs and functionality loss associated with each of the damage states.

Damage State	Cost (€)		Repair Duration (days)		Functionality Loss
	Mean	SD	Mean	SD	
0	0	0	0	0	None
1	10,000	2,150	14	1.4	None
2	50,000	8,600	32	3.2	Track Closure
3	150,000	21,500	112	11.2	Track Closure

Table 29: Repair cost, durations and functionality loss for rail sections due to rainfall-triggered landslides

6.6.6 Travel Delays

The potential transport disruption for the Croatian rail network was analysed in terms of the passenger and freight demand for the rail lines analysed. The effect on passenger trains was assessed by examining timetable information for the Croatian network (www.prodaja.hzpp.hr) to find the number of trains per day using the relevant lines.

Similar information was not available for freight trains. Therefore, European Transport policy Information System data was employed (www.etisplus.eu) that provided transport statistics for European regions. This data provided the amount of rail freight (in tonnes) that is transported from eastern Croatia to western Croatia and vice versa. In the analysis, it was assumed that this freight is transported on the rail line through the Karlovac region as this is the only railway line that links the eastern and western regions of Croatia. The rail passenger and freight information considered in the analysis is summarised in Table 30.

Croatian Rail Line	Number of Passenger Trains Per Day (in each direction)	Tonnes of Freight Per Day (in each direction)
Zagreb – Duga Resa	37	2597
Karlovac – Bubnjarci	18	Not available
Zagreb – Varazdin	27	Not available

Table 30: Passenger and freight rail demand for selected Croatian rail lines

6.7 Risk Estimation

This section will describe the application of the 'Estimate risk' task in the risk assessment process described by Hackl et al. (2016) to perform stress tests for the Croatian case study. The methodologies and tools, as well as the format of the data employed at each stage of the analysis will be described. The stress test performed considered extreme, low-probability flood hazard scenarios. Two types of stress tests were performed: 1) extreme values of river flow in the vicinity of the Kupa Karlovac Bridge and corresponding values of water depth adjacent to a number of sections of the rail line and 2) extreme values of rainfall in the vicinity of Novi Marof in northern Croatia. The objective of the stress tests was to determine the associated risk and to ensure an acceptable level of risk.

6.7.1 Methodology

Stress tests were performed for the selected Croatian rail network for a variety of low probability, high consequence flood hazard scenarios based on the flood hazard model described in Section 6.6.1 and the network vulnerabilities described in Sections 6.6.3 to 6.6.2. For the purpose of the analysis, three return periods were considered for the flood hazard: 200, 500 and 1000 years. The impacts to the network were assessed in terms of the potential for damage to the rail track due to rainfall triggered landslides, bridge scour and track inundation. These network vulnerabilities were evaluated at particular locations along the selected rail lines that were deemed to be most vulnerable.

To assess the potential for rainfall-triggered landslides, a visual inspection of slopes was carried out using Google Earth combined with geographically referenced data available for the selected case study area. A more comprehensive approach would be to consult an existing database of slopes, giving details of the associated geological conditions, geometry, proximity to track etc. However, since such information was unavailable for the Croatian case study, the visual inspection was employed.

Four locations were identified along the selected railway lines where the potential for damage to the rail track due to rainfall-triggered landslides was deemed to be present, as outlined in Appendix B.

Although there may have been other locations along the selected rail network potentially vulnerable to rainfall-triggered landslides, the locations identified in this study were limited to those that: 1) were typical of engineered slopes on the network, 2) were in close proximity to a meteorology station that provided historic rainfall data, 3) had geological information available, 3) had geometric information available for the slope.

To identify rail bridges along the selected network that were vulnerable to scour, a visual inspection was also conducted using Google Street View. The analysis was limited to those bridges that also had sufficient data available (i.e. geometry, river bed information, flood hazard data, etc.) to perform a scour analysis. The Kupa Karlovac bridge was identified as being susceptible to scour since the bridge has a central pier located in the Kupa river. Furthermore, historic river discharge data was available for a nearby hydrological data station and detailed information was available for the bridge. As such, the vulnerability of this bridge to scour was considered in the analysis.

To identify sections of rail track along the selected network that were vulnerable to inundation, a preliminary study was carried out. This consisted of a high level comparison between flood hazard maps and the location of the rail lines in conjunction with a visual inspection using Google Street View that considered the following: 1) the proximity of the railway line to water courses, and 2) the elevation of the rail track relative to the surrounding topography. Additionally, the analysis was limited to those rail sections for which a nearby hydrological data station was present. Overall, three sections of the railway line were identified as potentially vulnerable to track inundation and were considered to be suitable for the analysis, as outlined in Table 31 and illustrated in Figure 89.

Site No.	Rail line	Section Length	No. of 1km Segments	No. of 1km Segments Analysed*	River	Hydrological Station
1	Karlovac – Slovenia	6 km	6	4	Kupa	Kamanje
2	Karlovac – Jastrebarsko	0.2 km	1	1	Kupcina	Lazina Brana
3	Karlovac – Duga Resa	5 km	5	5	Mreznica	Mrzlo Polje

*Some segments were not deemed to be susceptible to flooding and were omitted from the analysis

Table 31: Summary of network locations identified as vulnerable to inundation.

A more structured approach to the identification of the locations along the selected rail network which are vulnerable to the three failure mechanisms considered in the analysis due to flooding (see Table 13) is the ORT, as described in Section 6.5. However, due to time limitations the two approaches adopted for the Croatian case study (i.e. qualitative and quantitative) were conducted concurrently.

A summary of the identified locations along the selected rail network vulnerable to rainfall-triggered landslides, bridge scour, and track inundation is illustrated in Figure 89. Two main types of stress tests were performed for the Croatian case study. The first consisted of an extreme rainfall event in the vicinity of the town of Novi Marof where the four locations along the rail network vulnerable to rainfall-triggered landslides were identified. The second type of stress test considered an extreme river discharge event in the vicinity of the Kupa Karlovac bridge and track inundation and the identified network locations vulnerable to inundation. The two types of stress test were each performed for three return periods: 200, 500 and 1000 years.

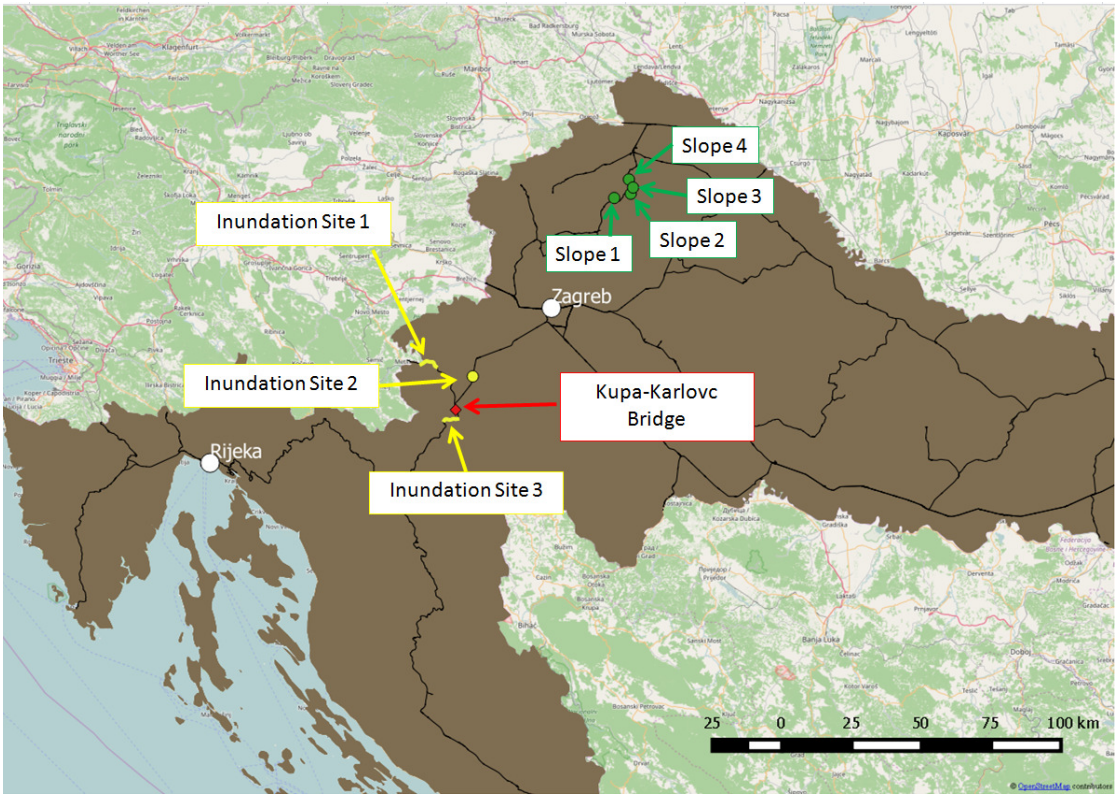

Figure 89: Network locations identified as vulnerable to rainfall-triggered landslides, bridge scour and track inundation

6.7.2 Software and Hardware

To perform stress tests for the selected Croatian railway lines, the data related to the various aspects of the flood hazard model described in Section 6.6.1 was imported into Matlab software and the various methodologies employed were subsequently applied. Fragility functions for each of the network elements, as described in Sections 6.6.2 and 6.6.3, were also generated using Matlab. The various stress tests were subsequently performed using Matlab according to a Monte Carlo simulation (MCS) approach to consider the associated uncertainties in the analysis. This software was also employed to post process the results.

The computation of the stress tests was performed using a 12 Core 3.50 GHz Intel Xeon desktop computer with 16,292 MB of memory, running on a 64 bit operating system. The stress tests that considered an extreme rainfall event required approximtely 30 minutes to compute. The stress tests that considered an extreme river discharge event and associated track inundation required approximately 2 hours to compute.

6.7.3 Simulation Workflow

The process employed to conduct a stress test that considered an extreme rainfall event is described in Figure 90. MCS sampling was performed to evaluate the network damage, associated repair costs, durations, and functionality loss of the rail network for a given return period. To do so, 1,000,000 MCS loops were performed for each of the three return periods considered (200, 500 and 1000 years). For each MCS loop, a rainfall duration was randomly sampled for each rainfall intensity considered based on the fragility functions presented in Table 15. Based on the sampled rainfall

duration, the associated damage state of the slope was determined by selecting a random number between 0 and 1 and then using this number to assign a unique damage state for a particular element by identifying the most onerous damage state probability that was greater than the random number. This process was repeated for the four vulnerable locations identified along the network and for each rainfall intensity. For each damage sample, the associated repair cost and duration was randomly sampled from the distributions described in Table 29 and the associated functionality loss of that section of rail line was also determined. For each MCS loop, the total cost of network repairs and duration was determined by summing the repair costs and duration associated with each of the four vulnerable locations.

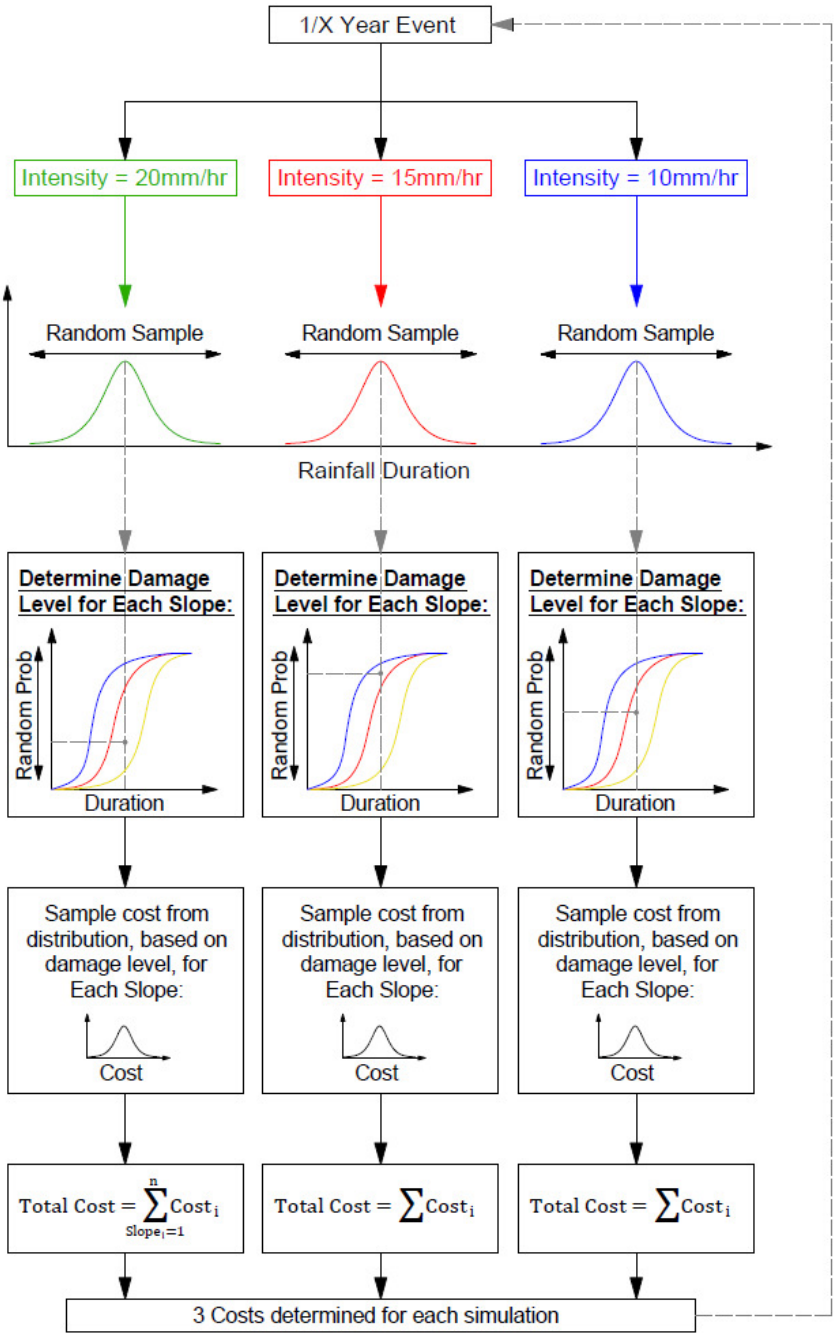

Figure 90: MCS to perform stress tests for an extreme rainfall event

A similar approach was adopted to conduct the stress tests due to an extreme river discharge event in the vicinity of the Kupa Karlovac Bridge and track inundation downstream. It is noted that while the flood hazard models described in Section 6.6.1 provided an approach which allowed the calculation of discharge levels and water heights corresponding to the same flood event of a given return period, this was only applicable when considering flooding of the river from which the measurements were taken. When considering flooding of the various rail sections, records from the nearest river were used. All of these rivers were located very close to each other, with the rail sections considered for inundation all within approximately 30 km of each other. It was considered reasonable to assume that these sites were located within the same catchment area and consequently, it was assumed that the predicted water levels associated with a given return period would occur simultaneously for the sites examined. Figure 89 clearly shows the close proximity of the Kupa Karlovac Bridge and the three inundation sites considered, relative to the four slopes assessed which are located over 100 km away in the North-East of the region.

MSC sampling was also conducted for these stress tests, where the associated functionality loss for each network element was assigned in terms of axle weight limits or speed limits on a given line, as presented in Table 26 and Table 28. Additionally, the disruption to freight transport and passenger trains was determined based on the information provided in Table 30 and the duration for which individual rail sections were out of operation.

6.8 Stress Test Results

In this section the results of stress tests performed for the Croatian case study are presented, which considered: i) an extreme rainfall event and the potential for rainfall-triggered landslides, and ii) an extreme river discharge event and the potential for bridge scour and track inundation downstream.

6.8.1 Solution Convergence

The number of network elements considered along the Croatian rail network was relatively small (i.e. one bridge, 10 segments of railway line and three slopes) and, therefore, a large number of MCS sampling loops were conducted in a relatively short time period: 1,000,000 samples were performed in 2 hours. An increase in the number of MCS loops showed no change in the solution.

6.8.2 Direct Consequences

This section presents the results of the stress tests performed in terms of the direct consequences, which are considered to be directly attributable to the rail infrastructure operator. Figure 91 presents the CDF of the total network repair costs for the stress tests that considered an extreme rainfall event. The resulting CDF is multimodal due to the nature of the fragility curves and the significant difference in the mean value of the costs for each damage state. The total network repair costs were almost identical for each of the return periods considered due to the fact that the observed rainfall intensities reached an upper bound that resulted in an almost assymptotic curve in the extrapolation analysis. Figure 91 demonstrates that the potential losses in terms of network repair costs due to rainfall-triggered landslides are relatively low; there is a 42% probability that the network repair costs will not exceed zero.

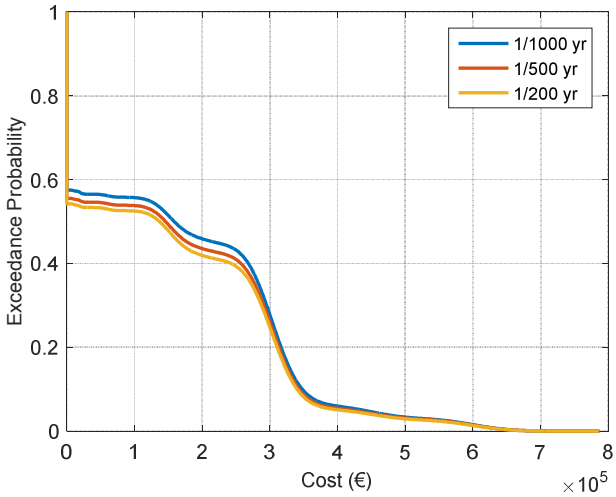

Figure 91: Total network repair costs due to rainfall-triggered landslides

Figure 92 presents the CDF of the total network repair costs for the stress tests that considered an extreme river discharge event and track inundation downstream. The results of the three return periods analysed demonstrated a similar trend that consisted of a 'stepped' shape. This was due to the fact that the total network costs were governed by the damage caused to the Kupa Karlovac bridge due to scour since track inundation was not significant for the rail sections analysed. Therefore, the stepped shape of the CDF corresponded to shifts between each of the damage states associated with bridge scour.

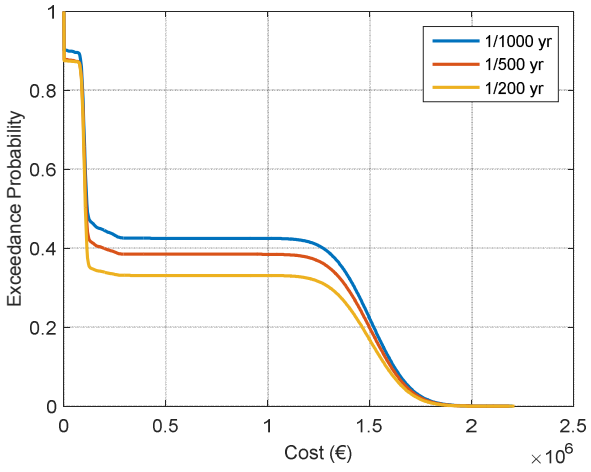

Figure 92: Total network repair costs due to bridge scour and track inundation

The total repair time for the network was also considered in terms of the direct consequences. Figure 93 illustrates the total cumulative time required to repair the network elements for the three return periods considered. Again, the results demonstrated that the potential network damage due to rainfall-triggered landslides was low since there was approxiamtely a 48% probability that no netowrk repairs would be required.

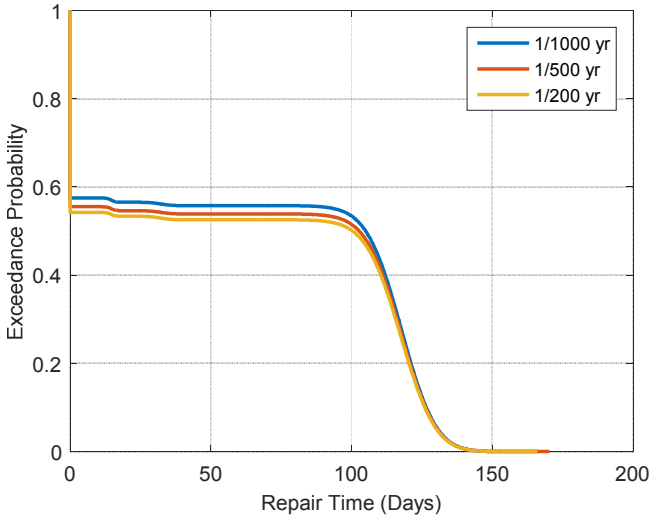

Figure 93: Total network repair time due to rainfall-triggered landslides

Figure 93 presents the results in terms of the total time required to carry out the necessary earthworks design and construction of slopes. However, the time required to resume operation of the rail network is much less since landslide debris that covers the track can generally be removed in a matter of days, as shown in Figure 94, which presents the actual rail downtime due to rainfall-triggered landslides, after which the rail can be re-opened, with necessary safety precautions, during the rehabilitation works to the adjacent slopes.

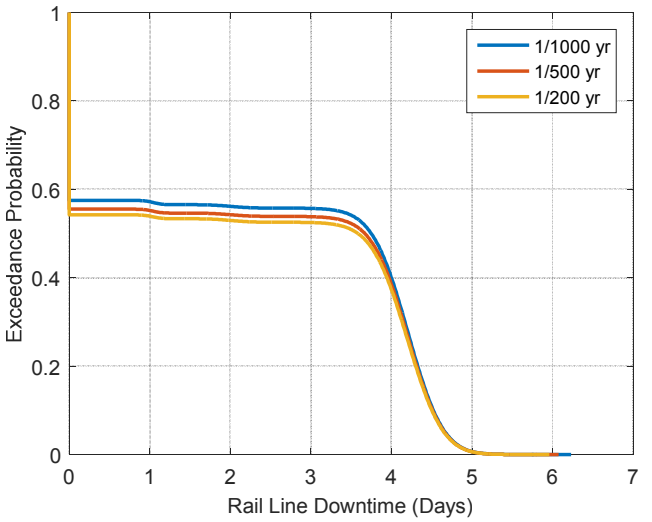

Figure 94: Total rail downtime due to rainfall-triggered landslides

Figure 95 illustrates the total network restoration period (i.e. the time taken to restore the network back to its original state) based on the stress tests that considered bridge scour and track inundation. To calculate the duration of the restoration period, it was assumed that three repair crews were available to carry out repairs on the network simultaneously, and the time taken to restore the network back to full functionality was calculated on this basis. The CDF for the various

return periods followed a ‘stepped’ trend that was due to the shift between each of the damage states associated with bridge scour, which governed the duration of the restoration period since damage to the network due to inundation of the rail track was not significant.

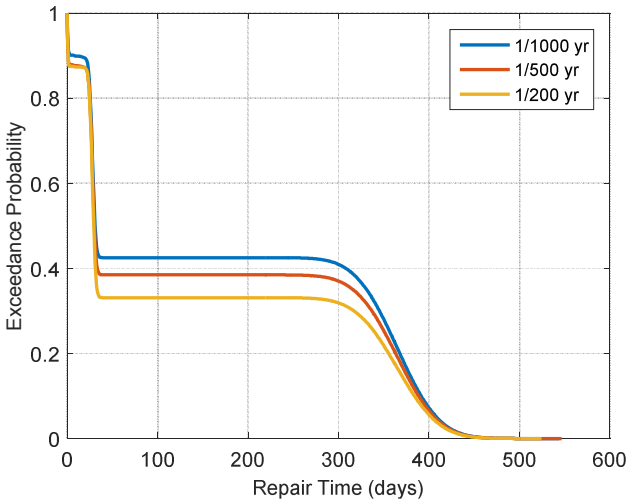

Figure 95: Total duration of restoration period due to scour & inundation

The impact of the loss of functionality of the rail network was subsequently evaluated in terms of the travel disruption to passenger trains due to the flood scenarios considered. In many countries, the railway operator is obliged to compensate train passengers due to travel delays and, therefore, the travel disruption to passenger trains was classified as a direct consequence.

To determine the travel disruption to passengers trains, timetable information (see Section 6.6.6) was used to determine the number of trains that would be disrupted due to the loss of functionality of the rail lines due to the extreme flood scenarios considered. This involved the calculation of the total number of passenger trains which were unable to travel as a result of the damage to the network. Delays to individual trains due to speed restrictions during repairs were not considered as they were shown to be negligible. Figure 96 illustrates the results of the stress tests that considered extreme rainfall scenarios in the vicinity of Novi Marof where the potential for rainfall-triggered landslides was analysed. The CDFs for each of the return periods considered demonstrated similar results: there was approximately a 50% probability that up to 100 passenger trains would be impacted.

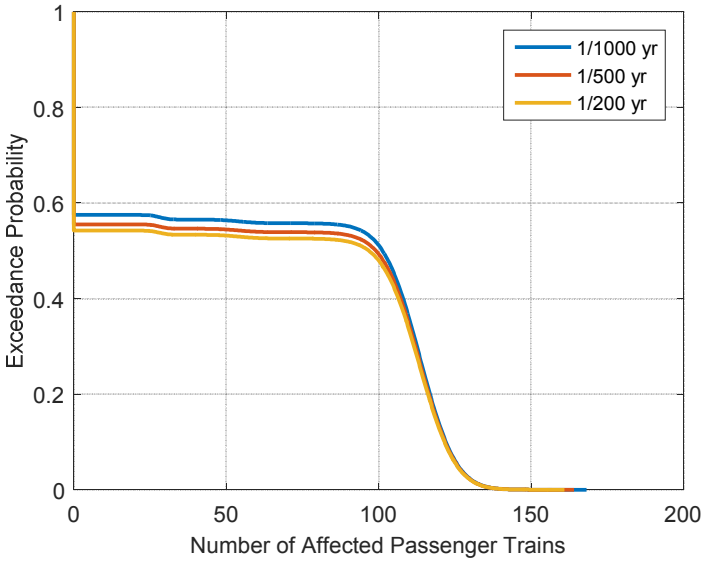

Figure 96: Number of passenger trains affected due to rainfall-triggered landslides

Figure 97 presents the results of the stress tests that considered an extreme river discharge scenario and associated water levels in terms of the number of passengers trains affected due to the rail network disruption. The travel disruption was far greater than due to rainfall-triggered landslides and demonstrated approximately a 40% probability that up to 12,000 passenger trains would be impacted.

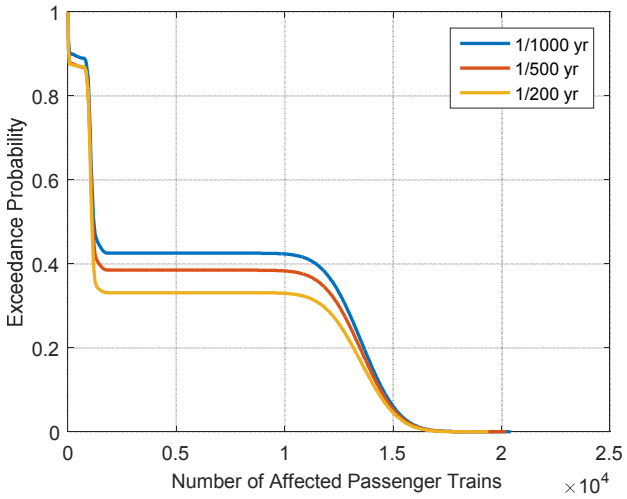

Figure 97: Number of affected passenger trains due to bridge scour and track inundation

6.8.3 Indirect Consequences

The indirect consequences were evaluated in terms of the potential disruption to freight transport along the rail network. In some cases, the rail operator may also be obliged to provide compensation due to travel disruption. However, in this case the disruption to freight transport was deemed to be an indirect consequence of an extreme flood scenario.

Based on the data described in Section 6.6.6, the freight is transported along the rail lines that connect Duga Resa to the city of Zagreb. Based on the stress tests performed for the Croatian case study, the potential for freight disruption was only due to the stress tests that considered bridge scour and track inundation. Figure 98 illustrates the results, wherein the CDFs for each of the return periods considered were similar; there was approximately a 40% probability that up to 750,000 tonnes of freight will be affected.

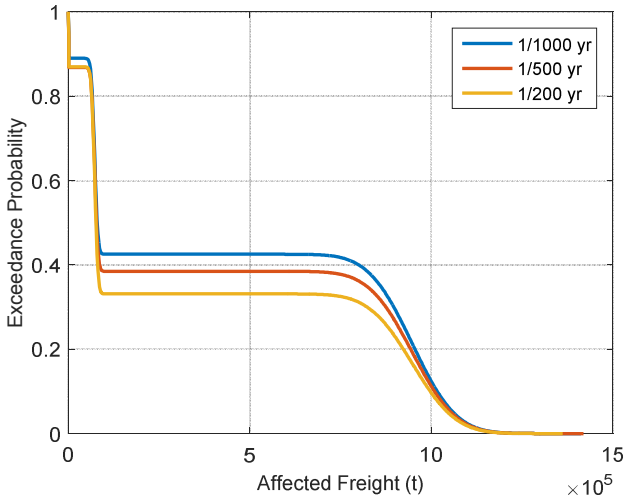

Figure 98: Tonnes of freight affected due to bridge scour and track inundation

6.9 Stress Test Outcome

The results of the stress tests performed for the Croatian case study have been presented in terms of the direct and indirect consequences, as described in Sections 6.8.2 and 6.8.3. This was deemed to be an appropriate means by which to present the results of the stress tests described herein since just three return periods were considered in terms of the flooding hazard. The analysis of supplementary stress tests based on additional return periods would facilitate the presentation of the associated risk, such as the annualised risk, as described by Hackl et al. (2016).

The goal of the stress test framework applied to the Croatian case study was to determine whether or not the potential losses were deemed to be acceptable (see van Gelder and van Erp (2016)). In reality, stress tests are performed based upon evaluation criteria, e.g. total monetary losses. As such, the results of the stress tests performed for the Croatian case study were analysed based on the criteria outlined in Table 32. It is noted that due to the fact that the landslide assessment of the north easterly section of the rail line was carried out separately to the scour and inundation assessment for the rest of the line, a separate threshold was considered appropriate for each of these analyses.

Evaluation Criteria	Threshold
Total repair cost	€150,000* / €750,000**
Freight affected	250,000 t
No. of passenger trains affected	2,100

*Threshold for rainfall-triggered landslide analysis
**Threshold for bridge scour and track inundation analysis

Table 32: Evaluation criteria employed to assess outcome of stress tests for Croatian case study

Figure 99 illustrates the evaluation of the stress tests that considered rainfall-triggered landslides according to the 'repair costs' evaluation criterion. Based on the imposed threshold, there was approximately a 50% probability that the threshold value would be exceeded for each of the return periods considered since the results were very similar. The outcome of probabilistic stress tests depends on the risk acceptability of the infrastructure owner or manager. However, we will assume that a 50% probability of exceedance would be unacceptable and, therefore, that the stress tests have failed in this instance.

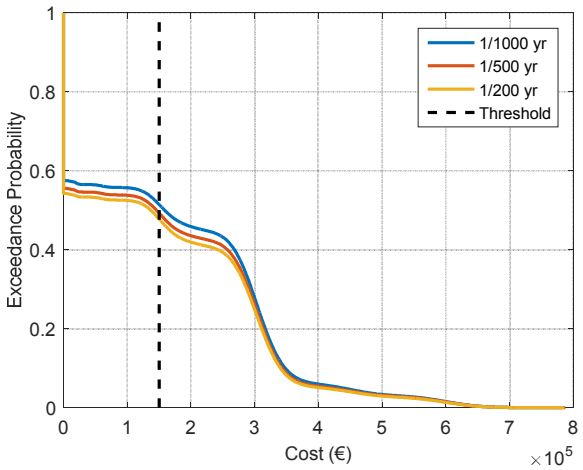

Figure 99: Stress test results: total network repair costs due to rainfall-triggered landslides

Figure 100 presents the evaluation of the stress tests according to the 'repair costs' evaluation criterion for the extreme river discharge (i.e. bridge scour) and track inundation scenarios examined. Based on the imposed threshold, the exceedance probability ranged between 37% and 42% depending on the return period considered. Again, it is likely that an infrastructure owner or manager will not be willing to accept this risk (i.e. stress test failure) and may subsequently decide to analyse parts of the network in greater detail to reduce the uncertainty associated with the risk estimate or to implement intervention measures to mitigate against these potential losses. To do so, the decision theory proposed by van Gelder and van Erp (2016) has the potential to be used to determine the optimal intervention strategy for the network.

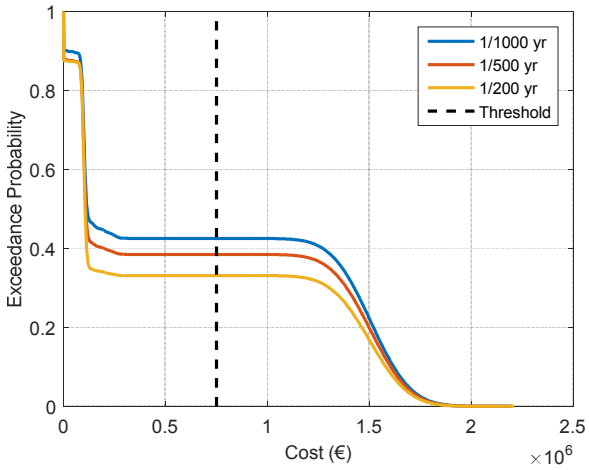

Figure 100: Stress test results: total network repair costs due to bridge scour and track inundation

The outcomes of the stress tests performed for the Croatian case study were subsequently assessed according to the number of passenger trains affected. For the stress tests that evaluated the impact of an extreme rainfall event and the associated potential for rainfall-triggered landslides, the threshold value was far greater than the results of the stress tests for the three return periods analysed (see Figure 96). However, for the stress tests that considered the potential for bridge scour and track inundation, the evaluation of the results according to the 'number of passenger trains affected' criterion is presented in Figure 101, whereby the exceedance probability ranged between 33% and 42% for the three return period considered. If an infrastructure manager/owner is unwilling to accept this level of risk then the stress tests are deemed to have failed and further analysis or the implementation of an intervention programme is required.

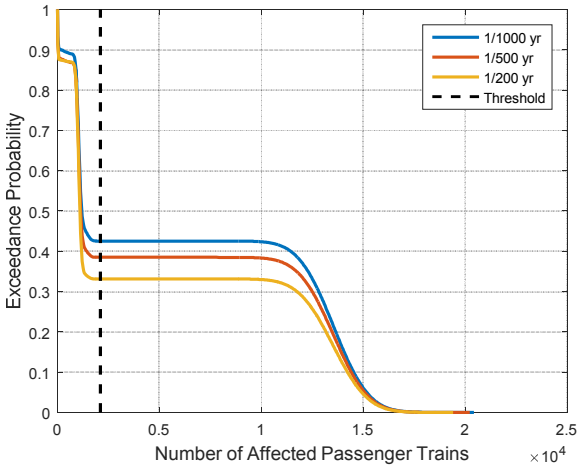

Figure 101: Stress test results: number of passenger trains affected by bridge scour and track inundation

Finally, the outcome of the stress tests that considered an extreme river discharge scenario and the potential for bridge scour, as well as track inundation downstream, were evaluated in terms of the total amount of affected freight, as shown in Figure 102. The probability that the threshold value

would be exceeded ranged between 37% and 42% since the results for all three return periods were similar. Again, the outcome of the stress tests is dependent on the willingness of the infrastructure manager/owner to accept this level of risk. However, in this case it is assumed that the risk is too large and that the stress tests have failed.

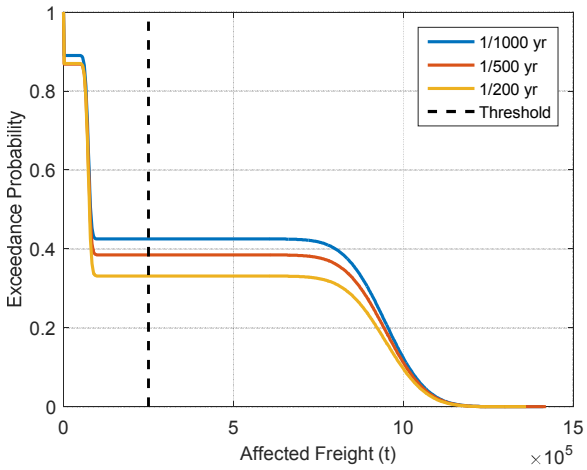

Figure 102: Stress test results: tonnes of freight affected by bridge scour and track inundation

6.10 Discussion

The Croatian case study has demonstrated the application of the methodologies developed within the INFRARISK project to perform stress tests on a railway network subjected to low probability, high consequence flooding scenarios, following the overarching risk assessment methodology proposed by Hackl et al. (2016). The results illustrate the potential impacts of: i) an extreme rainfall event and the associated potential for rainfall-triggered landslides and ii) an extreme river discharge event and the associated potential for bridge scour and track inundation downstream.

The stress tests were performed in modular format; more advanced modelling approaches could be employed for the various model components, where deemed necessary. For example, due to the limitations of the flood hazard model adopted, it was not possible to correlate the extreme rainfall event in the vicinity of Novi Marof to the values of river discharge in the vicinity of the Kupa Karlovac bridge. The use of more advanced hydraulic modelling, along with the neccessary data inputs, would facilitate the analysis of stress test scenarios that consider the source hazard (i.e. rainfall) and the correlated effects, in terms of bridge scour and track inundation, as well as other failure mechanisms for railway networks that have not been examined herein. However, such detailed approaches require substantial computational effort, as well as a great deal of data.

Similarly, more advanced traffic modelling could be employed to simulate the movement of passenger and freight trains to provide more detailed results in terms of the losses due to extreme flood scenarios. For instance, freight goods can generally be moved to trucks and transported by roads and passenger trains can be replaced by bus transfers. Many railway lines have contingency measures for rail closures due to natural hazards. For example, Network Rail in the UK have a Railway Operational Code (Network Rail, 2010), which includes procedures for responding to extreme weather events. However, such modelling also requires significant computational effort,

along with substantial data inputs. Furthermore, since alternative transport modes would generally be employed in the case of rail disruption (i.e. transporting of freight goods via road as an alternative), more advanced transport modelling could be employed to consider the multi-modal transport networks and the potential for transport via an alternative means. Additionally, more detailed information in relation to passenger and freight movements, such as origin-destination information, would facilitate the use of a methodology similar to that described for the Italian case study in Section 5.3.7 to quantify the impacts of extreme flood hazard events in terms of economic losses due to rail disruption as part of the overall stress test framework.

The stress tests performed for the Croatian case study have the potential to be extended to consider the impact of a network intervention program. For example, the stress test framework could be used to determine the potential losses for the Croatian railway line if flood defences, scour protection or slope strengthening interventions were to be implemented. Based on such stress tests, the decision-making protocol proposed by van Gelder and van Erp (2016) could subsequently be employed to determine the optimal intervention programme for the railway network. In addition, the stress test framework has the potential to consider future scenarios, which could also be advantageous as part of the decision making process during planning.

7.0 CONCLUSION

This deliverable has presented the results of two case studies for which stress tests have been conducted to evaluate the potential impacts of extreme natural hazard scenarios on distributed transport infrastructure networks. The case studies consisted of existing road and rail transport networks located along the European TEN-T network, which is considered to be critical infrastructure for the European Union. The stress tests were performed according to the stress test framework proposed in work package 6 of the INFRARISK project and according to the overarching risk assessment methodology proposed in work package 4. The objective was to demonstrate how the various tools and methodologies developed in the various other work packages could be systematically applied to determine whether or not the risks associated with a transport network due to extreme natural hazards were deemed to be acceptable.

The Italian case study conducted stress tests for a regional road network in the vicinity of Bologna city in northern Italy to evaluate the potential losses due to low probability, high consequence seismic hazard scenarios. The Croatian case study, on the other hand, conducted stress tests for a significant portion of the Croatian rail network to evaluate the potential losses due to low, probability, high consequence flood hazard scenarios. For both case studies, cascading hazard effects were considered (i.e. earthquake-triggered and rainfall-triggered landslides) and the potential impacts were evaluated according to the direct consequences (i.e. those that were deemed to be directly attributable to the infrastructure owner or manager) and the indirect consequences (i.e. additional losses encountered).

The case studies have demonstrated how the overarching risk assessment methodology proposed in the INFRARISK project can be adapted for different transport network types at various scales to evaluate the potential impacts associated with different types of extreme natural hazard events. The methodology offers flexibility in relation to the level of detail required or the specific aspects of a transport network that are examined as part of the stress tests. Consequently, the stress test framework proposed in the INFRARISK project has the potential to be adapted for other infrastructure network types, such as power, telecommunication and water distribution networks to evaluate the potential losses associated with extreme natural hazard events.

REFERENCES

Adey, B., and J. Hackl. *INFRARISK Terminology.* European Commission, 2014.

Adey, B., J. Hackl, M. Heitzler, and I. Iosifescu. *Infrarisk Deliverable D4.1 Preliminary Model, Methodology and Information Exchange.* European Commission, 2014.

Adey, Bryan, et al. "Ensuring acceptable levels of infrastructure related risls due to natural hazards with emphasis on conducting stress tests." 2016.

Alipour, A., B. Shafei, and M. Shinozuka. "REliability-Based Calibration of Load and Resistance Factors for Design of RC Bridges under Multiple Extreme Events: Scour and Earthquake." *Journal of Bridge Engineering* 18 (2013): 362-271.

Apel, H., A. H. Thieken, B. Merz, and G. Bloschel. "Flood risk assessment and associated uncertainty." *Natural Hazards and Earth System Sciences* 4 (2004): 295-308.

Apel, H., H. Thieken, B. Merz, and G. Bloschl. "A Probabilistic Modelling System for Assessing Flood Risks." *Natural Hazards* 38 (2006): 79-100.

Argyroudis, S., and A. M. Kaynia. "Fragility functions of highway and railway infrastructure." In *SYNER-G: Typology Definition and Fragility Functions for Physical Elements at Seismic Risk*, by K. Pitilakis, H. Crowley and A. M. Kaynia, 299-326. Springer, 2014.

Argyroudis, S., J. Selva, and P. Gehl. "Systematic seismic risk assessment of road networks considering interactions with the built environment." *Computer-Aided Civil and Infrastructure Engineering* 30 (2015): 524-540.

Atkinson, G., and J. Adams. "Ground motion prediction equations for application to the 2015 Canadian national seismic hazard maps." *Canadian Journal of Civil Engineering* 40, no. 10 (2015): 988-998.

Avdeeva, Y., and P. van Gelder. *INFRARISK Deliverable D6.1 Stress Test Methodologies.* Brussels: European Commission, 2014.

Baker, Jack W. *An Introduction to Probabilistic Seismic Hazard Analysis (PSHA).* White Paper, Version 2.0, 2013.

Bekic, D., and D. Oskorus. "Sediment status Croatia." *www.sednet.org/download/Sava-ssm_croatia_bekic-oskorus.pdf.* 2012.

Beniston, M., et al. "Future extreme events in European climate: an exploration of regional climate model projections." *Climatic Change* 81, no. 1 (2007): 71-95.

Cagnan, Zehra, and Rachel Davidson. "Post-earthquake restoration modeling of electric power systems." *13th World Conference on Earthquake Engineering.* Vancouver, 2004.

Cardinali, M., et al. "A geomorpohologial approach to the esimation of landslide hazards and risks in Umbria, Central Italy." *Natural Hazards and Earth System Science* 2 (2002): 57-72.

CEN. *EN 1991-1-2:2002 Eurocode 1: Actions on structures, Part 2: Traffic loads on bridges.* European Committee for Standardisation, 2010.

Chang, S. E., M. Shinozuka, and J. E. Moore. "Probabilistic earthquake scenarios: extending risk analysis methodologies to spatially distributed systems." *Earthquake Spectra*, 2000: 557-572.

Collin, J. G. *Timber pile design and construction manual.* American Wood Preservers Institute, 2002.

Commission, European. *Infrastructure TEN-T Connecting Europe.* http://ec.europa.eu/transport/themes/infrastructure/index_en.htm (accessed August 18, 2016).

Crowley, H., and J. J. Bommer. "Modelling seismic hazard in earthquake loss models with spatially distributed exposure." *Bulletin of Earthquake Engineering* 4 (2006): 249-273.

Davidson, J., G. E. Ramey, M. L. Hughes, M. Schambeau, and J. Kang. *Stability of highway bridges subject to scour-phase IV: screening tool for bridges supported by timber pile bents.* Alabama Department of Transportation, 2011.

D'Ayala, D., and P. Gehl. *INFRAISK Deliverable D3.4 Single Risk Analysis.* European Commission, 2015.

D'Ayala, D., and P. Gehl. *Infrarisk Deliverable D3.1 Hazard Distribution Matrix.* European Commission, 2014.

D'Ayala, D., and P. Gehl. *Infrarisk Deliverable D3.2 Fragility Functions Matrix.* European Commission, 2015.

D'Ayala, D., and P. Gehl. *INFRARISK Deliverable D3.3 Uncertainty Quantification.* European Commission, 2015.

D'Ayala, Dina, et al. "Guidelines for Analytical Vulnerability Assessment of low/mid-rise Buildings, Vulnerability Global Component project." 2014.

D'Ayala, Dina, et al. *Hazard Distribution Matrix, INFRARISK D 3.1 Report.* University College London, London: University College London, 2014.

DeBlasio, A. J., A. Zamora, F. Mottley, R. Brodesky, M. E. Zirker, and M. Crowder. *Effects of Catastrophic Events on Transportation System Management and Operations, Northridge Earthquake - January 17, 1994.* U.S. Department of Transportation, 2002.

DEFRA. *National Appraisal of Assets at Risk from Flooding and Coastal Erosion, including the potential impact of climate change.* Department for Environment, Food and Rural Affairs, 2001.

Directorate-General for Energy and Transport. *Modern rail, modern Europe: Towards an integrated European railway area.* European Commission, 2008.

ETISPLUS. *D4 ETISPLUS FInal Database Specification.* European Commission, 2012.

European Commission and the European Soil Bureau Network. "The European Soil Database distribution version 2.0." *EUR 19945 EN.* 2004.

European Commission. *EU transport in figures: statistical pocketbook.* Luxembourg: European Union, 2015.

European Commission. *Road Transport: A change of gear.* Luxembourg: European Union, 2012.

European Commission. *Roadmap to a single European transport area - towards a competitive and resource effecient transport system.* Brussels: European Union, 2011.

European Environment Agency. *Mapping the impacts of natural hazards and technological accidents in Europe.* Luxembourg: European Union, 2010.

Eurostat. *Regions in the European Union: Nomenclature of territorial units for statistics.* European Union, 2015.

FEMA. *HAZUS 99 Estimated Annualized Earthquake Losses for the United States.* Washington DC: Federal Emergency Management Agency, 2000.

FEMA. *Multi-hazard Loss Estimation Methodology Earthquake Model, HAZUS MR4 Technical Manual.* Washington DC: Federal Emergency Management Agency , 2003.

Giardini, D., et al. "SHARE European Seismic Hazard Map for Peak Ground Acceleration, 10% Exceedance Probability in 50 years." 2013. http://www.share-eu.org/node/90 (accessed 2016).

Gunther, A., M. Van den Eeckhaut, J. P. Malet, and J. Hervas. "European Landslide Susceptibility Map (ELSUS1000), European Soi Portal." 2013. http:\\esdac.jrc.ec.europa.eu/ (accessed 2016).

Hackl, J., M. Heitzler, J. C. Lam, B. Adey, and L. Hurni. *INFRARISK Deliverable D4.2 Final Model, Methodology and Information Exchange.* European Commission, 2016.

Hall, J. W., R. J. Dawson, P. B. Sayers, C. Rosu, J. B. Chatterton, and R. Deakin. "A methodology for national-scale flood risk assessment." *Proceedings of the Institution of Civil Engineers Water and Maritime Engineering* 156 (2003): 235-247.

Han, Y., and R. A. Davidson. "Probabilistic seismic hazard analysis for spatially distributed infrastructure." *Earhtquake Engineering and Structural Dynamics* 41, no. 15 (2012): 2141-2158.

Hancilar, Ufuk, and Fabio Taucer. *Guidelines for typology definition of European physical assets for earthquake risk assessment.* Luxembourg: Joint Research Centre, 2013.

Huppert, H., and S. Sparks. "Extreme natural hazards: population growth, globalization and environmental change." *Philosophical Transactions of the Royal Society A* 364 (2006): 1875-1888.

HZ Infrastruktura. "Unpublished Internal Report." 2013.

Intergovernmental Panel on Climate Change. "Climate Change 2014, Synthesis Report, Summary for Policymakers." 2014.

International Strategy for Disaster Reduction. *Hyogo Framework for Action 2005-2015: Building the Resilience of Nations and Communities to Disasters.* United Nations, 2005.

Jaiswal, P., J. van Westen, and V. Jetten. “Quantitative assessment of direct and indirect landslide risk along transportation lines in southern India.” *Natural Hazards Earth System Science*, 2010: 1253-1267.

Jayaram, N., and J. W. Baker. “Correlation model for spatially distributed ground modtion intensities.” *Earthquake Engineering and Structural Dynamics* 38, no. 15 (2009): 1687-1708.

Jayaram, N., and J. W. Baker. “Efficient sampling and data reduction techniques for probabilistic sesimc lifeline risk assessment.” *Earthquake Engineering and Structural Dynamics* 39, no. 10 (2010): 1109-1131.

Jibson, R. W., E. L. Harp, and J. A. Michael. “A method for producing digital probabilistic seismic landslide hazard maps.” *Engineering Geology* 58 (2000): 271-289.

Jiménez, M. J., and M. García-Fernández. *Development of seismic hazard modelling for low-probability extreme ground motions. INFRARISK Technical Report.* European Commission, 2016.

Jonkman, B. N., M. Bockarjova, M. Kok, and P. Bernardini. “Integrate hydrodynamic and economic modelling of flood damage in the Netherlands.” *Ecological Economics*, 2008: 77-90.

Kameshwar, S., and J. E. Padgett. “Multi-hazard risk assessment of highway bridges subjected to earthquake and hurricance hazards.” *Engineering Structures* 78 (2014): 154-166.

Kellermann, P., A. Schobel, G. Kundela, and A. H. Thieken. “Estimating flood damage to railway infrastructure - the case study of the March River flood in 2006 at the Austrain Northern Railway.” *Natural Hazards Earth Systems Science* 15 (2015): 2485-2496.

Kok, M., H. J. Huizinga, A. C. W. M Vrouwenvelder, and A. Barendregt. *Standard Method 20014 Damage and Casualties Caused by Flooding.* Road and Hydraulic Engineering Institute, 2005.

Librić, L., M. Bačić, and M. S. Kovačević. *A framework for risk management in rockfall protection.* Vol. 2, in *Engineering Geology for Society and Territory, Landslide Processes*. 2014.

Mackie, Kevin, and Bozidar Stojadinovic. *Fragility basis for California Highway Overpass Bridges Seismic Decision Making.* Berkeley: Pacific Earthquake Engineering Research Center, 2005.

MATLAB 2013. MathWorks Inc., 2013.

Medda, F., and F. Taalab. “INFRARISK Deliverable D5.3: Infrastructure Platform.” 2016.

Medda, F., and M. Wang. *INFRARISK Deliverable D6.5 The wider economic impact of a natural hazard - an agent based approach.* European Commission, 2016.

Menzel, L., A.H. Thieken, D. Schwandt, and G. Burger. “Impact of climate change on the regional hydrology - scenario-based modelling studies in the German Rhine catchment.” *Natural Hazards* 38 (2006): 45-61.

Messner, F., E. Penning-Rowsell, C. Green, V. Meyer, S. Tunstall, and A. van der Veen. “FLOODsite Project Deliverable D9.1 'Evaluating flood damages: guidance and recommendations on principles and methods'.” 2007.

Miller, M., and J. W. Baker. “Coupling mode-destination accessibility with seismic risk assessment to identify at-risk communities.” *Reliability Engineering and System Safety* 147 (2016): 60-71.

Moran, Andrew, Annegret H. Thieken, A. Schobel, and C. Rachoy. “Documentation of Flood Damage on Railway Infrastructure.” In *Data and Mobility*, 61-70. Springer Berlin Heidelberg, 2010.

Mujkanovic, N., D. Marcic, M. S. Kovacevic, and V. Dragcevic. *Kategorizacika Nosivosti Celicnih Mostova, Sveuciliste u Zagrebu.* Faculty of Engineering, University of Zagreb, 2013.

National Institute of Building Sciences. *HAZUS-MHL User's Manual and Technical Manuals.* Washington, D. C.: Report prepared for the Federal Emergency Management Agency, 2004.

Network Rail. “Railway Operational Code.” 2010.

Newmark, N. M. “Effects of earthquakes on dams and embankments.” *Geotechnique 15*, 1965: 271-289.

Nguyen, M. H., T. K. Nguyen, T. V. Ho, and M. D. Do. “Modeling and simulation of the effects of landslide on circulation of transport on the mountain roads.” *International Journal of Advanced Computer Science and Applications*, 2015.

Ni Choine, M., and , K. Martinovic. *INFRARISK Deliverable D8.1 Critical Infrastructure Case Studies.* European Commission, 2014.

Penning-Rowsell, E., et al. “The Benefits of Flood and Coastal Risk Management: A Handbook of Assessment Techniques.” 2005.

Phoon, K. K., and F. H. Kulwahy. “Characterisation of geotechnical variability.” *Canadian Geotechnical Journal* 36, no. 4 (1999): 612-624.

Pitilakis, Kyriazis, et al. *Physical vulnerability of elements at risk to landslides: Methodology for evaluation, fragility curves and damage states for buildings and lifelines.* Thessaloniki: AUTH, 2011.

Remondo, J., J. Bonachea, and A. Cendrero. “A statistical apprroach to landslide risk modelling at basin scale: from landslide susceptibility to quantitative risk assessment.” *Landslides* 2 (2005): 321-328.

Saygili, G., and E. M. Rathje. “Probabilistcally based seismic landslide hazard maps: an application in Southern California.” *Engineering Geology* 109, no. 3-4 (2009): 183-194.

Saygili, G., and Ellen M. Rathje. “Probabilistically based seismic landslide hazards maps: An application in Southern California.” *Engineering Geology* 109, no. 3-4 (2009): 183-194.

Scawthorn, C., et al. “HAZUS-MH Flood Loss Estimation Methodology. 1: Overview and Flood Hazard Characterization.” *Natural Hazards Review* 7, no. 1 (2006): 60 - 71.

Shinozuka, M., M. Q. Feng, J. Lee, and T. Naganuma. “Statistical analysis of fragility curves.” (Journal of Engineering Mechanics), no. 126 (2000).

Shiraki, N., M. Shinozuka, J. E. Moore, S. E. Chang, H. Karneda, and S. Tanaka. “System risk curves: probabilistic performance scenarios for highway networks subject to earthquake damage.” *Journal of Infrastructure Systems* 13, no. 1 (2007).

Silva, V., H. Crowley, and M. Colombi. “Fragility function manager tool.” In *SYNER-G: Typology Definiation and Fragility Functions for Physical Elements at Seismic Risk*. 2014.

Sivakumar Babu, G. L., and D. S. Murthy. “Reliability analysis of unsaturated slopes.” *Journal of Geotechnical and Geoenvironmental Engineering* 131, no. 11 (2005): 1423-1428.

Šustić, D, , Z Tadić, L Tadić, and T Kržak. “Hydrologic and hydraulic analysis of less studies watersheds.” *24th Conference on the Danubian Countries on the Hydrological Forecasting and Hydrological Bases of Water Management.* 2008.

Tacnet, J.M., E. Mermet, and S. Maneerat. “Analysis of importance of road networks exposed to natural hazards.” *Proceedings of the AGILE2012 Conference on Geographic Information Science.* Avignon, 2012.

Tanasic, N., V. Ilic, and R. Hajdin. “Vulnerability Assessment of Bridges Exposed to Scour.” *Transportation Research Record: Journal of the Transportation Research Board* 2360 (2013): 36-44.

Taylor, J. “Basic Controls and User Interfaces of NeXTA Appendix 1: NeXTA Data Structure.” 2013.

Tomlinson, M., and J. Woodward. *Pile design and construction practice.* CRC Press, 2014.

U.S. Army Corps of Engineers. “HEC-RAS River Analysis System, Version 4.1.0.” 2010.

United Nations. *Sendai Framework for Disaster Risk Reduction 2015-2030.* United Nations Office for Disaster Risk Reduction (UNISDR), 2015.

van Gelder, P., and N. van Erp. *INFRARISK Deliverable D6.2 Stress Test Framework for Systems.* European Commission, 2016.

van Gelder, P., and N. van Erp. *INFRARISK Deliverable D6.3 Decision-making Protocal.* European Commission, 2016.

van Mierklo, M. C. L. M., et al. “Assessment of flood risk accounting for river sustem behaviour.” *Interntaiontal Jounral of River Basin Management* 5, no. 2 (2007): 93-104.

Vorogushyn, S., B. Merz, K. E. Lindenschmidt, and H. Apel. “A new methodology for flood hazard assessment considering dike breaches.” *Water Resources Research*, 2010.

Werner, S. D., et al. *{REDAR 2} methodology and software for seismic risk analysis of highway systems.* Buffalo: MCEER, 2006.

Woessner, J., et al. “The 2013 European Seismic Hazard Model: Key Components and Results.” *Bulletin of Earthquake Engineering* 13 (2015): 3353-3596.

Zhang, L. L., J. Zhang, L. M. Zhang, and W. H. Tang. “Stability analysis of rainfall-induced slope failures: a review.” *Proceedings of the Institute of Civil Engineering: Geotechnical Engineering* 164, no. 5 (2011): 299-316.

Zhou, X., and J. Taylor. “DTALite: A queu-based mesocopic traffic simulator for fast model evaluation and calibration.” *Cogent Engineering* 1, no. 1 (2014).

Žic, E., M. Vranješ, and N. Ožanić. “Methods of roughness coefficient determination in natural riverbeds.” *11th International Symposium on Water Management and Hydraulic Engineering.* 2009.

APPENDIX A: Italian Road Network Data

ID	Coordinates (CRS = UTM32N)		Typology	ID	Coordinates (CRS = UTM32N)		Typology
	X	Y			X	Y	
1	679670.8	4928137	1	159	686209	4918803	18
2	677952.9	4929169	1	160	671522.1	4919544	18
3	677263.5	4929499	1	161	686671.8	4920050	18
4	678753.2	4932782	1	162	670848.7	4919663	18
5	675720.1	4905073	2	163	690279.3	4920391	18
6	679779.7	4918224	2	164	690309.5	4920549	18
7	680886.5	4928618	2	165	686926	4921082	18
8	680657.2	4928728	2	166	690983.9	4922149	18
9	680625.2	4930159	2	167	691548.9	4923131	18
10	689439.6	4930470	2	168	673574.4	4922929	18
11	689317.3	4930777	2	169	687280.9	4923442	18
12	681289.1	4931755	2	170	694131.1	4924148	18
13	688499.5	4932256	2	171	687737	4924063	18
14	681810.9	4932618	2	172	687610.4	4924113	18
15	685559.1	4933587	2	173	681115.1	4924067	18
16	684669.6	4933572	2	174	674629.3	4924270	18
17	695116.4	4937861	2	175	688223	4924942	18
18	675905.2	4897393	3	176	694279.6	4925590	18
19	675896.3	4897393	3	177	689212.2	4925689	18
20	675637.3	4898461	3	178	689448.8	4925860	18
21	675616	4898468	3	179	698210.1	4926474	18
22	675340.7	4898890	3	180	694971	4926458	18
23	675346.7	4898898	3	181	689864.5	4926401	18
24	679437.3	4915632	3	182	690538.3	4926665	18
25	679367.8	4917580	3	183	690521.5	4927119	18
26	680711	4926714	3	184	691013.2	4927238	18
27	694080.8	4928151	3	185	700052.8	4927773	18
28	681085.2	4928593	3	186	681240.8	4927477	18
29	681877.8	4928998	3	187	680732.5	4927583	18
30	677088.8	4928927	3	188	694162.1	4928348	18
31	682035.9	4929066	3	189	692559.3	4928472	18
32	690107.7	4929479	3	190	678105.2	4928256	18
33	682506.8	4929363	3	191	677085.3	4928641	18
34	683154.1	4929992	3	192	681421	4928761	18
35	683305.8	4930122	3	193	692299.9	4930045	18
36	695613.5	4930721	3	194	682024.7	4930534	18
37	679431.8	4933124	3	195	696341.5	4931204	18
38	702019.3	4935237	3	196	696340.6	4931209	18
39	688350.3	4935393	3	197	682215.2	4931099	18
40	688589.2	4935944	3	198	678060.1	4931914	18
41	689139.1	4937211	3	199	681542.4	4932191	18
42	689460.9	4937951	3	200	683195.8	4932744	18
43	689754.8	4938627	3	201	679903.1	4932892	18
44	690066	4939339	3	202	679912.3	4932912	18

45	680265.7	4942776	3	203	686037.6	4933479	18
46	679264.4	4928507	4	204	699522.2	4934361	18
47	692011.6	4939197	4	205	686445.7	4934430	18
48	678474.4	4928920	5	206	688859.6	4935161	18
49	689901	4929785	5	207	700117.2	4935564	18
50	690319.1	4939923	5	208	687169.4	4935791	18
51	690480.9	4940296	5	209	689624.3	4935867	18
52	686421.2	4915493	6	210	687922.5	4936513	18
53	681265.3	4925254	6	211	688634.6	4938193	18
54	678060.6	4932411	6	212	692919.7	4938826	18
55	693875.6	4924430	7	213	692857.3	4938853	18
56	679582.6	4935725	7	214	693150.3	4939119	18
57	668550.4	4905321	9	215	689490.1	4939793	18
58	679925.4	4918234	9	216	689830.3	4940178	18
59	679897.5	4918235	9	217	683612.6	4942154	18
60	680763.2	4928061	9	218	693247.9	4928128	19
61	689251	4931248	9	219	679977.7	4928335	19
61	688945.9	4931789	9	220	680123.4	4928424	19
63	688087.3	4932516	10	221	680849.6	4930991	19
64	689786.8	4902726	11	222	680945.6	4931160	19
65	667813.7	4905477	11	223	681402.3	4931949	19
66	674363.7	4910828	11	224	681561.8	4932224	19
67	669115.7	4912185	11	225	687658.9	4933789	19
68	694188.5	4924360	11	226	690600.7	4905112	20
69	698505.4	4926365	11	227	679670.8	4915545	20
70	693785	4928143	11	228	680581.4	4920556	20
71	692028.9	4928366	11	229	680566.8	4920560	20
72	691525.3	4928825	11	230	680962.3	4925839	20
73	680042.6	4928972	11	231	699599.7	4926653	20
74	680545.5	4929138	11	232	680885.3	4926435	20
75	701098.2	4931903	11	233	680595.8	4926850	20
76	682258.1	4931889	11	234	680196.4	4927393	20
77	682289.4	4931932	11	235	680083.3	4927556	20
78	682289.4	4931932	11	236	690246.8	4927959	20
79	682271	4931937	11	237	692467.9	4928180	20
80	682271	4931937	11	238	680677.8	4928105	20
81	693510.9	4932845	11	239	691535.5	4928578	20
82	681317.6	4932587	11	240	691334.3	4928664	20
83	682528.7	4932780	11	241	680909.3	4928612	20
84	682559.5	4932886	11	242	690664.2	4928955	20
85	701955.1	4933858	11	243	677421.2	4928704	20
86	682841.2	4934997	11	244	681534.9	4928841	20
87	682830.1	4935002	11	245	680458.3	4928823	20
88	681297.8	4935230	11	246	680473.4	4928858	20
89	680001.3	4935840	11	247	680165.7	4928941	20
90	688359.4	4940892	11	248	688861.2	4929407	20
91	687901.7	4940942	11	249	688843.9	4929410	20
92	683814	4942153	11	250	688613	4929722	20
93	683422.9	4942158	11	251	688639.8	4929748	20
94	685521.8	4933598	12	252	688656.7	4929765	20

95	684913	4933629	12	253	688055.6	4930046	20
96	684957.5	4933635	12	254	687637.8	4932125	20
97	678604.1	4928864	13	255	687854.6	4932663	20
98	676095.3	4905741	14	256	678151.3	4932458	20
99	679851	4927888	15	257	680684.3	4932547	20
100	680817.6	4921247	16	258	681473.4	4932587	20
101	681161.1	4922293	16	259	681101.5	4932627	20
102	681405	4924093	16	260	687597.4	4932824	20
103	699161.5	4926131	17	261	682500.5	4932680	20
104	697676.4	4926678	17	262	687408.1	4932941	20
105	696770.3	4927162	17	263	680774.6	4932776	20
106	696132.6	4927478	17	264	687212.3	4933067	20
107	695509.6	4927722	17	265	686808.6	4933241	20
108	694884.3	4927965	17	266	683991.5	4933178	20
109	680018	4933134	17	267	679670.5	4933171	20
110	681901.4	4894658	18	268	686495.8	4933365	20
111	681978.4	4894747	18	269	687799.9	4934118	20
112	672646.2	4897704	18	270	702660.2	4934887	20
113	677609.8	4898815	18	271	702543.7	4934974	20
114	674321.9	4899117	18	272	701776.6	4935424	20
115	674211.4	4899429	18	273	677065	4907008	21
116	677517.6	4900896	18	274	680220.8	4914262	21
117	675130.3	4900909	18	275	679910.6	4915179	21
118	675120.3	4900909	18	276	679865.5	4915418	21
119	675326.6	4901271	18	277	679865.5	4915418	21
120	675315.6	4901275	18	278	678176.4	4928373	21
121	674560.3	4901621	18	279	693370	4932532	21
122	676759.6	4903468	18	280	701480.8	4932808	21
123	682921	4904222	18	281	693669.3	4933188	21
124	675524.4	4904059	18	282	693893	4933850	21
125	675533.3	4904060	18	283	694719	4935040	21
126	675237.3	4904634	18	284	695179.9	4935608	21
127	675678.2	4904721	18	285	695362.9	4936302	21
128	675668.9	4904722	18	286	689969.6	4940093	21
129	675513.8	4904852	18	287	687854.7	4938410	21
130	668612.7	4906006	18	288	676108.2	4906254	22
131	691283.4	4907460	18	289	676099.9	4906260	22
132	679503	4908879	18	290	686467.5	4930753	23
133	679482.5	4908904	18	291	678835	4917655	24
134	679880.1	4909270	18	292	670205.9	4907439	25
135	688404.4	4909642	18	293	672554.4	4908813	26
136	679755.2	4910245	18	294	689948.1	4929063	27
137	679796.6	4910248	18	295	681509.6	4931538	28
138	691737.6	4910637	18	296	669246.9	4917774	29
139	689090.8	4910875	18	297	687676.3	4930255	29
140	689210.7	4911466	18	298	687098.2	4930553	29
141	674331.1	4911054	18	299	688052	4930099	30
142	673552.9	4911374	18	300	680578.9	4910574	31
143	672564.5	4911616	18	301	668404.6	4905339	32
144	680727.6	4912037	18	302	680587.4	4910400	33

145	680702.2	4912053	18	303	688165.9	4940920	34
146	691792.9	4913048	18	304	681055.5	4930969	35
147	691969.8	4913524	18	305	691259.8	4928379	36
148	692180.2	4913728	18	306	687620	4932136	36
149	681175	4915629	18	307	686297	4916129	37
150	686432.9	4915799	18	308	667488.2	4905542	38
151	693311.5	4916339	18	309	672811	4908971	39
152	677777.4	4916426	18	310	682175.5	4898246	40
153	677107.3	4916641	18	311	681889.2	4894804	41
154	686168.7	4917047	18	312	688961.3	4928258	42
155	693538.6	4918003	18	313	674962.3	4925827	43
156	678936.8	4917590	18	314	674938.5	4925734	44
157	679785	4917965	18	315	702205.3	4934490	45
158	690579.6	4918883	18				

Table A 1: Road bridges along selected road network

ID	Coordinates (CRS = UTM32N)		Typology	ID	Coordinates (CRS = UTM32N)		Typology
	X	Y			X	Y	
1	676419.6	4896317	3	13	689670.3	4925967	5
2	676460.7	4896322	3	14	690233	4926545	5
3	675499.5	4898719	4	15	693248.4	4927335	5
4	675540.5	4898725	4	16	680354.8	4927160	5
5	675155	4899575	4	17	692564.4	4927663	5
6	675180.9	4900593	4	18	690241.4	4929232	5
7	675189.2	4900604	4	19	696317.9	4930735	4
8	678661.7	4907567	5	20	687456.8	4931200	5
9	678652	4907576	5	21	687387.3	4931461	5
10	679452.8	4908679	2	22	683926.8	4931563	1
11	679428.5	4908688	2	23	679932.7	4931899	5
12	680000.8	4916808	1	24	680762.5	4936198	5

Table A 2: Road tunnels along selected road network

Typology	MM1	MM2	DSS	PDC	PT	Sp	LS
1	C	PC	Ssu	Is	McP	Ms	NSD
2	C	PC	Ssu	Is	McP	Ms	LC
3	C	PC	Ssu	Is	McP	Ms	MC
4	C	PC	Ssu	Is	McP	Ms	HC
5	C	PC	Ssu	Is	ScP	Ms	LC
6	C	PC	Ssu	Is	ScP	Ms	MC
7	C	PC	Ssu	Is	ScP	Ms	HC
8	C	PC	Co	Is	McP	Ms	MC
9	C	PC	Co	Is	ScP	Ms	MC
10	C	RC	X	X	X	Ssp	LC
11	C	RC	X	X	X	Ssp	MC
12	S	X	Ssu	Is	ScP	Ms	LC
13	S	X	Ssu	Is	ScP	Ms	MC
14	S	X	Ssu	X	X	Ssp	LC
15	S	X	Ssu	X	X	Ssp	MC
16	S	X	Co	Is	ScP	Ms	MC
17	S	RC	Co	Is	ScP	Ms	MC
18	X	X	X	X	X	X	X
19	C	PC	X	X	X	Ssp	LC
20	C	PC	X	X	X	Ssp	MC
21	C	PC	X	X	X	Ssp	HC
22	C	PC	X	X	McP	X	X
23	C	PC	Co	NIs	McP	Ms	HC
24	C	PC	X	X	X	X	X
25	C	PC	X	Is	ScP	Ms	MC
26	C	PC	X	Is	ScP	Ms	HC
27	C	RC	Co	NIs	ScP	Ms	MC
28	C	RC	X	X	X	Ms	HC
29	C	X	X	X	X	Ms	MC
30	C	X	X	X	X	Ssp	MC
31	C	URM	X	X	X	Ssp	MC
32	C	URM	X	X	ScP	Ms	MC
33	S	RC	X	X	X	Ssp	MC
34	S	X	Ssu	Is	McP	Ms	MC
35	S	X	X	X	X	Ssp	LC
36	S	X	X	X	X	Ssp	MC
37	M	URM	X	X	ScP	Ms	LC
38	M	URM	X	X	ScP	Ms	MC
39	M	URM	X	X	X	Ssp	MC
40	M	S	X	X	ScP	Ssp	MC
41	M	S	X	X	ScP	Ms	MC
42	M	X	X	X	X	Ms	MC
43	M	X	X	X	ScP	Ms	MC
44	C	PC	X	X	ScP	Ms	X
45	C	PC	X	X	X	Ssp	X

Table A 3: Bridge typology structural characteristics
Note: 'X' is denoted where parameters were unspecified

Typology	CM	Sh	D	Geo	Ss
1	B	C	D	A	C
2	B	C	D	R	C
3	CC	H	D	A	C
4	CC	H	S	A	C
5	CC	R	S	A	C

Table A 4: Tunnel typology structural characteristics

Typology	DS 1		DS 2		DS 3		DS 4	
	μ	β	μ	β	μ	β	μ	β
1	0.22	1.56	0.65	0.65	0.95	0.87	1.31	1.68
2	0.22	1.56	0.65	0.65	0.95	0.87	1.31	1.68
3	0.18	1.76	0.61	0.59	0.80	0.56	1.13	0.72
4	0.18	1.76	0.61	0.59	0.80	0.56	1.13	0.72
5	0.17	1.83	0.52	0.75	0.52	0.22	0.74	0.46
6	0.26	1.38	0.68	0.56	1.10	0.73	1.01	0.69
7	0.26	1.38	0.68	0.56	1.10	0.73	1.01	0.69
8	0.27	1.42	0.81	0.60	0.65	0.90	1.40	1.00
9	0.34	1.27	0.66	0.69	0.92	0.67	0.92	0.75
10	0.50	0.94	0.72	1.03	1.09	1.53	1.01	1.62
11	0.77	0.72	1.03	1.02	1.35	1.39	1.67	1.37
12	0.47	0.81	1.05	0.69	1.46	0.96	1.33	0.90
13	0.47	0.81	1.05	0.69	1.46	0.96	1.33	0.90
14	0.61	0.70	0.86	0.73	1.11	0.95	1.66	1.53
15	0.69	0.64	1.49	1.48	1.90	1.71	2.39	2.10
16	0.84	0.62	1.07	0.71	1.36	0.95	1.69	1.23
17	0.84	0.62	1.07	0.71	1.36	0.95	1.69	1.23
18	0.28	1.34	0.62	0.87	0.88	1.13	1.21	1.52
19	0.52	0.78	0.66	0.65	0.83	0.67	1.16	0.92
20	0.72	0.64	1.19	1.17	1.48	1.35	1.90	1.70
21	0.72	0.64	1.19	1.17	1.48	1.35	1.90	1.70
22	0.29	1.31	0.75	0.77	0.93	0.99	1.56	1.74
23	0.75	0.60	1.04	0.79	1.47	1.34	2.22	2.57
24	0.24	1.46	0.67	0.67	0.86	0.88	1.26	1.45
25	0.25	1.51	0.63	0.67	0.92	0.67	0.88	0.70
26	0.25	1.51	0.63	0.67	0.92	0.67	0.88	0.70
27	0.40	1.14	0.67	0.88	0.95	1.05	1.38	1.87
28	0.35	1.21	0.67	0.80	0.93	0.91	1.28	1.52
29	0.27	1.39	0.64	0.77	0.84	0.90	1.18	1.40
30	0.80	0.76	1.07	1.07	1.42	1.51	1.91	2.32
31	0.72	0.64	1.19	1.17	1.48	1.35	1.90	1.70
32	0.72	0.60	0.91	0.61	1.15	0.77	1.46	1.04
33	0.72	0.64	1.19	1.17	1.48	1.35	1.90	1.70
34	0.39	1.00	0.58	0.66	0.79	0.58	1.11	0.78
35	0.55	0.74	0.65	0.66	0.76	0.63	1.09	0.82
36	0.72	0.64	1.19	1.17	1.48	1.35	1.90	1.70
37	0.25	1.39	0.33	1.13	0.82	0.34	0.53	0.76
38	0.59	0.63	0.83	0.56	1.10	0.73	1.38	0.93
39	0.65	0.65	1.21	1.25	1.54	1.45	1.97	1.81
40	0.69	0.59	1.33	1.48	1.65	1.67	2.02	1.98
41	0.59	0.63	0.83	0.56	1.10	0.73	1.38	0.93
42	0.57	0.69	0.85	0.57	1.15	0.77	1.52	1.10
43	0.59	0.63	0.83	0.56	1.10	0.73	1.38	0.93
44	0.29	1.36	0.64	0.67	0.88	0.66	0.91	0.72
45	0.62	0.69	0.91	0.93	1.14	1.06	1.53	1.38

Table A 5: Bridge typology parameters (combined fragility functions) *values are Peak Ground Acceleration (PGA) given in terms of gravitational acceleration (*g*)

Typology	Median								Upper Confidence Bound								Lower Confidence Bound							
	DS 1		DS 2		DS 3		DS 4		DS 1		DS 2		DS 3		DS 4		DS 1		DS 2		DS 3		DS 4	
	μ	β	μ	β	μ	β	μ	β	μ	β	μ	β	μ	β	μ	β	μ	β	μ	β	μ	β	μ	β
1	0.25	0.16	0.67	0.42	1.07	0.81	1.17	0.68	0.31	0.22	0.82	0.54	1.31	1.02	2.14	1.38	0.13	0.10	0.44	0.26	0.53	0.32	0.76	0.44
2	0.25	0.16	0.67	0.42	1.07	0.81	1.17	0.68	0.31	0.22	0.82	0.54	1.31	1.02	2.14	1.38	0.13	0.10	0.44	0.26	0.53	0.32	0.76	0.44
3	0.14	0.13	0.63	0.25	0.83	0.37	1.11	0.56	0.54	0.29	0.80	0.44	1.18	0.78	1.52	0.87	0.07	0.47	0.43	0.39	0.49	0.38	0.83	0.36
4	0.14	0.13	0.63	0.25	0.83	0.37	1.11	0.56	0.54	0.29	0.80	0.44	1.18	0.78	1.52	0.87	0.07	0.47	0.43	0.39	0.49	0.38	0.83	0.36
5	0.12	0.06	0.51	0.19	Inf	1.00	0.75	0.32	0.35	0.14	0.63	0.26	Inf	1.00	0.83	0.42	0.11	0.05	0.43	0.18	Inf	1.00	0.66	0.28
6	0.25	0.84	0.64	0.27	1.02	0.77	0.94	0.49	0.63	0.40	0.97	0.68	1.48	0.92	1.62	0.98	0.11	0.06	0.52	0.21	0.81	0.37	0.68	0.32
7	0.25	0.84	0.64	0.27	1.02	0.77	0.94	0.49	0.63	0.40	0.97	0.68	1.48	0.92	1.62	0.98	0.11	0.06	0.52	0.21	0.81	0.37	0.68	0.32
8	0.22	0.09	1.02	0.62	0.60	0.49	1.34	0.87	0.70	0.53	1.35	0.76	1.39	0.94	1.89	1.13	0.17	0.21	0.39	0.41	0.27	0.07	1.05	0.60
9	0.53	0.23	0.65	0.28	0.94	0.62	1.03	0.54	0.91	0.71	1.08	0.70	1.41	0.90	1.69	1.08	0.08	0.79	0.38	0.32	0.53	0.45	0.50	0.28
10	0.53	0.36	0.66	0.54	1.00	0.69	0.81	0.47	0.96	0.69	1.81	1.50	2.63	1.83	2.06	1.33	0.30	0.24	0.41	0.27	0.50	0.43	0.48	0.73
11	0.70	0.43	0.93	0.58	1.25	0.79	1.70	1.10	1.07	0.71	1.74	1.24	2.44	1.25	3.97	1.61	0.53	0.29	0.58	0.36	0.74	0.44	0.81	0.44
12	0.45	0.49	Inf	1.00	Inf	1.00	1.23	0.81	0.65	0.43	Inf	1.00	Inf	1.00	1.78	1.04	0.35	0.13	Inf	1.00	Inf	1.00	1.00	0.45
13	0.45	0.49	Inf	1.00	Inf	1.00	1.23	0.81	0.65	0.43	Inf	1.00	Inf	1.00	1.78	1.04	0.35	0.13	Inf	1.00	Inf	1.00	1.00	0.45
14	0.77	0.52	1.07	0.71	1.36	0.88	1.90	1.29	0.96	0.63	1.44	0.96	1.93	1.24	3.01	1.76	0.31	0.21	0.42	0.28	0.53	0.35	0.76	0.54
15	0.65	0.43	1.05	0.70	1.46	0.97	1.83	1.21	0.96	0.63	3.29	1.92	3.43	1.96	3.77	2.12	0.54	0.36	0.88	0.65	1.21	0.91	1.65	1.34
16	0.81	0.67	1.07	0.71	1.35	0.90	1.69	1.12	1.09	0.72	1.09	0.72	1.46	0.96	1.74	1.14	0.65	0.43	1.05	0.69	1.26	0.83	1.65	1.09
17	0.81	0.67	1.07	0.71	1.35	0.90	1.69	1.12	1.09	0.72	1.09	0.72	1.46	0.96	1.74	1.14	0.65	0.43	1.05	0.69	1.26	0.83	1.65	1.09
18	0.26	0.18	0.65	0.53	0.92	0.68	1.16	0.74	0.75	0.52	1.09	0.75	1.67	1.32	2.17	1.37	0.12	0.14	0.34	0.24	0.44	0.38	0.64	0.49
19	0.47	0.57	0.61	0.68	0.76	0.84	1.06	0.91	0.92	0.62	1.06	0.70	1.36	0.86	1.89	1.18	0.32	0.20	0.42	0.24	0.51	0.27	0.73	0.39
20	0.65	0.42	1.05	0.70	1.26	0.83	1.73	1.14	1.05	0.69	1.96	1.44	2.35	1.50	2.76	1.60	0.53	0.28	0.68	0.45	0.86	0.61	1.11	0.76
21	0.65	0.42	1.05	0.70	1.26	0.83	1.73	1.14	1.05	0.69	1.96	1.44	2.35	1.50	2.76	1.60	0.53	0.28	0.68	0.45	0.86	0.61	1.11	0.76
22	0.25	0.16	0.73	0.53	1.09	0.85	1.56	1.15	0.70	0.47	1.09	0.73	1.47	1.04	2.53	1.57	0.16	0.10	0.43	0.23	0.44	0.32	0.79	0.50
23	0.74	0.51	1.09	0.72	1.26	0.83	1.64	1.10	1.09	0.71	1.62	1.08	2.98	1.67	3.93	2.00	0.53	0.23	0.65	0.29	0.80	0.40	0.97	0.64
24	0.23	0.17	0.68	0.48	1.02	0.75	1.28	0.90	0.58	0.37	1.05	0.69	1.30	0.89	1.89	1.19	0.12	0.08	0.42	0.22	0.45	0.31	0.63	0.34
25	0.21	0.13	0.62	0.27	0.94	0.62	0.83	0.44	0.76	0.62	1.07	0.69	1.41	0.90	1.69	1.06	0.09	0.34	0.42	0.33	0.53	0.45	0.52	0.28
26	0.21	0.13	0.62	0.27	0.94	0.62	0.83	0.44	0.76	0.62	1.07	0.69	1.41	0.90	1.69	1.06	0.09	0.34	0.42	0.33	0.53	0.45	0.52	0.28
27	0.39	0.34	0.67	0.59	0.97	0.74	1.20	0.82	0.92	0.80	1.17	0.97	1.59	1.10	2.39	1.48	0.23	0.24	0.48	0.37	0.59	0.44	0.70	0.62
28	0.34	0.31	0.69	0.58	0.96	0.68	1.16	0.71	0.85	0.64	1.07	0.71	1.44	0.92	2.17	1.21	0.14	0.35	0.44	0.34	0.58	0.45	0.70	0.59

29	0.27	0.18	0.63	0.37	0.90	0.66	1.12	0.67	0.69	0.51	1.08	0.70	1.44	0.93	1.90	1.11	0.11	0.09	0.39	0.23	0.45	0.35	0.65	0.46
30	0.75	0.42	0.98	0.64	1.27	0.81	1.73	1.15	1.19	0.93	1.93	1.37	2.84	1.50	3.74	1.79	0.53	0.31	0.59	0.37	0.74	0.47	0.79	0.52
31	0.65	0.42	1.05	0.70	1.26	0.83	1.73	1.14	1.05	0.69	1.96	1.44	2.35	1.50	2.76	1.60	0.53	0.28	0.68	0.45	0.86	0.61	1.11	0.76
32	0.65	0.42	1.05	0.69	1.26	0.83	1.65	1.09	1.09	0.71	1.10	0.71	1.48	0.92	1.79	1.04	0.53	0.23	0.65	0.28	0.81	0.37	1.06	0.50
33	0.65	0.42	1.05	0.70	1.26	0.83	1.73	1.14	1.05	0.69	1.96	1.44	2.35	1.50	2.76	1.60	0.53	0.28	0.68	0.45	0.86	0.61	1.11	0.76
34	0.52	0.27	0.65	0.28	0.82	0.36	1.08	0.48	0.56	0.31	0.92	0.59	1.28	0.80	1.89	1.08	0.20	0.04	0.34	0.07	0.48	0.12	0.68	0.19
35	0.52	0.77	0.60	0.65	0.68	0.57	0.96	0.72	0.95	0.63	1.05	0.70	1.24	0.84	1.79	1.14	0.32	0.20	0.42	0.24	0.51	0.27	0.73	0.39
36	0.65	0.42	1.05	0.70	1.26	0.83	1.73	1.14	1.05	0.69	1.96	1.44	2.35	1.50	2.76	1.60	0.53	0.28	0.68	0.45	0.86	0.61	1.11	0.76
37	0.26	0.83	0.34	0.77	Inf	1.00	0.52	0.91	0.53	0.22	0.65	0.27	Inf	1.00	1.09	0.46	0.12	0.18	0.17	0.27	Inf	1.00	0.25	0.37
38	0.58	0.34	0.79	0.60	1.02	0.77	1.29	0.81	0.65	0.41	1.06	0.68	1.48	0.92	1.79	1.04	0.53	0.23	0.65	0.28	0.81	0.37	1.07	0.50
39	0.60	0.38	0.97	0.66	1.35	0.90	1.78	1.18	0.90	0.63	2.47	1.66	2.80	1.67	3.15	1.72	0.52	0.27	0.65	0.38	0.82	0.50	1.05	0.67
40	0.65	0.42	1.05	0.70	1.45	0.97	1.73	1.15	0.96	0.63	3.26	1.87	3.37	1.84	3.59	1.83	0.53	0.23	0.63	0.32	0.79	0.42	1.02	0.58
41	0.58	0.34	0.79	0.60	1.02	0.77	1.29	0.81	0.65	0.41	1.06	0.68	1.48	0.92	1.79	1.04	0.53	0.23	0.65	0.28	0.81	0.37	1.07	0.50
42	0.55	0.32	0.91	0.60	1.26	0.83	1.74	1.14	0.65	0.41	1.06	0.68	1.48	0.92	1.88	1.09	0.52	0.27	0.65	0.28	0.81	0.37	1.06	0.50
43	0.58	0.34	0.79	0.60	1.02	0.77	1.29	0.81	0.65	0.41	1.06	0.68	1.48	0.92	1.79	1.04	0.53	0.23	0.65	0.28	0.81	0.37	1.07	0.50
44	0.35	0.14	0.62	0.27	0.94	0.62	0.83	0.44	0.73	0.49	1.06	0.69	1.34	0.86	1.68	1.06	0.11	0.05	0.42	0.21	0.50	0.26	0.53	0.28
45	0.65	0.42	0.94	0.62	1.26	0.83	1.65	1.09	0.97	0.64	1.12	0.77	1.51	0.99	1.99	1.22	0.35	0.15	0.43	0.24	0.53	0.33	0.78	0.50

Table A 6: Bridge typology parameters (median fragility functions with confidence bounds) *values are Peak Ground Acceleration (PGA) given in terms of gravitational acceleration (g)

Typology	DS 1		DS 2		DS 3		DS 4	
	μ	β	μ	β	μ	β	μ	β
1	0.57	0.71	0.84	0.44	Inf	1.00	Inf	1.00
2	0.51	0.62	0.75	0.46	1.10	0.50	Inf	1.00
3	0.44	0.63	0.67	0.49	0.95	0.50	Inf	1.00
4	0.42	0.54	0.60	0.52	0.95	0.50	Inf	1.00
5	0.44	0.60	0.72	0.61	1.16	0.59	Inf	1.00

Table A 7: Tunnel typology parameters (combined fragility functions) *values are Peak Ground Acceleration (PGA) given in terms of gravitational acceleration (g)

T	Median								Upper Confidence Bound								Lower Confidence Bound							
	DS 1		DS 2		DS 3		DS 4		DS 1		DS 2		DS 3		DS 4		DS 1		DS 2		DS 3		DS 4	
	μ	β	μ	β	μ	β	μ	β	μ	β	μ	β	μ	β	μ	β	μ	β	μ	β	μ	β	μ	β
1	0.57	0.71	0.84	0.44	23.2	0.21	Inf	1.00	0.61	0.71	0.91	0.44	23.2	0.21	Inf	1.00	0.53	0.73	0.77	0.46	23.2	0.21	Inf	1.00
2	0.55	0.60	0.80	0.43	Inf	1.00	Inf	1.00	0.65	0.62	0.90	0.43	Inf	1.00	Inf	1.00	0.36	0.47	0.57	0.43	Inf	1.00	Inf	1.00
3	0.48	0.55	0.70	0.46	Inf	1.00	Inf	1.00	0.57	0.71	0.86	0.38	Inf	1.00	Inf	1.00	0.31	0.46	0.47	0.44	Inf	1.00	Inf	1.00
4	0.47	0.47	0.66	0.47	Inf	1.00	Inf	1.00	0.53	0.53	0.74	0.53	Inf	1.00	Inf	1.00	0.30	0.40	0.45	0.40	Inf	1.00	Inf	1.00
5	0.43	0.52	0.73	0.55	1.06	0.55	Inf	1.00	0.64	0.58	1.01	0.61	1.62	0.57	Inf	1.00	0.32	0.48	0.53	0.49	0.96	0.51	Inf	1.00

Table A 8: Tunnel typology parameters (median fragility functions with confidence bounds) *values are Peak Ground Acceleration (PGA) given in terms of gravitational acceleration (g)

Origin	Destination																				
	6	**8**	**9**	**11**	**19**	**21**	**30**	**31**	**34**	**36**	**40**	**41**	**42**	**44**	**46**	**47**	**51**	**54**	**57**	**59**	**60**
6	0	952	2384	3400	1862	1692	1764	20	36	116	70	142	328	98	1258	1126	18	2518	658	70	2304
9	2014	0	72	48	176	530	330	0	2	4	2	12	6	44	194	36	2	320	12	14	60
11	2014	32	0	232	130	72	80	2	10	6	2	4	28	24	42	20	0	66	40	6	218
8	4228	86	358	0	240	112	128	2	0	36	12	14	86	62	90	66	0	150	334	42	918
57	2892	64	188	184	0	104	232	0	4	14	0	8	16	56	70	36	0	130	26	4	132
19	2358	302	90	80	122	0	246	2	2	6	2	10	16	36	180	92	0	362	10	2	70
44	2094	124	80	72	164	202	0	0	4	4	2	10	10	36	64	32	4	126	26	4	58
21	210	4	18	66	12	6	12	0	2	76	2	0	0	92	4	20	28	4	176	268	38
34	392	10	10	18	10	22	16	0	0	2	78	66	2	34	32	416	6	54	26	4	16
40	498	6	48	222	24	18	20	8	4	0	2	0	20	36	22	68	4	26	640	106	128
46	208	4	18	10	8	16	6	0	156	4	0	60	0	14	26	116	36	20	26	14	14
36	798	42	20	20	14	104	36	0	42	2	24	0	2	30	218	54	2	328	2	0	18
47	1520	14	166	580	62	32	56	4	0	22	2	6	0	28	24	26	2	44	116	18	732
59	572	2	54	210	18	18	16	14	56	62	10	4	10	0	8	146	32	32	358	26	106
60	1656	108	50	64	52	230	92	2	6	4	0	52	14	32	0	90	2	776	10	2	54
51	2146	44	64	122	62	150	78	2	48	14	12	18	0	60	108	0	6	358	66	0	60
31	208	2	14	44	6	0	8	10	50	14	58	8	10	118	2	36	0	6	88	26	38
30	4266	158	144	182	162	458	226	0	12	6	8	58	8	98	426	270	12	0	22	0	130
41	1454	20	172	738	64	46	60	0	10	112	10	4	96	76	34	108	16	62	0	42	348
54	262	6	32	64	20	6	4	76	0	118	2	0	42	16	6	40	2	6	160	0	60
42	2280	38	292	896	110	74	76	2	0	20	8	8	216	52	66	40	0	60	130	10	0

Table A 9: O-D matrix for regional traffic analysis

APPENDIX B: Croatian Rail Network Data

B.1 Kupa Karlovac Bridge

The 'Kupa Karlovac' bridge was originally built in 1873. Up until World War II the bridge carried two tracks but the bridge and the upper part of the substructure was destroyed during the war. In 1945, the bridge was rebuilt with smaller dimensions to accommodate a single track. Although the piers and abutments were rebuilt with smaller dimensions, appropriate for a single track, the lower part of the foundations was not altered. The current steel structure was built on the existing substructure in 1989.

The bridge structure is of steel construction and is continuous over 3 spans (32.02 m + 38.42 m + 32.02 m), with a total length of 103.56 m (including 0.55 m behind the bearings at each abutment). The bridge is 5.50 m wide. The superstructure cross section consists of two main solid web beams at a distance of 5.5 m; cross beams at intervals of 4 m in the end spans and 3.84 m in the middle span; and two longitudinal girders at a 1.8 m spacing support the tracks. The bridge also supports a pedestrian walkway on the downstream side. Figure B 1 illustrated the elevation, plan and cross section of the bridge.

A geotechnical investigation was conducted for the bridge in 2012 as part of a project to assess the capacity of a number of steel bridges across Croatia. The investigation consisted of a single borehole adjacent to the track at Abutment U1 and comprised of drilling with continuous coring, sampling and SPT tests as well as laboratory tests. The results are summarised in Figure B 2, as well as Table B 2 and Table B 2.

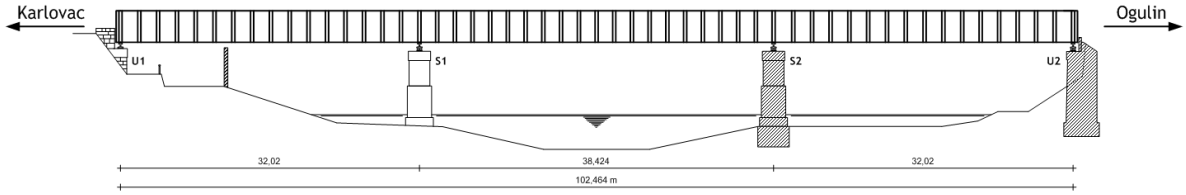

a) Elevation of bridge

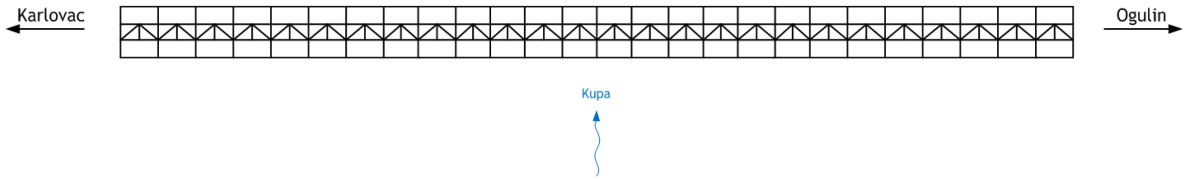

b) Plan view showing structural members of superstructure

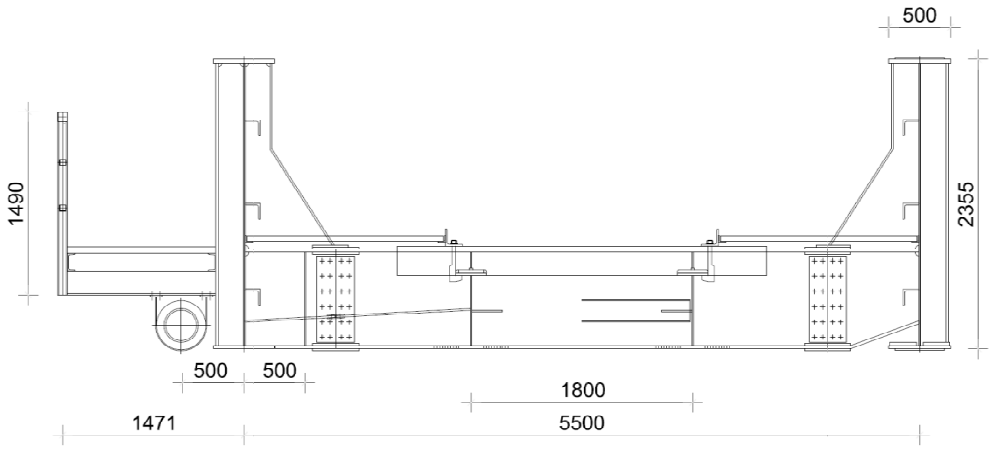

c) Cross section

Figure B 1: Geometry of Kupa Karlovac bridge (HZ Infrastruktura, 2013)

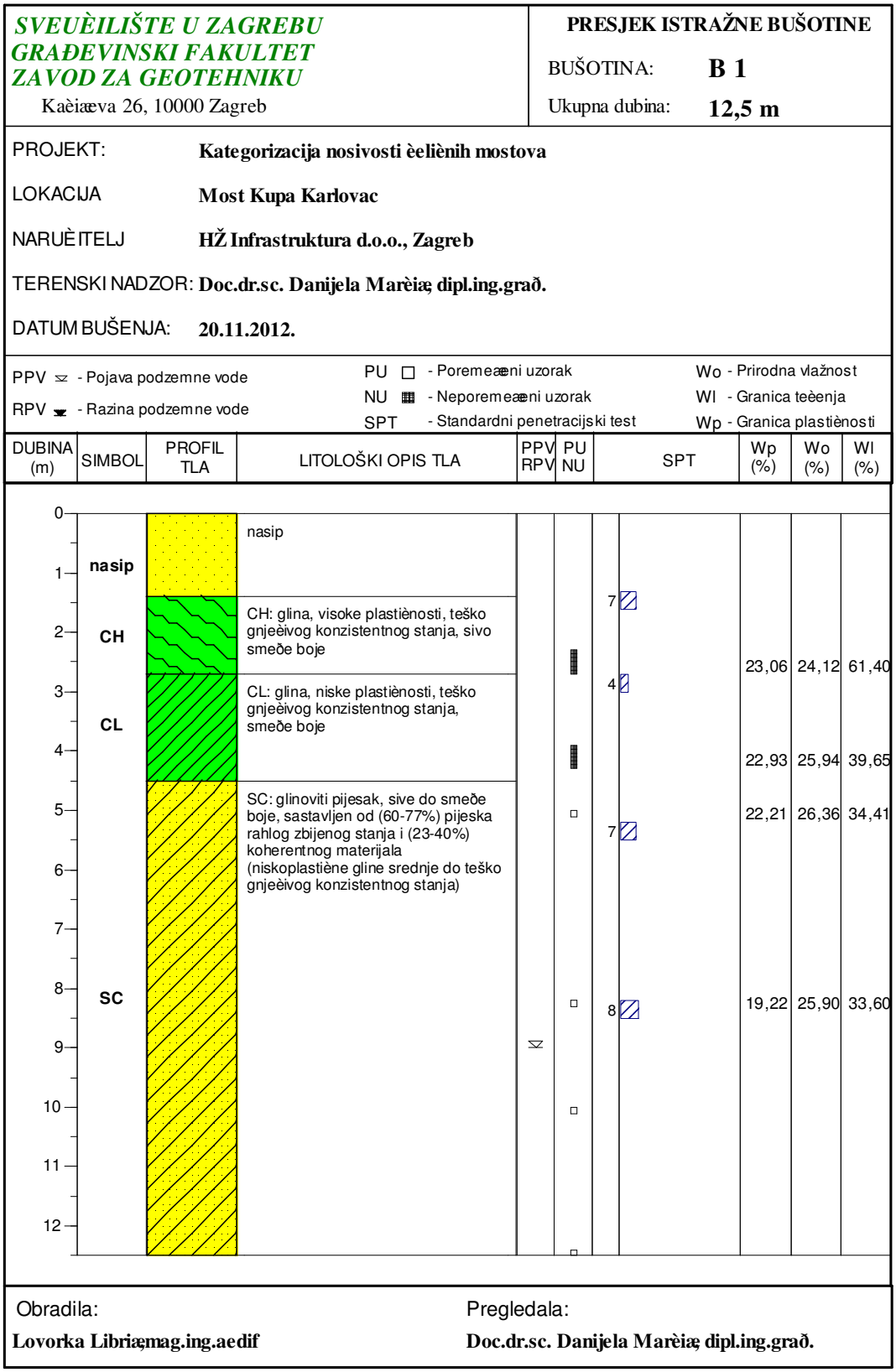

Table B 1: Borehole log from geotechnical investigation – translation and legend below (HZ Infrastruktura, 2013)

Nasip: Embankment

CH: clay, high plasticity, stiff with a gray-brown color

CL: clay, low plasticity, stiff with a brown color

SC: clayey sand, gray to brown in color, composed of (60-77%) loosely compacted sand and (23-40%) coherent materials (low plasticity clay, medium to stiff)

PPV - The emergence of groundwater

RPV - Groundwater level

PU – Disturbed sample

NU - Undisturbed sample

Wo – Natural moisture content

Wl – Liquid limit

Wp – Plastic limit

SPT - Standard penetration test

Soil Type	γ [kN/m^3]	c' [kPa]	φ' [°]
Nasip	18	0	28
CH	20	20.6	22.3
CL	20	4.5	26.9
SC	19	3.0	32.0

Table B 2: Summary of soil properties (HZ Infrastruktura, 2013)

The borehole testing was only conducted in one location, at the top of the river bank beside the abutment (U1) protected from scour by the flood wall. The borehole depth was 12.5 m which is approximantely the level where the timber piles meet the bottom of the piers/abutment. Due to this limited information, some assumptions need to be made about the soil properties around the piles. The analysis assumes that both the piers and the abutments are founded in the clayey sand (SC) layer and that this layer extents infinitely beyond the bottom of the borehole.

B.2 Network Locations Potentially Impacted by Rainfall-Triggered Landslides

Four network locations were identified as susceptible to potential damage due to rainfall-triggered landslides, as illustrated in Figure B 2 to Figure B 5. These were all located near the hydrological station in the town of Novi Marof, approximately 54 km north of Zagreb.

Figure B 2: Location 1

Figure B 3: Location 2

Figure B 4: Location 3

Figure B 5: Location 4